PERFORMANCE ANALYSIS AND TOPOLOGY CONTROL OF LARGE WIRELESS NETWORKS WITH FADING

A Dissertation

Submitted to the Graduate School
of the University of Notre Dame
in Partial Fulfillment of the Requirements
for the Degree of

Doctor of Philosophy

by

Xiaowen Liu, B.S., M.S.

Martin Haenggi, Director

Graduate Program in Electrical Engineering
Notre Dame, Indiana
April 2007

PERFORMANCE ANALYSIS AND TOPOLOGY CONTROL OF LARGE WIRELESS NETWORKS WITH FADING

Abstract

by

Xiaowen Liu

For the performance analysis of multihop wireless networks, the key issues are energy consumption, end-to-end reliability, delay and throughput. In the research of wireless multihop networks, the "disk models" that are often employed assume that the radius for a successful transmission of a packet has a fixed and deterministic value, irrespective of the condition of the wireless channel. Taking into account the stochastic nature of the fading channel, the Rayleigh fading link model includes fading as a random variation in the path loss. As a result, all properties of the network become random variables, in particular the signal-to-noise-and-interference ratio (SINR) that determines the success of a transmission.

This thesis explores the performance of one- and two-dimensional networks with equidistant nodes and uniformly randomly placed nodes. For regular two-dimensional networks, three topologies are studied based on a uniform traffic model and a simple random MAC scheme. Square networks are explored in more detail for their load distribution. By comparing the energy consumption and the achievable throughput for random and regular networks, we demonstrate that random distributions incur substantially higher energy expenditures at a lower achievable throughput.

Xiaowen Liu

For sensor networks with a slotted ALOHA MAC protocol in Rayleigh fading channels, we present closed-form expressions of the average link throughput, and we compare networks with three regular topologies in terms of throughput, transmit efficiency, and transport capacity. For random networks with nodes distributed according to a two-dimensional Poisson point process, the average throughput is analytically characterized and numerically evaluated.

Uniformly random or Poisson distributions are widely accepted models for the location of the nodes in wireless sensor networks if nodes are deployed in large quantities and there is little control over where they are dropped. On the other hand, by placing nodes in regular topologies, we expect benefits both in coverage and efficiency of communication. We describe and analyze quasi-regular networks, which only use nodes as sentries and relays that are approximately evenly spaced, thereby emulating a regular grid topology. It is shown that quasi-regular networks have a significant energy and lifetime advantage compared with purely random networks.

CONTENTS

FIGURES

TABLES

CHAPTER 1

INTRODUCTION

1.1 Overview

An ad hoc network is a collection of nodes setting up peer-to-peer communication without the use of any infrastructure. The term "ad hoc" means "can take different forms" and "can be static or mobile" [74]. The broadcast nature of the radio channel of wireless ad hoc networks enables nodes to communicate with high probability if the signal-to-noise-and-interference ratio (SINR) is high enough. Distant nodes may communicate indirectly over one or more relays. The source node, relay node(s) and destination node constitute a multihop connection or route. Multihop connections with the aid of peer nodes as relays and the lack of an infrastructure are the main differences that set the ad hoc wireless network apart from other classes of wireless network. Multihop routing is typically used to save transmit energy and consequently, increase the battery lifetime and decrease the interference between the nodes, thereby allowing spatial reuse of the communication channel.

With the development of micro-electro-mechanical-systems (MEMS) technology and digital electronics, sensor networks [4, 53] with small size, light weight, low cost, low power nodes have stimulated extensive research. In a sensor network, large numbers of sensor nodes are placed inside or near a phenomenon to collect

information about the phenomenon. One of the main discriminators of wireless sensor networks from other type of multihop networks is the fact that, in most cases, the sensor data has to be delivered to a common sink, the *observer* or *base station*.

In most applications, devices in a multihop network are powered by batteries with limited lifetime. Devices with a rechargeable battery, *e.g.*, cellular phones, must maximize lifetime between recharging. For devices with unrechargeable battery (for instance, in military applications, when nodes are distributed to the battlefield to collect data and it is impossible to recharge the batteries), energy conservation becomes imperative. So energy consumption plays a crucial role in the overall network performance [11, 59]. The traditional assumption is that transmit power dominates energy consumption although many researchers like [2] indicate that signal processing related to packet transmission and reception and hardware operation in a standby mode consume nonnegligible power as well. Our work does not focus on the energy consumption of the receiver and hardware. Rather, we focus on the transmit energy consumption so that the transmit traffic load of the node determines the node lifetime. For a sensor network, the load on the nodes near the base station is higher since those nodes have to forward all the traffic to the base station.

Throughput is a traditional measure of how much traffic can be delivered by the network [15, 16, 34, 75]. Although many papers on networks use the terms "capacity" or "throughput capacity" instead of throughput, we should clarify that this capacity is not the channel capacity in Shannon's theory. This capacity could be understood as the maximum throughput of the network when the rates of transmission on each link are fixed [11]. The throughput is intuitively related to the

error-free transmission rate of each transmitter, which, in turn, is upperbounded by Shannon's channel capacity. In this thesis, we define the throughput as the expected number of successful packet transmissions of a given node per timeslot. The end-to-end throughput over a multihop connection is the minimum of the link throughput values. End-to-end throughput is a performance measure of a route and the MAC scheme. We determined the throughput for different MAC schemes using analytic and simulation methods, yielding lower and upper bounds of the available throughput.

Our analysis is based on fading channel models, in contrast to the deterministic "disk model"(see Section 2.1), that is often used for the analysis of multihop packet networks [16, 62, 70, 77], where the radius for a successful transmission has a deterministic value, irrespective of the condition of the wireless channel, and interference is commonly taken account using the same geometric disk abstraction. The stochastic nature of the channel and thus the fact that the SINR is a random variable are neglected. However, the volatility of the channel cannot be ignored in wireless networks [11, 14]; the inaccuracy of "disk models" has also been pointed out in [67] and is easily demonstrated experimentally [13, 44]. In addition, the "prevalent all-or-nothing model" [64] leads to the assumption that a transmission over a multihop path either fails completely or is 100% successful, ignoring the fact that the end-to-end packet loss probabilities increase with the number of hops. To overcome some of these limitations of the "disk model", we employ a simple Rayleigh fading link model that relates transmit power, large-scale path loss, and the success of a transmission [21].

Based on the Rayleigh fading link model, we study regular one- and two-dimensional networks. To find the lower and upper throughput bounds, we present

several optimized MAC schemes. In particular, for regular two-dimensional networks, we consider three different topologies. At the other extreme, random networks whose nodes are uniformly randomly placed are explored. Comparisons between regular networks and their random counterparts are given.

Uniformly random or Poisson distributions are widely accepted models for the location of the nodes in wireless sensor networks if nodes are deployed in large quantities and there is little control over where they are dropped. On the other hand, by placing nodes in regular topologies, we expect benefits both in coverage and efficiency of communication. We describe and analyze a basic localized algorithm and three modifications for topology control that provide a tradeoff between performance and deployment cost. The objective is to regularize the topology for improved energy efficiency. The basic algorithm produces quasi-regular networks, which only use nodes as sentries and relays that are approximately evenly spaced, thereby emulating a regular grid topology. It is shown that quasi-regular networks have a significant energy and lifetime advantage compared with purely random networks.

1.2 Related Work

There is a rich literature on throughput capacity for ad hoc wireless networks [5, 15, 16, 23, 57, 65, 81]. The seminal paper [16] shows that, under certain assumptions, in a static two-dimensional network with N nodes and $N/2$ randomly selected source-destination pairs, the end-to-end throughput of a connection is at most $W/\sqrt{N}$, where W is the maximum transmission rate for each node. This result states that with an increasing number of nodes per unit area, the end-to-end throughput goes to zero. This work stimulated research in this problem (*e.g.*

[15, 61, 75]). However, such "order of" results do not provide any guidelines for protocol design, since the scaling behavior is very robust against changes in MAC and routing protocols [78]. Using ideal shortest path routing for the same ad hoc network model as in [16], [51] confirms the $1/\sqrt{N}$ decay of the throughput by an alternative approach and provides the relations of various network parameters. The authors in [49], claim that they computed an exact expression for throughput. They partition the network into non-overlapping square grid cells of equal size and assume that nodes can only communicate with the nodes in the same cell. This assumption neglects the fact that nodes within neighboring cells may have a higher SINR than nodes within the same cell.

All the above research work assumes networks with randomly located nodes. There are also research efforts focusing on networks with regular topologies which allow for mathematical tractability and provide valuable insight. In [65], the authors calculate the throughput of a regular square networks with a slotted ALOHA channel access scheme. For heavy traffic, they calculate the throughput as the expected number of successful packets received per slot summed over the whole network divided by the expected path length in hops. They find that the throughput grows proportionally to the square root of the number of nodes in the network if the number of nodes within transmission range is kept small. This result can be intuitively explained by spatial reuse. [63] also uses a square grid network to reveal the condition of connectivity and coverage if the nodes are unreliable. Moreover, when considering the exposure which is the capability of observing a target moving in a sensor field, [47] studies and compares three regular networks — square, triangle and hexagon networks. Their experimental results show that the exposure of the networks with regular topologies is higher than that with random

topology. Although some researchers focusing on random networks argue that it is more realistic and others argue that regular topologies are mathematically tractable, none of them have analyzed how big the performance gap is between these two classes of networks in terms of throughput, energy consumption and delay. We investigated the performance difference of these two classes networks.

Energy consumption is one of the most important performance metrics for wireless ad hoc networks with energy-constraint devices. It is often assumed that low-power transmissions reduce the interference and increase the throughput by spatial reuse, while, at the same time, consuming less energy. However, a route that contains more hops may experience a higher probability of route failure. [22] shows that routing as far as possible is a very competitive strategy in many cases. To achieve robustness, the use of multipath routing is suggested [33]. [29] proves that using a single path routing scheme with higher transmit power can also be an energy-efficient solution for robustness against node failures. Taking into account delay, throughput and reliability for specific MAC and routing protocols, minimizing the transmit power sustaining the connectivity may not be a desired strategy. All these considerations complicate the design of routing algorithms [60] and require the coordination of routing and access control protocols across the whole network. [59] presents a distributed protocol to find the minimum energy consumption topology for static ad hoc networks. Since the topology is found via a local search in each node's surrounding, they argue that it is applicable to a mobile scenario, which is "proved" by simulation. Since [68] shows that idle energy consumption can not be ignored compared to transmitting and receiving energy consumption, the authors in [79] present Geographical Adaptive Fidelity (GAF) — an energy saving protocol focusing on identifying nodes that are equivalent from

a routing perspective and then turning off unnecessary nodes, keeping a constant level of routing fidelity, which is defined as the uninterrupted connectivity between communicating nodes.

Most of the work above is based on a"disk model", often denoted as *protocol model* [16]. This model assumes every source node has the same transmission range r, and other transmitting nodes with distance further than $(1+\Delta)r$ to the source node do not interfere the source node for some $0 < \Delta \leq 1$. This disk model generates no interference outside a distance $(1+\Delta)r$, and it assumes the same received power level over the whole disk. Obviously, it is not a good model. The *physical model* [16] calculates the total interference over the whole network. The reception probability is 1 if the SINR is greater than a threshold Θ and 0 if it is less than Θ. We call this model *threshold model without fading* or simply *threshold model* in the thesis. It takes into account the power law path loss model and the interference over the entire network. But it is idealized, too, since even in the non-fading case, the actual reception probability is not a simple step function of the source-destination distance [83]. [32] examines the forwarding methods for wireless mobile multihop network both in Rayleigh fading [66] and non-fading channels. It models the channel power gain by an exponential distribution and assumes a path loss exponent α of 3. Adding the multipath fading effect and taking into account the total interference provides a more realistic model. However, it did not focus on the analytic study of the link model, instead simulations of different algorithms were provided. [82] extends the work in [67] which adopts a disk model without considering the random propagation effects, by combining both the fading and shadowing effects. As a result, the reception probability is a function of the threshold. Further, [28] characterizes the multipath fading

channel dynamics mostly by simulations at the packet level and examines the data queueing performance with respect to node speed, SNR, and average data message size. Although fading effects were considered in earlier work, their impact on the end-to-end reliability and the associated energy issues have not been addressed. Therefore, the detailed analysis of the performance of the multihop networks with fading is a very important research topic.

1.3 Contributions

The contributions made by this thesis are the following:

1. We analyze regular and random one-dimensioal (line) networks with Rayleigh fading channels [38], [39]. Based on a simple random MAC scheme, we show that regular line networks (equidistant nodes) outperform random line networks (uniformly randomly distributed nodes) in terms of throughput and, more drastically, in energy consumption. For regular line networks, we present the optimum scheduler that takes full advantage of spatial reuse and show that the throughput gain from the optimum scheduler is about 100% at nearly the same energy consumption. For random line networks, we present a throughput balancing strategy with power control and an energy balancing strategy without power control.

2. We study and compare the performance of several two-dimensional networks with regular topologies utilizing a Rayleigh fading link model [40]. For nearest-neighbor and shortest-path routing, analytical expressions of the path efficiency, delay, and energy consumption for a given end-to-end reception probability are derived. For the interference analysis, the maximum throughput and optimum transmit probability are determined, and a

simple MAC scheme is compared with an optimum scheduler, yielding lower and upper performance bounds.

3. We present closed-form expressions of the average per-node throughput for two dimensional sensor networks with a slotted ALOHA MAC protocol in Rayleigh fading channels [41], [42]. We compare networks with three regular topologies in terms of per-node throughput, transmit efficiency, and transport capacity. For random networks with nodes distributed according to a two-dimensional Poisson point process, the average per-node throughput is analytically characterized and numerically evaluated.

4. We describe and analyze a basic localized algorithm and three modifications for topology control that provide a tradeoff between performance and deployment cost [43]. The objective is to regularize the topology for improved energy efficiency. The basic algorithm produces quasi-regular networks, which only use nodes as sentries and relays that are approximately evenly spaced, thereby emulating a regular grid topology. We consider two specific types of quasi-regular networks: the ones that are based on a Gaussian deviation about an ideal grid point, and the ones that consist of a subset of nodes taken from a Poisson point process.

1.4 Organization of the Thesis

In the next chapter, the Rayleigh fading link model is introduced. Chapter 3 discusses the throughput and energy consumption for regular and random one-dimensional networks. For these two classes of networks, a simple random MAC scheme and an optimized scheduler are presented, yielding lower and upper throughput bounds. For random networks, two transmit power control strate-

gies are provided, and their energy consumption is compared. Chapter 4 deals with two-dimensional regular networks with three topologies — square, triangle, hexagon. Chapter 5 discusses the load distribution for regular square networks under the peer-to-peer traffic assumption (ad hoc network) and many-to-one traffic assumption (sensor network). Chapter 6 compares the performance of regular and random networks. In particular, for random sensor networks without power control, a strategy with retransmissions is discussed. Chapter 7 provides the analysis of the average link throughput for sensor networks of regular and random topologies with a slotted ALOHA MAC protocol in Rayleigh fading channels. Chapter 8 introduces and analyzes *quasi-regular networks*, where only nodes that are approximately evenly spaced to emulate a regular grid network are active and other nodes are put to sleep to save energy. Chapter 9 concludes the thesis.

CHAPTER 2

THE RAYLEIGH FADING LINK MODEL

2.1 Shortcomings of the Disk Model

The protocol or disk model in [16] assumes all nodes use the same transmit power which determines a circle with radius r, the so-called transmission radius [9, 27, 63, 65, 71]. The transmission is successful if the receiver lies inside the circle and every other simultaneously transmitting node lies outside the circle centered at the receiver with radius $r(1+\Delta)$ for some small positive Δ.

One of the drawbacks of the model is illustrated by Fig. 2.1. The transmit power determines the circle with radius r denoted by the solid circle. The dashed circle with radius of $r(1+\Delta)$ centered at the receiver determines the interference range, *i.e.*, any simultaneous transmission from a node within this circle leads to a collision. In Fig. 2.1 (a), the receiver is inside the solid circle and many other interfering nodes are outside the dashed circle, so the transmission is successful according to the model. In Fig. 2.1 (b), there is a collision since the interfering node is inside the dashed circle. However, from a communication theory point of view, it is clear that the SINR is the parameter that determines the success of a transmission. For example, let us assume all the nodes in Fig. 2.1 transmit at the same power level, and the noise power is zero. In Fig. 2.1(a), if $\overline{RI} = 2\overline{TR} = 2q$,

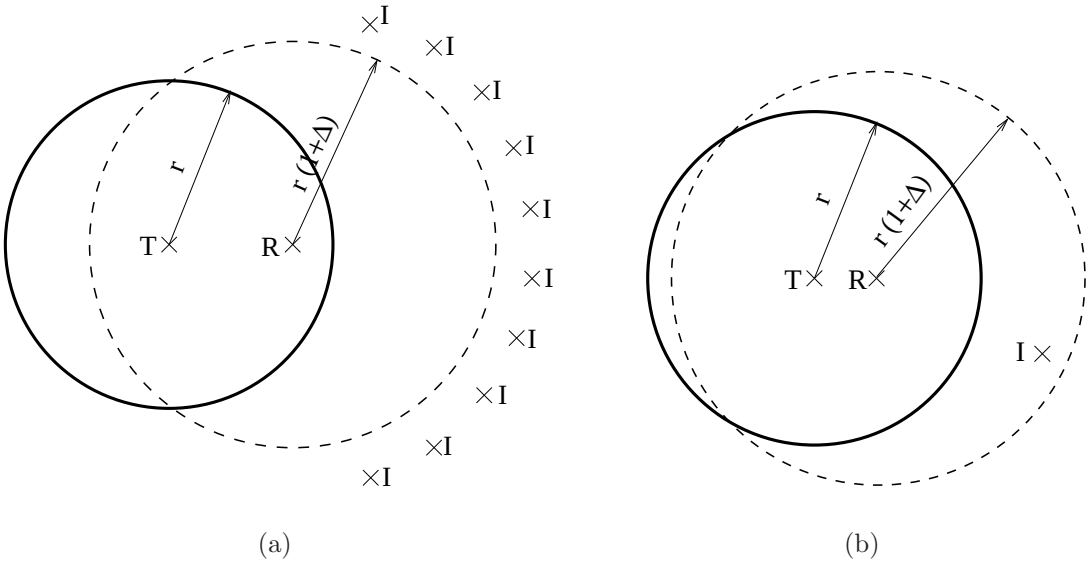

Figure 2.1. Shortcoming 1 of the disk model. T, R, and I denote transmitter, receiver, and interfering nodes, respectively. (a) Successful transmission. (b) Collision.

then the SIR is

$$\text{SIR} = \frac{q^{-\alpha}}{10 \cdot (2q)^{-\alpha}} = \frac{2^{\alpha}}{10}, \tag{2.1}$$

assuming the number of interferers is 10, where α is the path loss exponent. In Fig. 2.1 (b), if $\overline{RI} = 5\overline{TR} = 5q$, for example, the SIR is

$$\text{SIR} = \frac{q^{-\alpha}}{(5q)^{-\alpha}} = 5^{\alpha}. \tag{2.2}$$

Obviously, the SIR of Fig. 2.1(b) is much greater than that of Fig. 2.1 (a), about 25dB for $\alpha = 4$.

Another shortcoming can be explained by Fig. 2.2. The nodes use transmit power P_1 in Fig. 2.2 (a) and P_2 in Fig. 2.2 (b). $P_1 < P_2$ so that $r_1 < r_2$. The interferer is inside the dashed circle in Fig. 2.2 (a) but outside the dashed circle in Fig. 2.2 (b). So the transmission is successful in Fig. 2.2 (a) but fails in Fig. 2.2

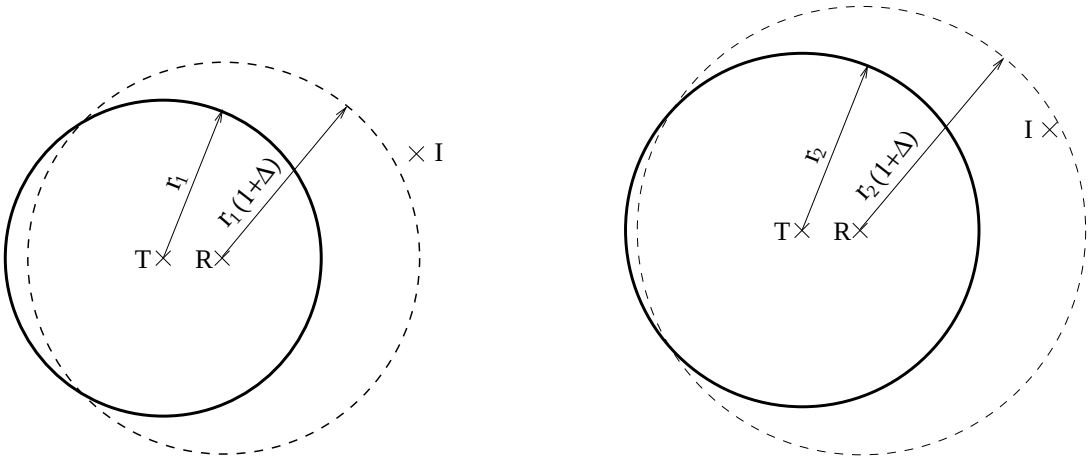

Figure 2.2. Shortcoming 2 of disk model. T, R, and I denote transmitter, receiver, and interference nodes, separately. $r_1 < r_2$. (a) Successful transmission. (b) Collision.

(b) although the SIR is the same for the two cases. The weakness of this disk model is that it does not take into account the difference of the distances if both transmitters are inside the solid circle.

The physical model [15, 16] is a threshold model (without fading). Let the desired source node transmit at power P_0 over a distance d_0 and have k interferers transmitting at power P_i, $i = 1, ..., k$ over distance d_i, $i = 1, ..., k$ respectively. The desired transmission is successful if

$$\frac{P_0 d_0^{-\alpha}}{N_0 + \sum_{i=1}^{k} P_i d_i^{-\alpha}} \geq \Theta. \tag{2.3}$$

where Θ is the SINR threshold and N_0 is the noise variance. Note that for $\alpha \to \infty$, this reduces to a disk model with transmission radius 1, irrespective of P_i. Without interference, the physical model assumes the reception probability is one if the

transmitter-receiver distance is smaller than a threshold and zero if it is greater than the threshold, like the disk model. In reality, even with long packets (and accordingly, long channel codes), the packet reception probability cannot reach 1. For example, with a one-hop link reception probability of 0.95, over a 10-hop connection, the end-to-end reliability is only 0.60 due to error propagation. However, by the above models, the end-to-end reliability is 1 or 0. Further, both models neglect the random fading effect of the radio channel.

2.2 The Rayleigh Fading Link Model

We assume a narrowband multipath wireless channel with a coherence time equal to or longer than the packet transmission time. The channel can then be modeled as a flat block Rayleigh fading channel [56] with an AWGN process z. Therefore the received signal at time k is $y_k = a_k\, x_k + z_k$, where a_k is the path loss multiplied by the fading coefficient. The variance of the noise process is denoted by N_0.

The transmission from node i to node j is successful if the SINR γ is above a certain threshold Θ that is determined by the communication hardware and the modulation and coding schemes (normally $2 \leq \Theta \leq 100$ or $3\text{dB} \leq \Theta \leq 20\text{dB}$) [11].

With the assumptions above, the SINR γ is given by

$$\gamma = \frac{Q}{N_0 + I}\,. \tag{2.4}$$

Q is the received power, which is exponentially distributed with mean $\bar{Q}$. Over a transmission of distance $d = \|x_i - x_j\|_2$ with an attenuation d^α, we have $\bar{Q} =$

$P_0 d^{-\alpha}$, where P_0 is the transmit power[1], and the path loss exponent is $2 \leqslant \alpha \leqslant 5$. I denotes the interference power affecting the transmission, *i.e.*, the sum of the received power from all the undesired transmitters.

Our analysis is based on the following Theorem [21]:

Theorem 1 *In a Rayleigh fading network, the mean reception probability* $\mathbb{P}[\gamma \geqslant \Theta]$ *can be factorized into the reception probability of a zero-noise network and the reception probability of a zero-interference network.*

Proof: Let Q_0 denote the received power from the desired source and Q_i, $i = 1, \ldots, k$, the received power from k interferers. All the received powers are exponentially distributed, *i.e.*, $p_{Q_i}(q_i) = 1/\bar{Q}_i \, e^{-q_i/\bar{Q}_i}$, where $\bar{Q}_i$ denotes the average received power $\bar{Q}_i = P_i d_i^{-\alpha}$. The probability of correct reception is[2]:

$$\begin{aligned} p_r &= \mathbb{E}_I\Big[\mathbb{P}[Q_0 \geqslant \Theta(I+N_0)]|I\Big] = \mathbb{E}_I\Big[\exp\Big(-\frac{\Theta(I+N_0)}{\bar{Q}_0}\Big)\Big] \\ &= \int_0^\infty \cdots \int_0^\infty \exp\Big(-\frac{\Theta(\sum_{i=1}^k q_i + N_0)}{\bar{Q}_0}\Big) \cdot \prod_{i=1}^k p_{Q_i}(q_i)\, \mathrm{d}q_i \\ &= \underbrace{\exp\Big(-\frac{\Theta N_0}{P_0 d_0^{-\alpha}}\Big)}_{p_r^N} \cdot \underbrace{\prod_{i=1}^k \frac{1}{1+\Theta\frac{P_i}{P_0}\big(\frac{d_0}{d_i}\big)^\alpha}}_{p_r^I} \cdot \end{aligned} \tag{2.5}$$

p_r^N is the probability that the SNR $\gamma^N := Q_0/N_0$ is above the threshold Θ, *i.e.*, the reception probability in a zero-interference network as it depends only on the noise. The second factor p_r^I is the reception probability in a zero-noise network. □

[1]This equation does not hold for very small distances. So, a more accurate model would be $\bar{Q} = P_0' \cdot (d/d_0)^{-\alpha}$, valid for $d \geqslant d_0$, with P_0' as the average value at the reference point d_0, which should be in the far field of the transmit antenna. At 916MHz, for example, the near field may extend up to 3-4ft (several wavelengths)[22].

[2]A similar calculation has been carried out in the Appendix of [82] for a network with spreading gain and equal transmit powers for all nodes.

This allows an independent analysis of the effect caused by noise and the effect caused by interference. For each interferer, there is one factor in the product. It assumes all the distances are known, and it is known precisely who is transmitting. Theorem 1 will be extended in Chapter 7 to the case of slotted ALOHA where the transmitting nodes are selected randomly. Note that this is still a threshold model, but it includes Rayleigh fading.

CHAPTER 3

PERFORMANCE ANALYSIS OF ONE-DIMENSIONAL NETWORKS

We study the performance of line networks — regular line networks (equidistant nodes) and random line networks (uniformly randomly distributed nodes) — since optimum routes in higher-dimensional networks approximately follow a straight line. Fig. 3.1 displays a 5-node regular line network and a typical random line network. It is assumed that the left end node is the source node and the right end node is the destination node. For every transmitting node, its next-hop receiver is its right neighbor. Both line networks have density one, *i.e.,* the expected number of nodes in an interval of length one is one. From Theorem 1, we know that the reception probability is the product of the reception probability in a zero-interference network p_r^N and the reception probability in a zero-interference network p_r^I. We fix p_r^N by fixing the transmit power P_0 and consider networks where the reception is only corrupted by interference, not by noise (interference analysis). The throughput is defined as the expected number of successful packet transmissions of a given node per timeslot. The end-to-end throughput over a multihop connection is the minimum of the link throughput values.

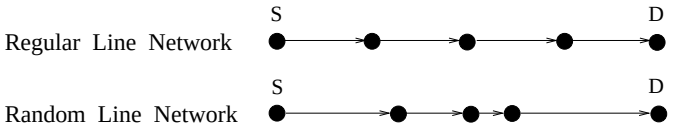

Figure 3.1. A 5-node regular line network and a 5-node random line network.

3.1 Regular Line Networks

3.1.1 Simple MAC scheme

First, we study a very simple MAC scheme, with the aim of finding a lower performance bound for more elaborate schemes. For the network, it is assumed that nodes are transmitting packets independently in every timeslot with transmit probability p at equal transmit power level. The same MAC scheme was considered in [27] and [65]. It is called slotted ALOHA MAC in [65]. The packets are of equal length and fit into one timeslot. In Fig.3.2 (a), the simulation results for various path loss exponents α are plotted.

3.1.2 Optimum scheduler

Exploiting spatial reuse, we can devise a scheduling scheme that maximizes the throughput. Assume that in a regular line network, every q-th link is used in a given timeslot for unidirectional traffic. Therefore, q phases are needed for all the nodes to make one transmission attempt. In Fig. 3.2 (b), the throughput as a function of q is plotted. Optimum scheduling is achieved at $q_{opt} = 8, 5, 4, 3$ and the throughput ratio between the simple MAC scheme and the optimum one is between $[0.5, 0.6]$ for $\alpha = 2, 3, 4, 5$. Since $p_{max} \approx 1/q_{opt}$ for all α, where p_{max} is the throughput-maximizing transmit probability of the simple MAC scheme, the

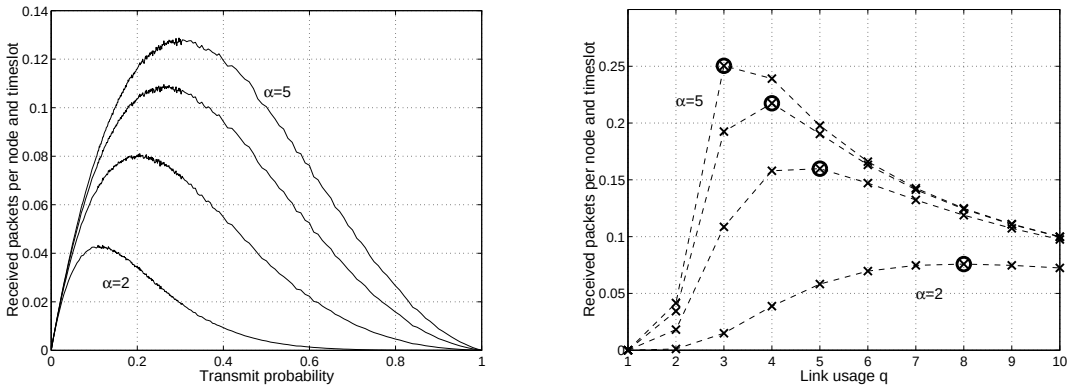

(a) (b)

Figure 3.2. (a). Simultion results of received packets per node and timeslot for $\Theta = 10$ and $\alpha = 2$, 3, 4, 5 for a large regular line network based on the simple MAC scheme. (b). Received packets per node and timeslot for $\Theta = 10$ and $\alpha = 2$, 3, 4, 5 for a large regular line network where every q-th link is used unidirectionally. The points marked with $\otimes$ are the throughput-optimum points.

link utilizations[1] (and thus the energy consumption) are almost identical for the two MAC schemes. The throughput gain from the optimum scheduler is about 100%. The comparison is shown in Table 3.1.

3.2 Random Line Networks

For regular line networks with equidistant nodes, a fixed p_r^N means that nodes transmit at equal transmit power level. However, for random line networks where nodes are uniformly randomly placed in a line, a fixed p_r^N requires transmit power adaptation. Different transmit power levels will cause some nodes to die soon, which will decrease the lifetime[2] of the whole network; on the other hand, the

[1]The fraction of timeslots that a node is transmitting.

[2]We assume the lifetime of the line network is the time until the first node dies. This definition is a consequence of the strict nearest-neighbor routing policy.

TABLE 3.1

COMPARISON OF SIMPLE MAC SCHEME WITH OPTIMUM SCHEDULER FOR A REGULAR NETWORK.

	$\alpha = 2$	$\alpha = 3$	$\alpha = 4$	$\alpha = 5$
p_{max} of simple MAC	0.1200	0.2060	0.2600	0.2970
$1/q_{opt}$ of optimum scheduler	0.1250	0.2000	0.2500	0.3333
maximum throughput of simple MAC	0.0433	0.0811	0.1096	0.1288
maximum throughput of optimum scheduler	0.0758	0.1599	0.2174	0.2504

equal transmit power strategy is energy balanced, but it results in different p_r^N. Therefore, we consider and compare two strategies — adaptive transmit power and equal transmit power.

3.2.1 Adaptive transmit power

From Chapter 2, we know that for a zero-interference network, the link reception probability over a link of distance d_0 is given by $p_r^N = e^{-\frac{\Theta N_0}{P_0 d_0^{-\alpha}}}$. Solving for P_0, we find the necessary transmit power to achieve a link reliability p_r^N to be

$$P_0 = \frac{d_0^\alpha \Theta N_0}{-\ln p_r^N}. \tag{3.1}$$

If the link reception probability p_r^N is fixed, we can adapt the transmit power based on (3.1).

3.2.1.1 Simple MAC scheme

Throughput. Again, we consider the simple MAC scheme for random line networks. We plot the average throughput for a large random line network in Fig. 3.3(a). In comparison with the regular line network in Fig. 3.2 (a), we can

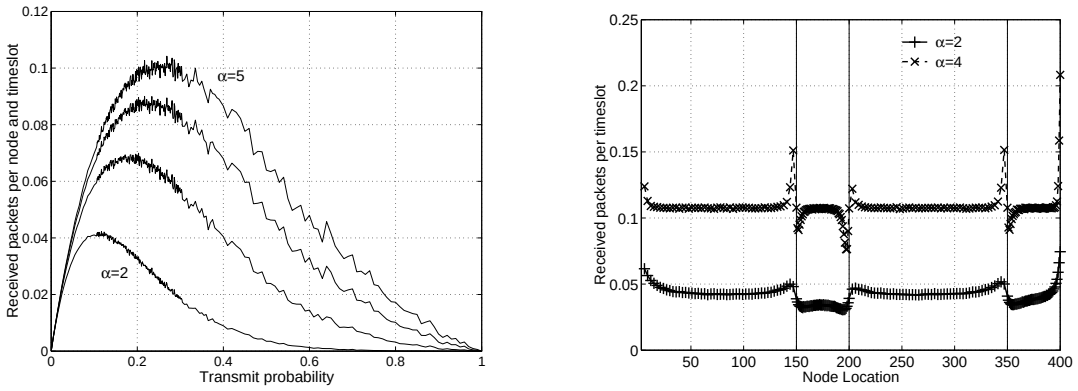

(a) (b)

Figure 3.3. (a) SImulation results of received packets per node and timeslot for simple MAC scheme of unidirectional traffic in a large random line network. (b) Throughput distribution of a network where nodes of 4 groups with 50 nodes each are placed in a line with distance 3 for the first group, distance 1 for the second group, distance 3 for the third group, and distance 1 for the fourth group.

see that the regular line network has a higher throughput than the random line network and that the difference is higher for larger α. To better understand how the distance interval distribution affects the throughput, we investigate the throughput distribution for a network with abruptly changing node density and plot the throughput distribution over the nodes for $\alpha = 2$ and $\alpha = 4$ in Fig. 3.3 (b), where 50 nodes are placed with distance 3 for the first group, 50 nodes with distance 1 for the second group, 50 nodes with distance 3 for the third group, and 50 nodes with distance 1 for the fourth group. Nodes in the dense area and close to the junction have lower throughput due to nearby interfering nodes with high transmit power.

Energy consumption. For a random line network of density one with n nodes and transmit probability p, the total expected energy consumption is

$$E_{tot} = np\frac{\Theta N_0}{-\ln p_r^N}\mathbb{E}[d_r^\alpha]$$

where d_r are the internode distances of the random line network. When normalized by $E_0 = \frac{\Theta N_0}{-\ln p_r^N}$, we get[3]

$$E_{tot}^{rm} = np\mathbb{E}[d_r^\alpha]. \tag{3.2}$$

d_r is a random variable with mean $\bar{d_r} = 1$ and exponential distribution

$$f_{d_r}(x) = \frac{1}{\bar{d_r}}e^{-x/\bar{d_r}}u(x) = e^{-x}u(x). \tag{3.3}$$

This holds when nodes form a (homogeneous) Poisson point process on a line. Therefore, $\mathbb{E}[d_r^\alpha] = \Gamma(1+\alpha) = 2, 6, 24, 120$ for $\alpha = 2, 3, 4, 5$. For an n-node regular line network with transmit probability p, the total expected energy consumption is $E_{tot}^{ed} = np\mathbb{E}[d_e^\alpha]$ normalized by $E_0 = \frac{\Theta N_0}{-\ln p_r^N}$, where p_r^N is the same as that of the random network and $d_e = 1$ is the internode distance of the equidistant line network. So $\mathbb{E}[d_e^\alpha] = 1$ for all α. For a regular line network, at $p = 0.25$ and $n = 100$, the total normalized energy consumption is $E_{tot}^{ed} = 25$ for all α. For random line networks, the total normalized energy consumptions are $E_{tot}^{rm} = 50, 150, 600, 3000$ for $\alpha = 2, 3, 4, 5$. Our simulation running on 3000 node distributions and 1000 timeslots for each distribution shows the total energy consumptions are 44.4, 160.4, 494.2, 2812.0 for $\alpha = 2, 3, 4, 5$. The simulation results are within $\pm 10\%$ of the total expected energy consumption, which confirms the theoretical results.

[3]It is assumed that E_0 expresses the energy required to send a packet at a power level $\frac{\Theta N_0}{-\ln p_r^N}$.

3.2.1.2 Throughput balancing strategy

Finding the globally optimum scheduling scheme for random networks is an NP-hard problem [52]. Here we propose a simple and scalable near-optimum scheduling scheme that takes nearest interferers into account and balances the throughput of each node to achieve higher end-to-end throughput[4].

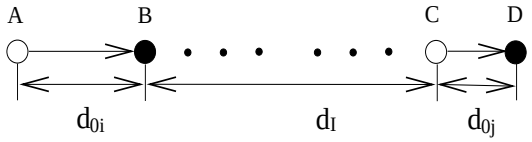

Figure 3.4. Distances in a random line network. The filled circles denote the receivers.

As shown in Fig. 3.4, if node A is transmitting in this timeslot, node C can be the nearest right neighbor that transmits if the reception probability of node B and node D is higher than some threshold. We know when only node A and node C transmit in the same timeslot,

$$p_{rB}^{I} = \frac{1}{1+\Theta/\mathrm{SIR}_B} = \frac{1}{1+\Theta\frac{P_C d_I^{-\alpha}}{P_A d_{0i}^{-\alpha}}} = \frac{1}{1+\Theta\frac{d_{0j}^{\alpha} d_I^{-\alpha}}{d_{0i}^{\alpha} d_{0i}^{-\alpha}}} = \frac{1}{1+\Theta\left(\frac{d_{0j}}{d_I}\right)^{\alpha}}. \tag{3.4}$$

and

$$p_{rD}^{I} = \frac{1}{1+\Theta\left(\frac{d_{0i}}{d_{0i}+d_I+d_{0j}}\right)^{\alpha}}. \tag{3.5}$$

[4]When this scheduler is applied to regular line networks, the optimum result of Fig. 3.2 is obtained. So we denote this scheduler as near-optimum scheduler.

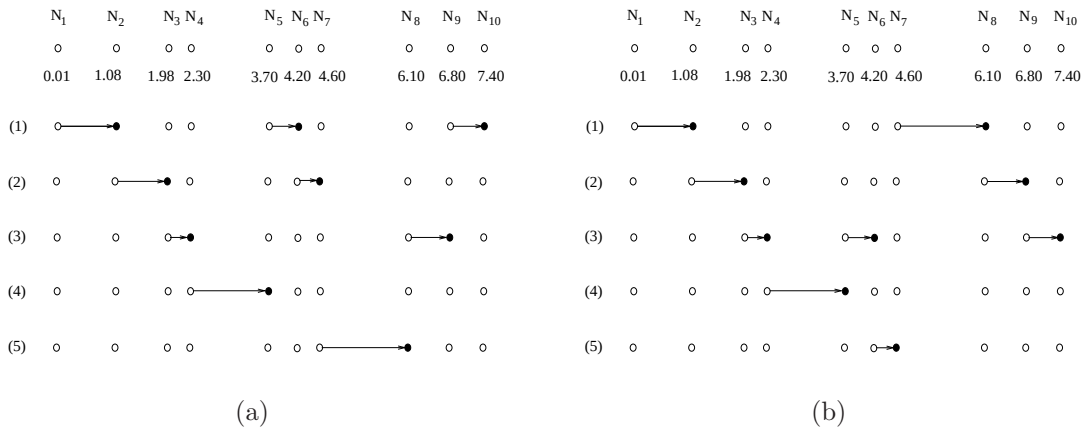

Figure 3.5. (a) The five phases of the scheduler of throughput balancing strategy with power adaptation of a random network. (b) The five phases of the scheduler of the energy balancing strategy with equal transmit power of the same random network.

If both p_{rB}^I and p_{rD}^I are higher than some threshold, then $(d_{0i} + d_I + d_{0j})/d_{0i} > \beta$ and $d_{0j}/d_I < 1/\beta$, where β is a function of the path loss exponent α. Therefore, for the nearest right node C of node A, if the distances satisfy the conditions

$$\begin{cases} (d_{0i} + d_I + d_{0j})/d_{0i} > \beta \\ d_{0j}/d_I < 1/\beta, \end{cases} \tag{3.6}$$

node C can transmit in the same timeslot as node A. Otherwise, the next nearest node that satisfies the above two conditions will be selected.

Fig. 3.5(a) exhibits the five phases of the near-optimum scheduler for a ten-node line network, where the ten nodes N_1, N_2, ..., N_{10} are uniformly randomly located. N_1 is the source, and N_{10} is the destination. The coordinates of the ten nodes are 0.01, 1.08, 1.98, 2.30, 3.70, 4.20, 4.60, 6.10, 6.80 and 7.40. Figs. 3.6(a), (b) compare the throughput distributions over the 10-node network and a 100-

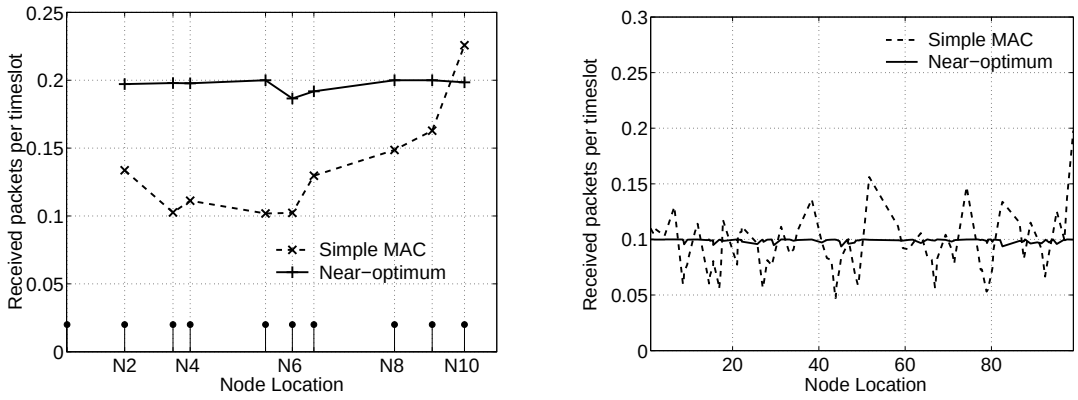

(a) (b)

Figure 3.6. Comparison of the throughput distribution for the simple MAC scheme and the near-optimum scheduler for $\alpha = 4$. (a) 10-node network. The short vertical lines with the circles on top indicate the locations of the nodes. Note that N_1 does not receive any packet. (b) 100-node network.

node network of the simple MAC scheme and the near-optimum scheduler for $\alpha = 4$. For the 100-node network, the end-to-end throughput is 0.0936 for the near-optimum scheduler and 0.0473 for the simple MAC scheme. For the simple MAC scheme, the average throughput is 0.0898 which is about twice the end-to-end throughput. Extensive simulation results confirm that the near-optimum scheduler achieves about twice the end-to-end throughput of the simple MAC scheme.

3.2.2 Equal transmit power without retransmissions

With power adaptation, the transmit power of each node of the previous analysis satisfies $P_0 \propto d_0^{\alpha}$, where d_0 is the distance between the transmitting node and the next-hop receiver. Therefore, the nodes with bigger d_0 suffer from higher energy consumption than those with shorter d_0. The unbalance of the energy

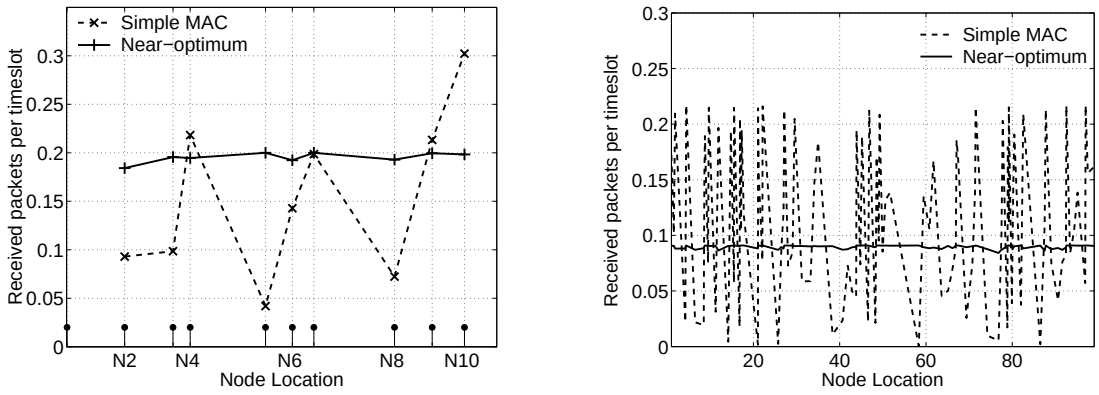

(a) (b)

Figure 3.7. Comparison of the throughput distribution for the simple MAC scheme and the energy balancing strategy for $\alpha = 4$ for random line networks. (a) 10-node network, (b) 100-node network.

consumption will cause some nodes to die fairly soon and decrease the lifetime of the whole network. To avoid this problem, we study an energy balancing strategy in which every node transmits at equal transmit power level. Again, spatial reuse is optimized for a high end-to-end throughput.

Energy balancing strategy. Similar to the scheduler of the throughput-balancing strategy, we get the conditions of the scheduler for the energy balancing strategy to be

$$\begin{cases} (d_{0i} + d_I + d_{0j})/d_{0j} > \delta \\ d_{0i}/d_I < 1/\delta. \end{cases} \tag{3.7}$$

Again, δ is a function of the path loss exponent α.

Fig. 3.5 (b) displays the five phases of the energy balancing strategy for the same ten-node random line network as Fig. 3.5 (a). Figs. 3.7 (a) and (b) present the throughput distribution comparison of the simple MAC scheme and the en-

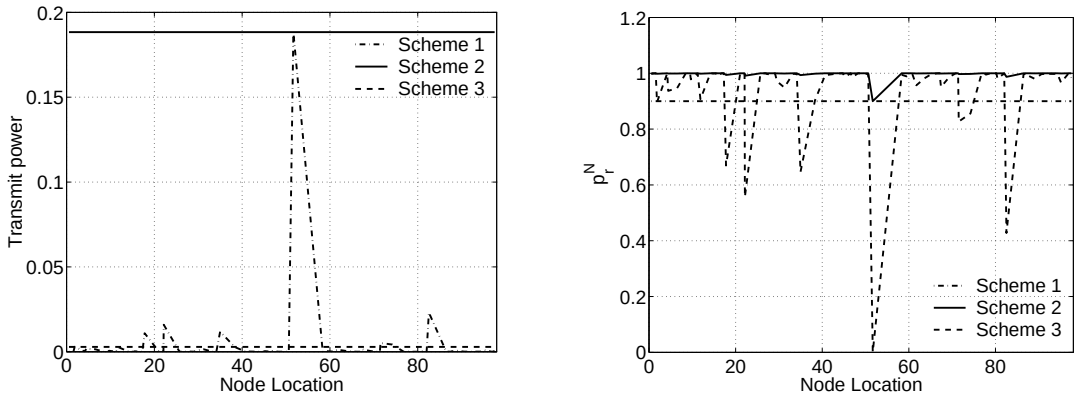

(a) (b)

Figure 3.8. Comparison of the transmit power and p_r^N for scheme 1, 2 and 3 for a random line network with 100 nodes for $\alpha = 4$. (a) Transmit power. (b) p_r^N.

ergy balancing strategy for random line networks with 10 nodes and 100 nodes. It is shown that the average throughput and end-to-end throughput of the two optimized schedulers with adaptive power and equal power are almost the same for zero-noise networks. However, for the simple MAC scheme, the throughput distribution of the strategy with equal transmit power is much more uneven than that of the strategy with adaptive transmit power, as shown in Figs. 3.6 and 3.7.

All the above analyses are based solely on interference. Considering both the noise and interference, the product of p_r^N (noise analysis) and p_r^I (interference analysis) gives the practical reception probability p_r. Although for the two optimized schedulers, the throughput performance from the interference analysis is similar, their p_r^N (thus the energy consumption) could be quite different, which results in different p_r. We investigate this problem with three schemes. Scheme 1 uses adaptive transmit power such that p_r^N is fixed at 0.9. Scheme 2 uses equal transmit power at the level of the *maximum* transmit power in scheme 1, which

means the minimum p_r^N of scheme 2 is 0.9. Scheme 3 uses equal transmit power at the level of the *average* transmit power in scheme 1. Fig. 3.8 displays the transmit power distribution and p_r^N distribution for scheme 1, 2 and 3. It is shown that scheme 2 consumes the highest total transmit energy although it has the same lifetime as scheme 1. Scheme 3 has the same energy consumption as scheme 1, but its minimum p_r^N is only 0.0001. A detailed probabilistic analysis shows that very small p_r^N always exist with a certain probability for scheme 3 (See Section 6.3). In summary, for scheme 1, 2 and 3, the minimum p_r^N are 0.9, 0.9, and 0.0001 and scheme 1 and 3 have the same total energy consumption which is smaller than that of scheme 2. Therefore, we conclude that the strategy with power control (scheme 1) outperforms the strategy with equal transmit power when considering both the total energy consumption and minimum p_r^N.

3.3 Conclusions

In this chapter, we investigated the throughput and energy consumption of line networks. For regular line networks, a simple random MAC scheme and optimum scheduler are studied. For random line networks, in addition to the simple MAC scheme, two near-optimum schedulers — one with transmit power adaptation to adjust the transmit power according to the link distance, the other with equal transmit power — are presented. By simulation, we show that the equal transmit strategy either consumes very high energy or suffers from very low link reception probability. In Section 6.3, we will demonstrate analytically that low link reception probabilities are unavoidable at medium transmit power levels. Hence, power control is crucial to avoid links with very low reception probability.

CHAPTER 4

PERFORMANCE ANALYSIS OF REGULAR TWO-DIMENSIONAL NETWORKS

For certain multihop networks, in particular, for sensor networks, we expect that in typical scenarios, the nodes are stationary for most of the time after deployment. For example, in the applications of monitoring environmental conditions, chemical/biological detection, security in a shopping mall or parking lot, the nodes are fixed at certain positions for most of the time. Moreover, to guarantee high exposure of the events of interest [47], uniform coverage is beneficial, suggesting the use of regular node placement schemes. Finding the optimal placement of nodes for a good trade-off between energy consumption, throughput, and delay is an important and challenging problem. In this chapter, we investigate networks with regular topologies (square, triangle, hexagon) in which each node has the same number of nearest neighbors and the distance between all pairs of nearest neighbors is the same. In [12], such networks are called perfect networks. We call them square, triangle, and hexagon networks.

4.1 Noise Analysis

First, we study the performance of zero-interference networks, where only one node is transmitting at transmit power P_0 in every timeslot. For each connection,

the source and destination are uniformly randomly chosen. For the network, it is assumed that the network is large (in terms of node numbers). Based on this assumption, the distributions of the Euclidean distance r between the source and destination are identical for all three networks, and the direction ϕ is uniformly distributed. We employ nearest-neighbor and shortest-path routing, which routes the packet via nearest neighbors along the shortest path toward its destination.

4.1.1 Square networks

We first analyze square networks with $N = m \times m$ nodes and distance d_0 between all pairs of nearest nodes. The next-hop receiver of each packet is a neighbor of the transmitter. For the 4-neighbor case, the four nearest neighbors (top, bottom, left and right) constitute the set of next-hop receivers. Because the 4-neighborhood may be not the best case, we also consider additional neighborhoods – the 8-neighbor and 12-neighbor cases. For the 8-neighbor case, the 4 diagonal neighbors with distance $\sqrt{2}d_0$ to the transmitter are included. For the 12-neighbor case, the nodes with distance $2d_0$ to the transmitter are added to the 8-neighbor case. We denote the hops of distance d_0, $\sqrt{2}d_0$, and $2d_0$ as unit, diagonal, and 2-unit hops, respectively.

In most cases, the diagonal hops are preferred in terms of hop numbers. We can measure the optimality of a path by the ratio between the Euclidean distance and the travelled distance. As in [20], we define the path efficiency as

$$\eta = \frac{\textit{Euclidean distance}}{\textit{travelled distance}}, \qquad 0 < \eta \leq 1. \tag{4.1}$$

In Fig. 4.1(a), O is the source and A is the destination, ϕ is the angle between $\overrightarrow{OA}$ and the horizontal axis. For the 4-neighbor case, by using nearest-neighbor

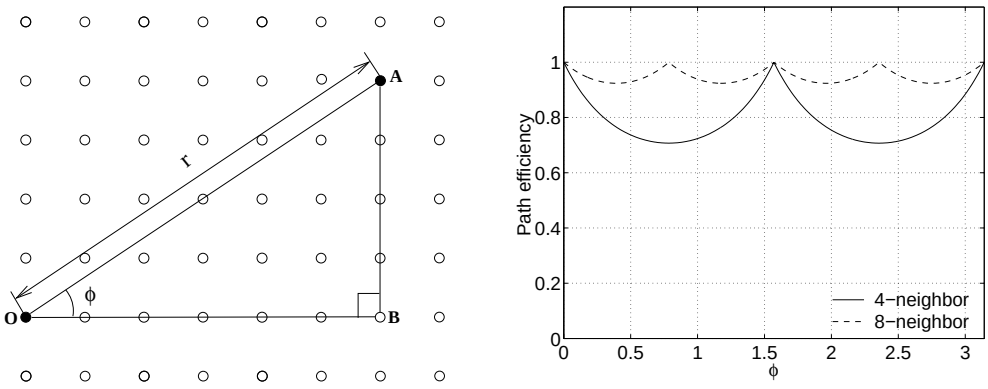

(a) (b)

Figure 4.1. (a) Path efficiency of square networks and (b) relationship between path efficiency and ϕ for the 4-neighbor case (solid) and 8-neighbor case (dashed).

and shortest-path routing, the Euclidean distance r is $|OA|$, and the travelled distance d_T is $|OB| + |BA|$. We have

$$\eta(\phi) = \frac{r}{d_T} = \frac{r}{|r\cos\phi| + |r\sin\phi|} = \frac{1}{|\cos\phi| + |\sin\phi|}. \tag{4.2}$$

If we move the destination along the line OA, the path efficiency will not change, so η is only a function of ϕ, and it is periodical with period $\pi/2$. Thus, although ϕ is a uniformly distributed random variable in $[0, 2\pi]$, we may restrict ϕ to be between 0 and $\pi/2$ in the following analysis. We can see that when $\phi = \pi/4$, $\eta_{min} = 1/\sqrt{2}$; when $\phi = 0$ or $\pi/2$, $\eta_{max} = 1$. The expected value of η is $\frac{2\sqrt{2}}{\pi}\arctan(\frac{\sqrt{2}}{2}) \approx 0.7935$. ϕ is uniformly distributed based on the previous assumptions.

For the 8-neighbor case, the travelled distance is $\sqrt{2}\ \min\{|OB|, |BA|\} +$

$\big||OB| - |BA|\big|$, so we find

$$\eta(\phi) = \frac{1}{\sqrt{2}\,\min\{\cos\phi,\ \sin\phi\} + |\cos\phi - \sin\phi|}. \tag{4.3}$$

For $\phi = \pi/8$ or $3\pi/8$, $\eta_{min} \approx 0.9239$; for $\phi = 0$ or $\pi/4$ or $\pi/2$, $\eta_{max} = 1$. The expected value of η is 0.9486. Fig. 4.1(b) displays the path efficiency as a function of ϕ between 0 and π. For the 12-neighbor case, the travelled distance is the same as that of the 8-neighbor case, so the path efficiency is the same. From Fig. 4.1(b), we can see that the introduction of diagonal neighbors increases the path efficiency. In the 8-neighbor case, the fraction of diagonal hops β depends on ϕ:

$$\beta(\phi) = \frac{\min\{\cos\phi,\ \sin\phi\}}{\min\{\cos\phi,\ \sin\phi\} + |\cos\phi - \sin\phi|}, \qquad 0 \le \phi \le \frac{\pi}{2}. \tag{4.4}$$

The mean of β is

$$\mathbb{E}[\beta] = \int_0^{\frac{\pi}{4}} \frac{\sin\phi}{\cos\phi}\frac{1}{\pi/2}\,d\phi + \int_{\frac{\pi}{4}}^{\frac{\pi}{2}} \frac{\cos\phi}{\sin\phi}\frac{1}{\pi/2}\,d\phi = \frac{2\ln 2}{\pi} \approx 0.4413. \tag{4.5}$$

Thus the expected distance covered by diagonal hops is about 53% of the total distance, which suggests diagonal hops and unit hops are almost equally important.

We assume that every packet has a given end-to-end reception probability P_{EE}, dictated by the application (or the transport) layer. From Chapter 2, we know the link reception probability over a link of distance d_0 is given by $P_L = e^{-\frac{\Theta N_0}{P_0 d_0^{-\alpha}}}$. Solving for P_0, we find the necessary transmit energy to achieve a link reliability P_L to be $E_L = \frac{d_0^{\alpha}\Theta N_0}{-\ln P_L}$. If there are h hops with equal distance d_0, the link reception

probability P_L is $P_{EE}^{1/h}$. Then the transmit energy at each hop is

$$E_L = h\frac{d_0^\alpha \Theta N_0}{-\ln P_{EE}}. \tag{4.6}$$

In the following, we investigate the total energy consumption of the 4-, 8- and 12-neighbor cases.

4.1.1.1 The 4-neighbor case

Using nearest neighbor and shortest path routing, the travelled distance is $d_T = r\cos\phi + r\sin\phi$, where r is the Euclidean distance. The number of hops is $h = d_T/d_0$. The total energy consumption of this route is

$$E_{tot}^4(\phi) = hE_L = h^2\frac{d_0^\alpha \Theta N_0}{-\ln P_{EE}} = \frac{r^2}{d_0^2}(\cos\phi + \sin\phi)^2\frac{d_0^\alpha \Theta N_0}{-\ln P_{EE}}. \tag{4.7}$$

Let $E_0 := \frac{d_0^\alpha \Theta N_0}{-\ln P_{EE}}$. Considering the uniform distribution of ϕ, we can find the expected total energy consumption in units of E_0 as

$$\frac{\overline{E}_{tot}^4}{E_0} = \frac{r^2}{d_0^2}\int_0^{\frac{\pi}{2}}(\cos\phi + \sin\phi)^2 f_\Phi(\phi)d\phi = \frac{r^2}{d_0^2}\left(1 + \frac{2}{\pi}\right) \approx 1.6366\frac{r^2}{d_0^2}. \tag{4.8}$$

Fig. 4.2(a) displays the total energy consumption in units of $E_0\frac{r^2}{{d_0}^2}$ for the 4-neighbor case. Note that the energy consumption increases with the hop number squared.

4.1.1.2 The 8-neighbor case

Strategies A and B. In the 4-neighbor case, a fixed transmit power level results in a fixed link reception probability since there exist only unit hops. However, in the 8-neighbor case, there are both diagonal hops and unit hops. If each link has the same reception probability, the nodes transmitting over diagonal hops need

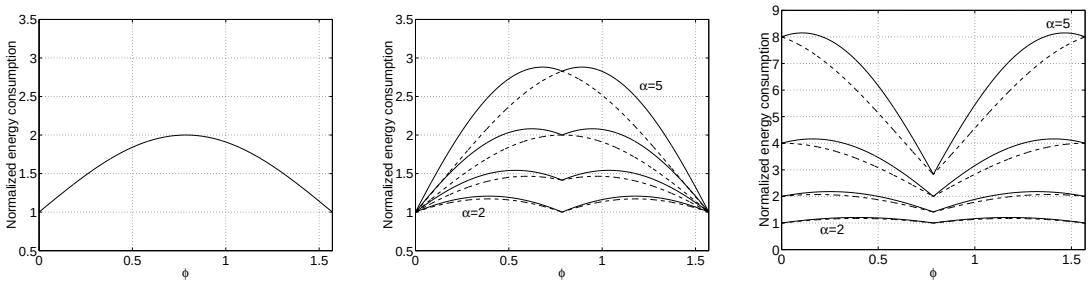

(a) 4-neighbor scheme (b) 8-neighbor scheme (c) 12-neighbor scheme

Figure 4.2. Normalized energy consumption for the 4-, 8- and 12-neighbor case. For (b),(c), the solid line is the energy consumption of strategies A and B, and the dashed line is the energy consumption of the minimum energy strategy.

more power; on the other hand, if each node transmits at the same power level, the diagonal hops suffer from a smaller reception probability. How to distribute the link reception probability to minimize the total energy consumption for a fixed P_{EE}? In strategy A, we assume that all the nodes transmit at a fixed link reception probability P_L. In strategy B, we assume all the nodes transmit at the same power level. Since neither A nor B might be optimal, we will also find the minimum energy strategy.

For each connection, let h_U and h_D denote the total number of unit hops and diagonal hops, respectively, and let P_{LU} denote the link reception probability over a unit hop, and P_{LD} the link reception probability over a diagonal hop; E_{LU} is the energy consumed at each node in a unit hop, and E_{LD} is the energy consumed at each node in a diagonal hop. For the 8-neighbor case, using nearest-neighbor and shortest-path routing, we have

$$h_U = \frac{r}{d_0}|\cos\phi - \sin\phi|, \quad h_D = \frac{r}{d_0}\min\{\cos\phi,\ \sin\phi\}, \quad h = h_U + h_D. \tag{4.9}$$

For strategy A, $P^A_{LU} = P^A_{LD} = P_L$,

$$E^A_{LU} = \frac{d_0^\alpha \Theta N_0}{-\ln P_L} = h\frac{d_0^\alpha \Theta N_0}{-\ln P_{EE}} = (h_U + h_D)E_0.$$
$$E^A_{LD} = \frac{(\sqrt{2}d_0)^\alpha \Theta N_0}{-\ln P_L} = 2^{\alpha/2}h\frac{d_0^\alpha \Theta N_0}{-\ln P_{EE}} = 2^{\alpha/2}(h_U + h_D)E_0. \tag{4.10}$$

For strategy B, $E^B_{LU} = E^B_{LD} = E_L$,

$$P^B_{LU} = e^{-\frac{d_0^\alpha \Theta N_0}{E_{LU}}}, \quad P^B_{LD} = e^{-\frac{(\sqrt{2}d_0)^\alpha \Theta N_0}{E_{LD}}} = (P^B_{LD})^{2^{\alpha/2}}.$$
$$P_{EE} = (P^B_{LU})^{h_U}(P^B_{LD})^{h_D} = (P^B_{LU})^{h_U + 2^{\alpha/2}h_D}, \tag{4.11}$$

from which we can find

$$P^B_{LU} = P_{EE}^{\frac{1}{h_U + 2^{\alpha/2}h_D}}, \quad P^B_{LD} = P_{EE}^{\frac{2^{\alpha/2}}{h_U + 2^{\alpha/2}h_D}}.$$
$$E^B_{LU} = \frac{d_0^\alpha \Theta N_0}{-\ln P_{LU}} = (h_U + 2^{\alpha/2}h_D)E_0. \tag{4.12}$$

Table 1 lists the expressions of both strategies for the 8-neighbor case.

In total, we have

$$E^{8A}_{tot} = h_U E_{LU} + h_D E_{LD} = (h_U + 2^{\alpha/2}h_D)(h_U + h_D)E_0,$$
$$E^{8B}_{tot} = (h_U + h_D)E_L = (h_U + 2^{\alpha/2}h_D)(h_U + h_D)E_0, \tag{4.13}$$

which shows that the total energy consumptions for the two strategies are equal. Strategy A may be preferred because every node in strategy A has the same lifetime since they transmit at the same power level. Substituting h_U and h_D into the above equation, we plot the total energy consumption in units of $E_0\frac{r^2}{{d_0}^2}$ of strategy A, B in Fig. 4.2(b) by solid lines. The expected total energy consumption

TABLE 4.1

PER-HOP ENERGY CONSUMPTION AND RECEPTION PROBABILITIES FOR STRATEGIES A AND B OF 8-NEIGHBOR CASE.

	Strategy A	Strategy B
E_{LU}	$(h_U + h_D)E_0$	$(h_U + 2^{\alpha/2}h_D)E_0$
E_{LD}	$2^{\alpha/2}(h_U + h_D)E_0$	$(h_U + 2^{\alpha/2}h_D)E_0$
P_{LU}	$P_{EE}{}^{\frac{1}{h_U+h_D}}$	$P_{EE}{}^{\frac{1}{h_U+2^{\alpha/2}h_D}}$
P_{LD}	$P_{EE}{}^{\frac{1}{h_U+h_D}}$	$P_{EE}{}^{\frac{2^{\alpha/2}}{h_U+2^{\alpha/2}h_D}}$

in units of $E_0\frac{r^2}{{d_0}^2}$ is $(\frac{1}{2} + \frac{2^{\alpha/2}}{\pi})$. For $\alpha = 2, 3, 4, 5$, this yields $\overline{E}_{tot}^{8A}/(E_0 r^2/{d_0}^2) = \overline{E}_{tot}^{8B}/(E_0 r^2/{d_0}^2) = 1.1366, 1.4003, 1.7732, 2.3006$.

Minimum energy strategy. With $\tau := \frac{E_{LD}}{E_{LU}}$, the total energy consumption is

$$\begin{aligned} E_{tot}(\phi) &= (h_U + \tau h_D)(h_U + \frac{2^{\alpha/2}}{\tau}h_D)E_0 \\ &= (|\cos\phi - \sin\phi| + \tau \min\{\cos\phi, \sin\phi\}) \qquad (4.14) \\ &\times \left(|\cos\phi - \sin\phi| + \frac{2^{\alpha/2}}{\tau}\min\{\cos\phi,\ \sin\phi\}\right) E_0\frac{r^2}{{d_0}^2}. \qquad (4.15) \end{aligned}$$

The optimal τ corresponding to the minimum E_{tot} does not depend on ϕ. At $\tau^{opt} = 2^{\alpha/4}$,

$$E_{tot}^{8min} = \left(|\cos\phi - \sin\phi| + 2^{\alpha/4}\min\{\cos\phi, \sin\phi\}\right)^2 E_0\frac{r^2}{{d_0}^2}. \qquad (4.16)$$

The minimum total energy consumption with various α is plotted in Fig. 4.2(b) by dashed lines. The expected minimum total energy consumption in units of $E_0 \frac{r^2}{{d_0}^2}$ is $\frac{4\tau - 2\tau^2 - 2}{\pi} + \frac{\tau^2 - 2\tau + 2}{2}$ at $\tau = \tau^{opt}$. For $\alpha = 2, 3, 4, 5$, this yields $\overline{E}_{tot}^{min}/(E_0 r^2/{d_0}^2) =$ 1.1132, 1.3368, 1.6366, 2.0411. The gains compared to strategies A and B are 2.0588%, 4.5347%, 7.7036%, 11.2797%. From Fig. 4.2(b), we can see the total energy consumptions for strategies A, B and minimum energy consumption at $\phi = \pi/4$ are equal, because there are only diagonal hops in these routes. In this case, minimum energy means equal transmit power which also means equal link reception probability. Also we can find that for strategies A, B the maxima are near $\phi = \pi/4$ and they depend on α. In fact, ϕ_{max} is $\arctan(2^{\alpha/2} - 1)/2$ for strategies A,B when ϕ is between 0 and $\pi/4$. Because when ϕ is increased, the hop number decreases (more diagonal hops), but increased diagonal hops consume more energy than unit hops. The combination of the two effects moves the maxima slightly away from $\pi/4$.

4.1.1.3 The 12-neighbor case

For large networks, we can neglect the number of unit hops since it is either 0 or 1. Denote the number of 2-unit hops as h_{2U}. We have

$$h_{2U} = \frac{|\cos(\phi) - \sin(\phi)|}{2} \frac{r}{d_0}, \quad h_D = \min\{\cos(\phi), \sin(\phi)\} \frac{r}{d_0}. \tag{4.17}$$

As in the 8-neighbor case, we have the same total energy consumption for strategies A and B:

$$E_{tot}^{12A} = E_{tot}^{12B} = 2^{\alpha/2}(h_D + h_{2U})(h_D + 2^{\alpha/2} h_{2U}) E_0 \tag{4.18}$$

The expected total energy consumption in units of $E_0\frac{r^2}{{d_0}^2}$ is $(\frac{2\alpha}{2\pi}+\frac{2^{\alpha/2}}{4})$. For $\alpha = 2$, 3, 4, 5, this yields $\overline{E}_{tot}^{12A}/(E_0r^2/{d_0}^2) = \overline{E}_{tot}^{12B}/(E_0r^2/{d_0}^2) = 1.1366$, 1.9803, 3.5465, 6.5074. For the minimum energy strategy, we have $E_{tot}^{12}(\phi) = 2^{\alpha/2}(h_D+\tau h_{2U})(h_D+\frac{2^{\alpha/2}}{\tau}h_{2U})E_0$. Inserting h_{2U} and h_D of (18), we find at $\tau^{opt} = 2^{\alpha/4}$,

$$E_{tot}^{12min} = 2^{\alpha/2}\left(\min\{\cos(\phi),\sin(\phi)\}+\frac{|\cos(\phi)-\sin(\phi)|}{2}\tau\right)^2 E_0\frac{r^2}{{d_0}^2}. \qquad (4.19)$$

The expected minimum total energy consumption is $\tau^2(\frac{4\tau-2\tau^2-2}{2\pi}+\frac{\tau^2-2\tau+2}{4})$ at $\tau = \tau^{opt}$. For $\alpha = 2$, 3, 4, 5, this yields $\overline{E}_{tot}^{min}/(E_0r^2/{d_0}^2) = 1.1132$, 1.8905, 3.2732, 5.7730. The gains are 2.0588%, 4.5347%, 7.7062% and 11.2856%. The total energy consumption of strategies A, B and minimum energy strategy are plotted in Fig. 4.2(c) by solid and dashed lines separately. From Fig. 4.2(c), we can see that for strategies A,B the minima are at $\pi/4$ instead and that the maxima are close to 0 and π. Compared with Fig. 4.2(b), the 12-neighbor case can be viewed as an 8-neighbor case rotated by $\pi/4$ and scaled by $\sqrt{2}$.

An interesting observation is that $E_{tot}^{8min}(\phi) = E_{tot}^{4}(\phi)$ for $\alpha = 4$ and $E_{tot}^{8}(\phi) = E_{tot}^{12}(\phi)$ for $\alpha = 2$ for strategies A,B and the minimum energy strategy. We can explain it in the following way: Between the 4-neighbor case and the 8-neighbor case (minimum energy strategy), the only difference is that one diagonal hop replaces two unit hops. Let the reception probability over one diagonal hop be the same as the one over two unit hops. The energy consumption for one diagonal hop is $\frac{(\sqrt{2}d_0)^\alpha\Theta N_0}{-\ln P_L} = 2^{\alpha/2}E_0$ and the total energy over two unit hops is $\frac{d_0^\alpha\Theta N_0}{-\ln P_L^{1/2}} = 2E_0$. For $\alpha < 4$, the first expression is smaller, for $\alpha = 4$ they are equal, and for $\alpha > 4$, the first one is greater. Similarly we can find when $\alpha = 2$, the energy consumption over one 2-unit hop is equal to that over two unit hops[1].

[1]In fact, for $\alpha = 2$, the energy consumption in a line network is completely independent of

From the above analysis, we see that introducing longer hops results in higher energy consumption and less delay. To resolve this, we need to take into account the end-to-end delay. The hop numbers for each case are

$$
\begin{aligned}
h^4 &= \frac{r}{d_0}(\cos\phi + \sin\phi), \\
h^8 &= \frac{r}{d_0}(\min\{\cos\phi,\ \sin\phi\} + |\cos\phi - \sin\phi|), \\
h^{12} &= \frac{r}{d_0}\left(\min\{\cos\phi,\ \sin\phi\} + \frac{|\cos\phi - \sin\phi|}{2}\right).
\end{aligned} \tag{4.20}
$$

Averaging over ϕ, the expected hop numbers $\overline{h}$ for fixed r are listed in Table 4.2, for $\alpha = 4$. When considering r as a random variable with source and destination uniformly distributed in a square network with $m \times m$ nodes, the expected value of r is $0.5214m$ [48]. For $d_0 = 1$, the expected number of hops for the 4-, 8- and 12-neighbor cases are $0.6639m$, $0.4694m$, and $0.3319m$. The 4-neighbor and 8-neighbor schemes consume the same energy on average; the former may be preferred since it uses the same energy at each hop. The 8-neighbor scheme is better in terms of delay and path efficiency. For a delay threshold less than $0.4694m$, the 12-neighbor scheme is to be chosen, albeit at higher energy cost. If we use the energy-delay product as the performance metric, we get $1.0865m$, $0.7682m$, $1.0865m$ for 4-, 8- and 12-neighbor cases. Therefore the 8-neighbor case is to be preferred in terms of the energy-delay product in light traffic which is noise-limited instead of interference-limited. The energy-delay products for the 4-neighbor and 12-neighbor cases are the same.

the number of hops.

TABLE 4.2

COMPARISON OF SQUARE NETWORKS FOR $\alpha = 4$ (NOISE ANALYSIS) WITH 4-, 8-, AND 12-NEIGHBOR.

	Energy (A,B)	Energy (Min.)	Hop nr. $\overline{h}/(r/d_0)$	Path efficiency $\overline{\eta}$
4-nbr	1.6366	1.6366	1.2732	0.7935
8-nbr	1.7732	1.6366	0.9003	0.9486
12-nbr	3.5465	3.2732	0.6366	0.9486

4.1.2 Triangle networks and hexagon networks

Two other regular topologies of interest are the triangle topology (each node has 6 nearest neighbors) and its dual, the hexagon topology (each node has 3 nearest neighbors). For each triangle, there are three vertices and six nearest neighbors for each vertex, while for the hexagon, there are six vertices for each hexagon and three nearest neighbors for each vertex. The distance between all pairs of nearest nodes is d_0. We use the same assumption as for the square networks, i.e., the networks are large (in terms of node numbers) such that the distribution of r and ϕ for all the topologies are identical, so we can compare the path efficiency, the energy consumption, and the hop numbers for different topologies.

Fig. 4.3(a) shows a triangle network. O is the source and A is the destination. We want to find the number of hops h by using nearest-neighbor and shortest-path routing. We can split the network into groups such that the members of the group are equidistant (in hops) to the source. These groups are the nodes in hexagons centered around the source as shown in Fig. 4.3(a). Thus, the first group will be 6

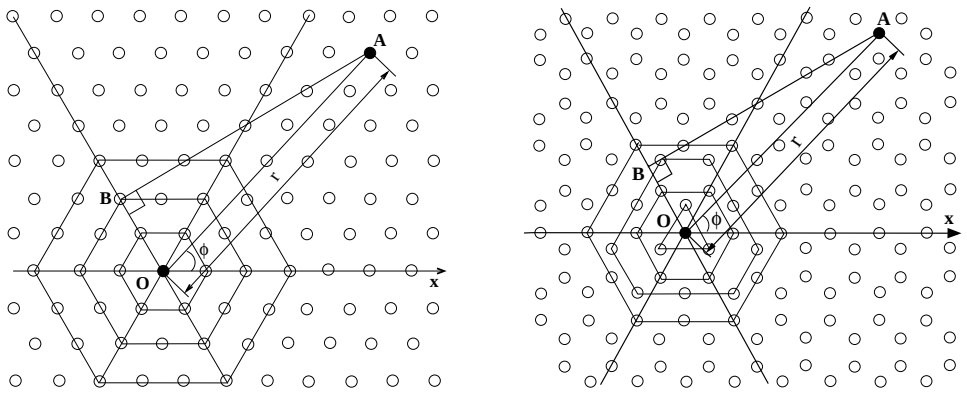

(a) Triangle Network (b) Hexagon network

Figure 4.3. Path efficiency of triangle network and hexagon network

nodes that are one hop away in the hexagon with perimeter $6d_0$, the second group will be 12 nodes that are two hops away in the hexagon with perimeter $12d_0$, and so on. In Fig. 4.3(a), because the angle ϕ between $\overrightarrow{OA}$ and the horizontal axis Ox is between 0 and $\pi/3$, we draw the vertical $|AB|$ to the line with $2\pi/3$ to Ox. The hop number h is $|AB|$ divided by $d_0 \sin(\pi/3)$. The travelled distance is hd_0. We will restrict ϕ within 0 and $\pi/3$ because h is a periodic function of ϕ with period $\pi/3$. Thus we have

$$h = \frac{r\sin(2\pi/3-\phi)}{d_0\sin(\pi/3)} = \frac{r}{d_0}\left(\cos\phi + \frac{1}{\sqrt{3}}\sin\phi\right), \qquad 0 \le \phi \le \pi/3. \tag{4.21}$$

The path efficiency is also a periodic function of ϕ:

$$\eta(\phi) = \frac{r}{d_T} = \frac{r}{hd_0} = \frac{\sqrt{3}}{2\sin(2\pi/3-\phi)} = \frac{\sqrt{3}}{\sqrt{3}\cos\phi + \sin\phi}, \qquad 0 \le \phi \le \pi/3. \tag{4.22}$$

The expected value of η is $\frac{3\sqrt{3}\ln 3}{2\pi} \approx 0.9085$.

For the hexagon topology, we use a similar method to find the group of nodes

that are equidistant (in hops) from the source. The first group consists of the vertices of an equilateral triangle centered at the source, all the other groups consists of hexagons. Some of them are equilateral hexagons, some are not. In Fig. 4.3(b), O is the source, A is the destination. To find the hop numbers from O to A by nearest-neighbor and shortest-path routing, we draw the vertical $|AB|$ to the line with $2\pi/3$ to Ox. If $|AB|$ divided by $3/2d_0$ is an integer, the hop number is twice the integer; if $|AB|$ divided by $3/2d_0$ is not an integer, the hop number is $\frac{|AB|-1/2d_0}{3/2d_0} \cdot 2 + 1$. Thus for ϕ within 0 and $\pi/3$, with $\rho := \frac{|AB|}{3/2d_0} = r\frac{\sin(2\pi/3-\phi)}{3/2d_0}$, we have

$$h = \begin{cases} 2\rho, & \rho \in \mathbb{N} \\ 2\rho + \frac{1}{3}, & \rho - \frac{1}{3} \in \mathbb{N}. \end{cases} \tag{4.23}$$

Because we assume that the number of hops between the source and the destination is large, we can neglect the $\frac{1}{3}$ term in the following analysis. The number of hops is again a periodic function of ϕ, this time with period $\pi/3$. So we have the expression for h and η as

$$h = \frac{2r\sin(2\pi/3-\phi)}{3/2d_0} = \frac{2r}{\sqrt{3}d_0}\left(\cos\phi + \frac{1}{\sqrt{3}}\sin\phi\right), \qquad 0 \le \phi \le \pi/3, \tag{4.24}$$

and the path efficiency

$$\eta(\phi) = \frac{r}{d_T} = \frac{r}{hd_0} = \frac{3/2}{2\sin(2\pi/3-\phi)} = \frac{3}{2\sqrt{3}\cos\phi + 2\sin\phi}, \qquad 0 \le \phi \le \pi/3. \tag{4.25}$$

The expected value of η is $\frac{9\ln 3}{4\pi} \approx 0.7868$. Fig. 4.4(a) shows the relationship between the path efficiency and ϕ for triangle and hexagon topology networks for ϕ within 0 and $2\pi/3$.

Similar to the square network, we determine the total transmit energy con-

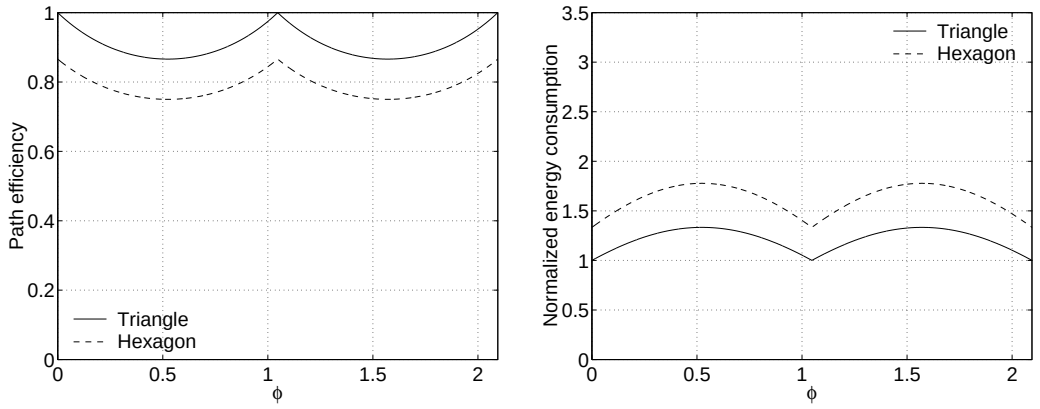

(a) Path efficiency

(b) Energy consumption

Figure 4.4. Path efficiency and energy consumption as a function of ϕ for triangle and hexagon networks.

sumption for a given end-to-end reception probability provided the Euclidean distance from the source to the destination is fixed for all the topologies. The total energy consumption is $E_{tot}(\phi) = hE_L = h^2 \frac{d_0^{\alpha} \Theta N_0}{-\ln P_{EE}} = h^2 E_0$. Inserting the expressions of h for the triangle and hexagon topologies yields the energy consumption in both topologies (Fig. 4.4(b)):

$$E_{tot}^T(\phi) = h^2 E_0 = \frac{(\sqrt{3}\cos\phi + \sin\phi)^2}{3} E_0 \frac{r^2}{{d_0}^2}, \qquad 0 \le \phi \le \pi/3,$$
$$E_{tot}^H(\phi) = h^2 E_0 = \frac{4(\sqrt{3}\cos\phi + \sin\phi)^2}{9} E_0 \frac{r^2}{{d_0}^2}, \qquad 0 \le \phi \le \pi/3. \tag{4.26}$$

The expected total energy consumption in units of $E_0 \frac{r^2}{{d_0}^2}$ is $\frac{\sqrt{3}}{\pi} + \frac{2}{3} \approx 1.2180$ for the triangle topology and $\frac{4}{\sqrt{3}\pi} + \frac{8}{9} \approx 1.6240$ for the hexagon topology. From the above equations and the plots, we can see that the path efficiency and energy consumption of the triangle network are a scaled version of those of the hexagon network. Averaging the number of hops of (22) and (25) over ϕ, the expected

TABLE 4.3

COMPARISON OF LATTICE, TRIANGLE, HEXAGON

NETWORKS FOR $\alpha = 4$ (NOISE ANALYSIS).

	Energy	Hop numbers $\overline{h}/(r/d_0)$	Path efficiency $\overline{\eta}$
Square network	1.6366	1.2732	0.7935
Triangle network	1.2180	1.1027	0.9085
Hexagon network	1.6240	1.4702	0.7868

hop numbers $\overline{h}$ for fixed r in unit of r/d_0 is $\frac{2\sqrt{3}}{\pi} \approx 1.1027$ and $\frac{8\sqrt{3}}{3\pi} \approx 1.4702$. We compare the parameters of the square network (4-neighbor case), triangle network, and hexagon network for $\alpha = 4$ in Table 4.3. We conclude that in a zero-interference network, the triangle topology is the best one due to its lowest energy consumption, least delay and highest path efficiency. However, it may not be the best one in the zero-noise network when considering the throughput, as we show in the following interference analysis.

4.2 Interference Analysis

In this section, we consider a network of N nodes, where every node always has a packet to transmit (heavy traffic assumption). The reception is only corrupted by interference, not by noise.

4.2.1 Analysis of the simple MAC scheme

For the network, it is assumed that nodes are transmitting packets independently in every timeslot with transmit probability p and the next-hop receiver

of every packet is one of its randomly chosen neighbors. The performance measurement is the throughput which is the expected number of successful packet transmissions per node in one timeslot. For a transmission over a distance d_0 with one interferer at distance d_i, the mean SIR is $\overline{\gamma}^I = (d_i/d_0)^\alpha$, yielding a reception probability of $p_r^{(1)} = e^{-\Theta(\frac{d_0}{d_i})^\alpha}$. If there are n interferers, the reception probability is

$$p_r^{(n)} = \prod_{i=1}^{n} e^{-\Theta(\frac{d_0}{d_i})^\alpha}. \tag{4.27}$$

If we let s_k denote the expected number of successful packet transmissions when k nodes transmit in one timeslot for a network with N nodes, then

$$s_k = c_k \mathbb{P}[k \text{ nodes transmit and } N-k \text{ nodes do not }] = c_k p^k (1-p)^{N-k}, \tag{4.28}$$

where p is the transmit probability of a node in every timeslot and c_k is the summation of the success probabilities given any k nodes transmit and the other $N-k$ nodes do not transmit in one timeslot. So s_k depends on the topology of the networks. For a simple line network with $N = 3$, $k = 2$ nodes transmitting at the same timeslot will cause interference. If the left end node and middle node transmit, the transmission success probability is $0.5e^{-\theta(\frac{d_0}{2d_0})^\alpha} = 0.5e^{-\theta 2^{-\alpha}}$. The 0.5 term comes from the fact that the middle node will transmit to its right neighbor with probability 0.5. Similarly, if the right end and middle node transmit, the successful transmission probability is also $0.5e^{-\theta 2^{-\alpha}}$. If the two outer nodes transmit, it is $2e^{-\theta}$. Then $s_2 = (e^{-\theta 2^{-\alpha}} + 2e^{-\theta})\, p^2(1-p)$. Generally we can write the total throughput for a network of N nodes as a polynomial of order N :

$$g_N(p) = \sum_{k=1}^{N-1} s_k(p) = \sum_{k=1}^{N-1} c_k p^k (1-p)^{N-k} \tag{4.29}$$

In the following, we will analyze the lattice, triangle and hexagon topology networks. We assume d_0 is one for all the topologies. For the square network, we study the 4-, 8- and 12-neighbor cases.

4.2.1.1 Square networks

The 4-neighbor case. We can derive the analytical expressions for the throughput of small networks. For $N = 2 \times 2$, $g_{2\times2}(p) = 4p(1-p)^3 + (4e_{\sqrt{2}} + 4e_1)p^2(1-p)^2 + 4e_1e_{\sqrt{2}}p^3(1-p)$. Table 4.4 presents the coefficients for $N = 2\times3$. The throughput functions for $N = 2 \times 2$ and $N = 2 \times 3$ are plotted in Fig. 4.5.

For small networks (small number of nodes) with N nodes and relatively small α, we may assume all N nodes can hear each other and interfere with each other. If more than one node is transmitting, there is a collision and all packets are lost. So the throughput is $\mathbb{P}[\text{success}] = Np(1-p)^{N-1}$. The optimal transmit probability is $1/N$, and the maximum throughput is $(1 - \frac{1}{N})^{N-1}$. If N goes to infinity, the throughput approaches $1/e$, as pointed out in [30, 65] as the maximum throughput of slotted ALOHA without spatial reuse. The network with 2×2 nodes satisfies the small networks requirement, so the optimal transmit probability is $1/4$. Similarly, the optimal transmit probability is $1/6$ for network with 2×3 nodes and small path exponents. We can see this from Fig. 4.5(a), (b) at $\alpha = 2$. However, if the network is larger or α is 4 or 5, nodes in different locations can use the channel simultaneously (spatial reuse) if they are sufficiently separated so that mutual interference will not prevent simultaneous successful transmissions. For large networks, we use simulation results instead of analytic calculations due to the "combinatoric explosion" of the number of terms. In Fig. 4.6(a), the simulation result is plotted for $\Theta = 10$ and various α for a network with 30×30 nodes. The

TABLE 4.4

COEFFICIENTS OF THE THROUGHPUT POLYNOMIAL $g_N(.)$

FOR $N = 2 \times 3$. $\quad e_t := e^{-\Theta t^{-\alpha}}$.

c_1	6
c_2	$\frac{26}{3}e_1 + \frac{26}{3}e_{\sqrt{2}} + \frac{10}{3}e_2 + \frac{10}{3}e_{\sqrt{5}}$
c_3	$\frac{8}{3}e_1e_1 + 14e_1e_{\sqrt{2}} + \frac{10}{3}e_1e_2 + \frac{10}{3}e_1e_{\sqrt{5}} + \frac{8}{3}e_{\sqrt{2}}e_{\sqrt{2}} + \frac{10}{3}e_{\sqrt{2}}e_2 + \frac{10}{3}e_{\sqrt{2}}e_{\sqrt{5}} + \frac{10}{3}e_2e_{\sqrt{5}}$
c_4	$\frac{16}{3}e_1e_1e_{\sqrt{2}} + \frac{16}{3}e_1e_{\sqrt{2}}e_{\sqrt{2}} + \frac{10}{3}e_1e_{\sqrt{2}}e_2 + \frac{10}{3}e_1e_{\sqrt{2}}e_{\sqrt{5}} + \frac{10}{3}e_1e_2e_{\sqrt{5}} + \frac{10}{3}e_{\sqrt{2}}e_2e_{\sqrt{5}}$
c_5	$\frac{8}{3}e_1e_1e_{\sqrt{2}}e_{\sqrt{2}} + \frac{10}{3}e_1e_{\sqrt{2}}e_2e_{\sqrt{5}}$

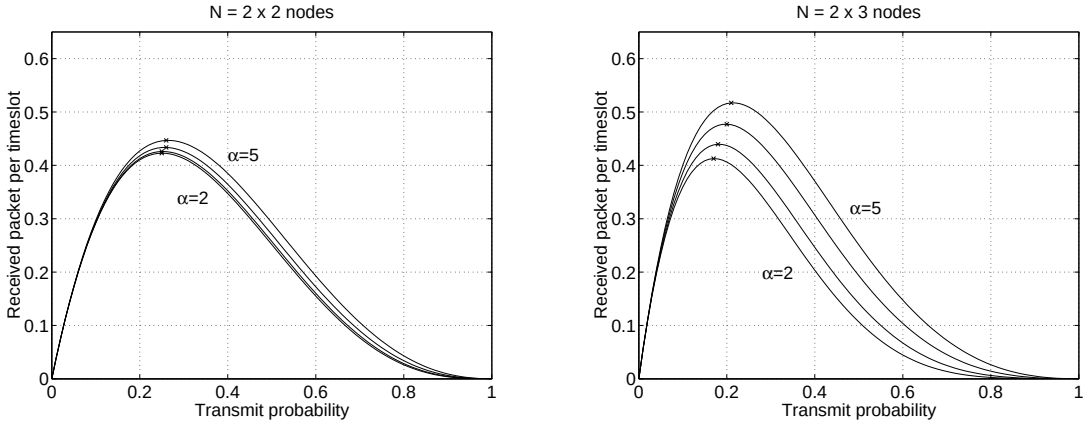

(a) (b)

Figure 4.5. Received packets per timeslot as a function of the transmit probability for a square network(4-neighbor) for $\alpha = 2, 3, 4, 5$ and $\Theta = 10$. The crosses indicate the maxima.

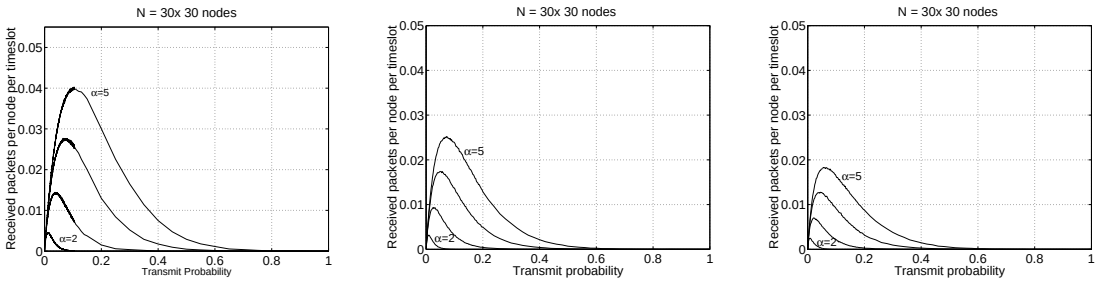

(a) 4-neighbor (b) 8-neighbor (c) 12-neighbor

Figure 4.6. Received packet per node per timeslot for $\Theta = 10$ and $\alpha = 2, 3, 4, 5$ for the 4-, 8- and 12-neighbor cases in a square network with $N = 30 \times 30$ nodes.

relationship between p_{max} and g_{max} can be linearly approximated. We find

$$g_{max} \approx 0.37 N p_{max}. \tag{4.30}$$

For $\alpha = 2, 3, 4, 5$, $p_{max} = 0.0128, 0.0397, 0.0748, 0.1044$, this yields $g_{max}/N = 0.0046$, 0.0144, 0.0277, 0.0403. Without interference, we would have $g_{max}/N = p_{max}$. We can define the *interference loss* as $L_I := 1 - \frac{g_{max}/N}{p_{max}}$ and its complement, the *transmission efficiency* as $T_{\mathit{eff}} := \frac{g_{max}/N}{p_{max}}$. In the 4-neighbor case, the transmission efficiency is about 0.37, which is similar to that of slotted ALOHA, namely e^{-1}.

The 8- and 12-neighbor cases. The simulation results for the 8-neighbor and the 12-neighbor cases are displayed in Fig. 4.6(b) and (c). The transmission efficiency is 0.34 for the 8-neighbor case and 0.31 for the 12-neighbor case.

To compare the 4-, 8- and 12-neighbor cases fairly, we use the *effective transport capacity*. We define the effective hop length as $\overline{l}_h = \mathbb{E}[r/h]$ for fixed r from the

TABLE 4.5

COMPARISON OF SQUARE NETWORKS FOR $\alpha = 4$

(INTERFERENCE ANALYSIS).

	Optimum probability	Maxi. throughput per node	Transmit efficiency	Effective hop length	Effective transport capacity
4-nbr	0.0748	0.0277	0.37	0.7935	0.0220
8-nbr	0.0590	0.0201	0.34	1.1222	0.0226
12-nbr	0.0466	0.0145	0.31	1.5870	0.0230

expressions in (21). The effective transport capacity is the distance-weighted throughput, defined as $Z := \frac{g_{max}}{N} \cdot \overline{l}_h$. We list the comparisons for $\alpha = 4$ in Table 4.5. We can see that the effective transport capacity is about 0.02 for the three cases. Hence on average, a packet can be successfully delivered over distance one every 50^{th} link in one timeslot. From the analysis, we find that 8-neighbor and 12-neighbor strategies can not increase the transport capacity in heavy traffic. This is because the gain of the hop length is offset by the decreased throughput due to the increased interference caused by additional neighbors at the same or smaller distance than the intended receiver.

4.2.1.2 Triangle and hexagon networks

Since including more neighbors barely improves the performance, we will not take into account different neighborhoods in the triangle and hexagon networks. Our comparison will be restricted to square (4-neighbor), triangle and hexagon networks. For triangle and hexagon networks, the relationship between the throughput and the transmit probability is displayed in Fig. 4.7.

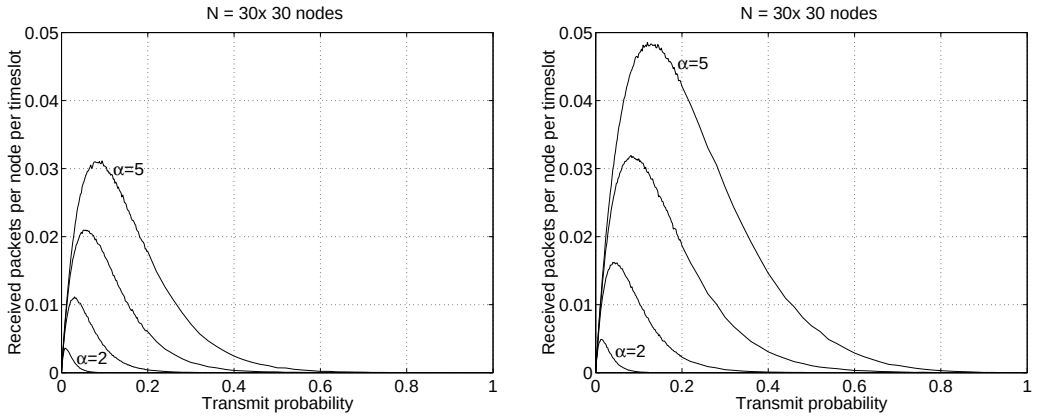

(a) Triangle network

(b) Hexagon network

Figure 4.7. Received packets per timeslot as a function of the transmit probability for $\Theta = 10$ and $\alpha = 2, 3, 4, 5$ for triangle and hexagon networks with $N = 30 \times 30$ nodes.

The transmission efficiency is about 0.37 for both topologies. However, g_{max} and p_{max} are larger in the hexagon topology than in the triangle topology. To interpret this, we can split the possible interferers into groups whose members have the same distance to the transmitter. For the transmitter in a hexagon network, the first group are the three neighbors at distance d_0, and the second group are nine nodes at distance $\sqrt{3}d_0$. For the 4-neighbor case in square network, there are four nodes in the first group with distance d_0 and four nodes in the second group with distance $\sqrt{2}d_0$ and four nodes in the third group with distance $2d_0$. Fewer nearest neighbors and other potential interferers further away can explain the larger p_{max} and g_{max} of hexagon networks.

The comparison of square (4-neighbor), triangle and hexagon networks for $\alpha = 4$ is shown in Table 4.6. The effective hop length of the three networks is identical to the path efficiency. We conclude that the hexagon network has the highest transmit probability, throughput and effective transport capacity, mainly

TABLE 4.6

COMPARISON OF LATTICE, TRIANGLE AND HEXAGON NETWORKS FOR $\alpha = 4$ (INTERFERENCE ANALYSIS).

	Optimum probability	Maxi. throughput per node	Transmit efficiency	Effective hop length	Effective transport capacity
Square	0.0650	0.0243	0.37	0.7935	0.0193
Triangle	0.0568	0.0210	0.37	0.9085	0.0191
Hexagon	0.0851	0.0320	0.37	0.7868	0.0252

since there are at most two interfering nodes at the same distance as the desired transmitter.

4.2.2 Comparison with optimum scheduler

Exploiting spatial reuse, we can devise a scheduling scheme that maximizes the throughput. There are several scheduling algorithms for general multihop wireless networks, e.g., [55]. Here we will deal with the scheduling problem in a square network for the 4-neighbor case. Assume that in every square area with q^2 nodes, one node is transmitting. Fig. 4.8(a) shows the optimum scheduling scheme for $q = 2$ for the first 4 phases (the number indicates the phase number). Shifting the four links connecting four nodes in the squares to their right and bottom squares, we can get another 4 phases. Since the traffic is bidirectional, 16 phases are needed. The total number of phases is $2q(q-1) + 4 + 2(q-2) = 4q^2$. In Fig. 4.8(b), the throughput as a function of q^2 is plotted. Optimum scheduling is achieved at $q = 16, 5, 3, 3$ for $\alpha = 2, 3, 4, 5$. The throughput ratio between the simple MAC scheme and the optimum one is 0.64, 0.44, 0.38 for $\alpha = 3, 4, 5,$

which shows that the relative performance of the simple MAC scheme is better for lower α than higher α.

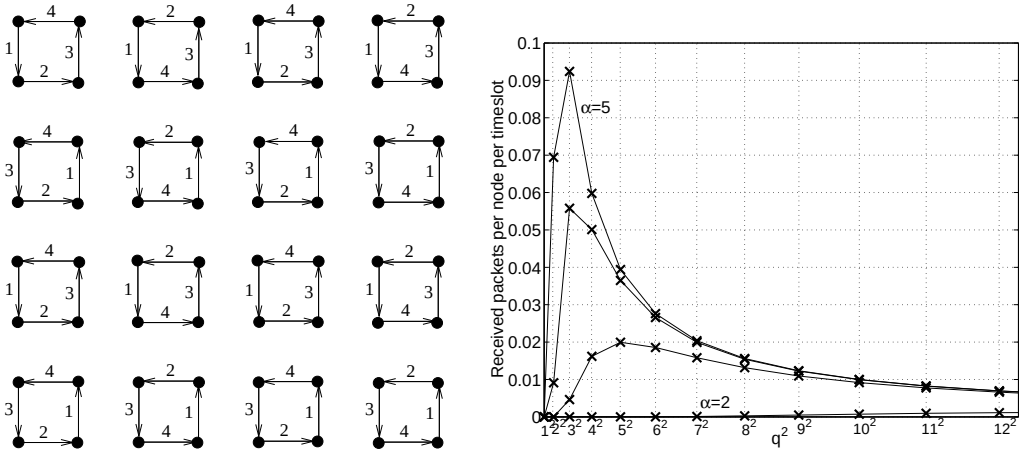

(a) (b)

Figure 4.8. (a). The optimum transmit scheduler for $q = 2$. (b). Received packets per node and timeslot for $\Theta = 10$ and $\alpha = 2$, 3, 4, 5 for a large square network (4-neighbor) where every q^2-th node is transmitting in every timeslot.

Interestingly, the curve for $\alpha = 2$ is quite different from the simulation results of the simple MAC scheme shown in Fig. 4.6(a). For $\alpha = 2$, the received interference power will be infinite for a receiver located in an infinite plane with a uniform and finite density of transmitters, as pointed out in [64, 67]. The results of the simple MAC scheme are for a 30×30 network, while the result of the optimum scheduler is for a very large network. So, in the latter case, the SIR is much smaller than in the first case since the fact that the per-node throughput for $\alpha = 2$ converges to zero with increasing network size. To see this, we carry out simulations for the

simple MAC scheme for $\alpha = 2$. For square networks (4-neighbor) with $m \times m$ nodes, Fig. 4.9(a) shows that the per-node throughput decreases with m (solid line). We approximate the relationship between the per-node throughput and m by $a/\ln(bm)$ with $a = 0.0062$ and $b = 0.1452$. The approximation is plotted in Fig. 4.9(a) by dashed line. We see they match perfectly. This confirms the result in [64], where it was shown that for $\alpha = 2$, the total interference power of a network of radius r is given by integrating c/r (for some constant c) from some R_0 to r. Hence, the SIR depends logarithmically on r. In Fig. 4.9(b), the throughput distribution over the location of the nodes is recorded for a network with 50×50 nodes at the optimal transmit probability $p_{max} = 0.0081$ with the per-node throughput $g_{max}/N = 0.0031$. We see that nodes at the boundary of the network, especially at the corner, contribute the most to the throughput, since they are subject to less interference. To show this more clearly, we plot the throughput distribution over the nodes in the main diagonal of the network and in an edge of the network as two profiles shown in Fig. 4.9(c). The average per-node throughput for nodes in the center, middle of the edge, and in the corner is 0.0024, 0.0038, and 0.0051, respectively. This shows that even for fairly large networks, the boundary nodes can not be neglected. On the contrary, routing algorithms should take advantage of the higher throughput that boundary nodes offer.

4.3 Conclusions

In the noise analysis, the triangle network gives the best performance due to its smallest energy consumption and delay and highest path efficiency. For the square network, we find that the 8-neighbor scheme is better than the 4-neighbor and 12-neighbor schemes in terms of the energy-delay product. If the delay is

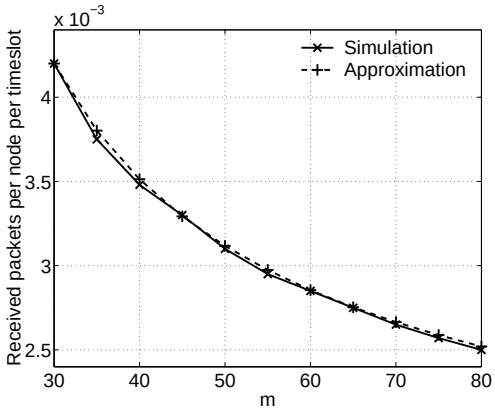

(a)

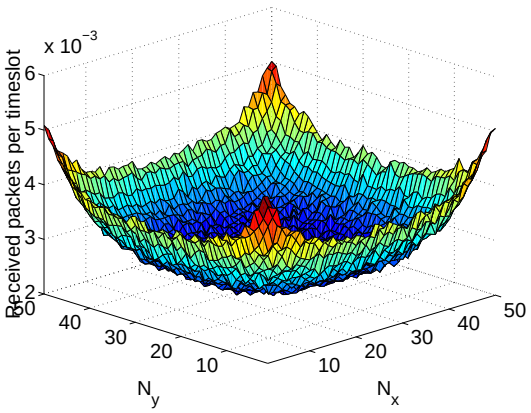

(b)

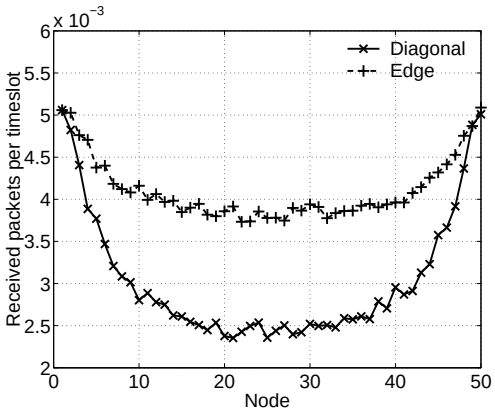

(c)

Figure 4.9. Throughput investigation for the simple MAC scheme with square networks (4-neighbor) for $\alpha = 2$. (a) The simulation result and approximation (by $a/\ln(bm)$ with $a = 0.0062$ and $b = 0.1452$) of the relationship between the per-node throughput and m. (b) Distribution of throughput over 50×50 nodes. (c) Distribution of the throughput over nodes in diagonal and edge profiles.

critical, longer hops (12-neighbor scheme) are preferred, albeit at higher energy expense.

In the interference analysis, the hexagon network exhibits the highest transmit probability, throughput, and effective transport capacity. By comparing the topologies and results, we find that connecting through fewer nearest neighbors can improve the throughput. An interesting observation for the square network is that for $\alpha = 4$, the transport capacities for the 4-, 8-, and 12-neighbor schemes are almost the same, since the gain of the hop length is offset by the decreased throughput due to increased interference. In the 4-neighbor case, for $\alpha > 2$, the throughput ratio between the simple MAC scheme and the optimum one is between $[0.35, 0.65]$ — the simple MAC is closer to the optimum for lower α. The performance of any practical MAC layer will lie between the bounds provided by these two MAC schemes. By investigating the distribution of the throughput over the nodes of the whole network, we find that for small α (in particular, for $\alpha = 2$), the per-node throughput is not a meaningful measure since a major part of the total network throughput comes from the boundary nodes, a fact that should be taken into account in routing protocols.

Thus, in the noise-limited regime (where the mean interference is much smaller than the noise), the triangle topology is best, whereas in the interference-limited regime, the best scheme is the hexagon topology.

Also we confirm that for $\alpha = 2$ (free space propagation), spatial reuse is not possible in large (in terms of node numbers) networks, since the interference power diverges to infinity as the number of nodes in the network grows.

CHAPTER 5

LOAD DISTRIBUTION FOR REGULAR SQUARE NETWORKS

In this chapter, we consider the load distribution in terms of the number of transmissions, *e.g.* the accumulated traffic at each node in the square network. Therefore, for each communication, we count the number of source and relay nodes as the load. We consider two classes of multihop networks — ad hoc networks and sensor networks. For ad hoc networks, we assume peer-to-peer traffic (source nodes and the destination nodes are uniformly randomly chosen); for sensor networks, we assume many-to-one traffic (the common destination node is the base station which is fixed at a corner of the network or in the center of the network).

5.1 Ad Hoc Networks

We use two strategies for nearest neighbor and shortest path routing in square networks (4-neighbor case) as shown in Fig. 5.1.

5.1.1 Strategy 1

In Fig. 5.1 (a), the source node O wants to send packets to destination node A. In Strategy 1 (4-neighbor case), the packet takes $2\min\{|OB|, |OA|\}/d_0$ hops along the diagonal direction first from O to C and then takes $||OB| - |BA||/d_0$ hops from C to A. With probability 0.5, it goes horizontal first or vertical first.

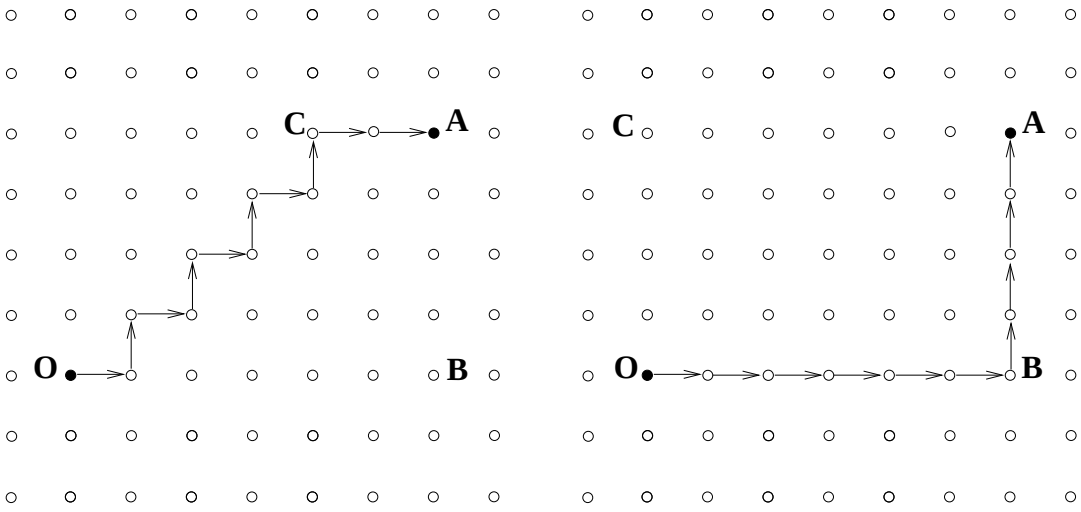

(a) Strategy 1 (b) Strategy 2

Figure 5.1. Two strategies of nearest neighbor and shortest path routing in square networks (4-neighbor case).

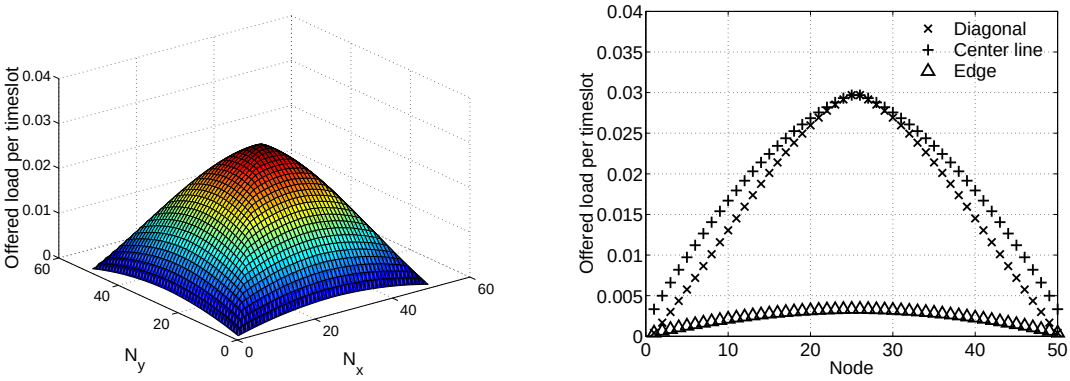

(a) Load distribution (b) Profiles

Figure 5.2. Analytically derived load distribution for Strategy 1 in a 50×50 ad hoc square network (4-neighbor case).

4-neighbor case. We derive the analytic function of the load for Strategy 1 in the 4-neighbor case. For any node with coordinate (x,y) in an $m \times m$ grid network, we obtain

$$\begin{aligned} L(x,y) &= -y^3 + \Big(-\frac{5}{2}m + \frac{3}{2}\Big)y^2 + \big(\frac{5}{2}m^2 - m - \frac{9}{2}\Big)y + (7m+7)xy - 7x^2y \\ &\quad + \Big(\frac{1}{2}m^2 - 3m - \frac{7}{2}\Big)x + \Big(-\frac{1}{2}m + \frac{7}{2}\Big)x^2 - \frac{3}{2}m^2 + \frac{1}{2}m + 2 \\ &\quad \text{for} \qquad 2 \le x \le m/2, \qquad 1 \le y \le x-1. \end{aligned} \tag{5.1}$$

The load of nodes in the diagonal lines is

$$\begin{aligned} L(x,y) &= -8y^3 + (4m+11)y^2 + (3m^2 - 3m - 7)y - 2m^2 + 2 \\ &\quad \text{for} \qquad 1 \le x \le m/2, \qquad y = x. \end{aligned} \tag{5.2}$$

The derivation of the analytic function is given in the Appendix to this chapter. By symmetry, (5.2) can be extended to the whole network. The load per communication is plotted in Fig. 5.2(a). Fig. 5.2(b) displays the load distribution of the nodes in the diagonal, center, and edge line. The average load for nodes in the center, middle of the edge, and in the corner is 0.03, 0.003, and 0.0004.

8-neighbor case and load balancing strategies. Similar to the 4-neighbor case, we can define the strategy 1 for 8-neighbor case – go along the diagonal direction first and then along the vertical or horizontal direction. Fig. 5.3 displays the simulation results. The expected load for nodes in the center, middle of the edge, and in the corner is 0.02, 0.003, 0.0004.

We can see the center nodes carry more traffic than the edge nodes, and much more than the corner nodes. To balance the load distribution, we route the packet

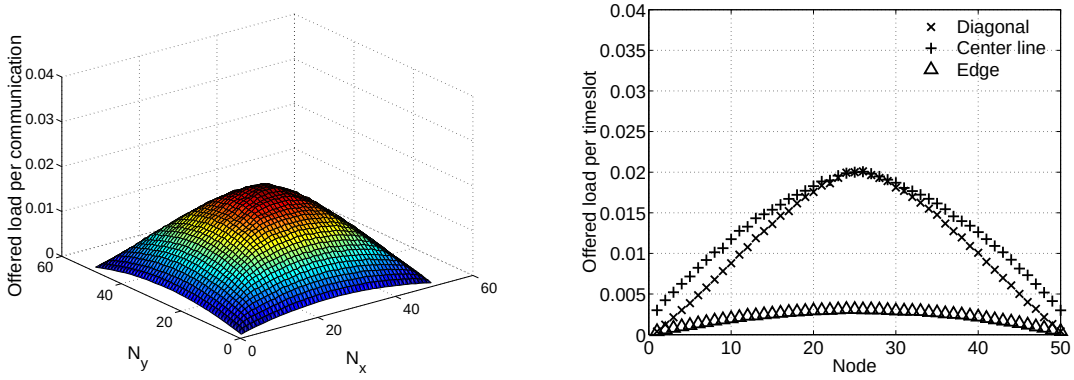

(a) Load distribution (b) Profiles

Figure 5.3. Simulation results of load distribution for Strategy 1 in a 50×50 ad hoc square network (8-neighbor case).

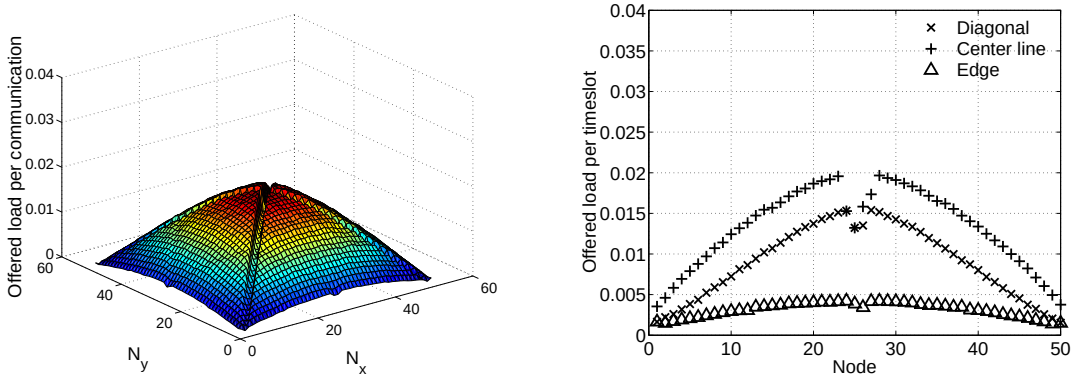

(a) Load distribution (b) Profiles

Figure 5.4. Simulation results of one-step strategy in a 50×50 ad hoc square network (8-neighbor case).

to a neighboring node which is not in the diagonal direction and has the longest distance from the center nodes for the first hop or the first two hops. The former is called the *one-step strategy*, while the latter is denoted as *two-step strategy*. Fig. 5.4 displays the simulation results for the one-step strategy. The average load for nodes in the center, middle of the edge, and in the corner is 0.0134, 0.0036 and 0.0016. Fig. 5.5 displays the simulation results for the two-step strategy. The average load for nodes in the center, middle of the edge, and in the corner is 0.0118, 0.0040 and 0.0041.

5.1.2 Strategy 2

In Fig. 5.1(b), the source node O sends packets to destination node A. In Strategy 2 (4-neighbor case), the packet takes $|OB|/d_0$ hops along the horizontal direction from O to B and then takes $|AB|/d_0$ hops along the vertical direction from B to A. With probability 0.5, it goes horizontal first or vertical first. For node (x, y), we find the load $L(x, y)$ to be

$$L(x,y) = (-2m+1)(x^2+y^2) + (2m^2+m-1)(x+y) - 2m^2, \quad (5.3)$$

which is derived in the Appendix of this chapter. The load distribution and corresponding profiles based on (5.3) are shown in Fig. 5.6. The average per-node load for nodes in the center, middle of the edge, and in the corner is 0.0198, 0.0103, and 0.0008.

5.2 Sensor Networks

For sensor networks, we assume the common destination node is the base station which is fixed at a corner of the network or in the center of the network.

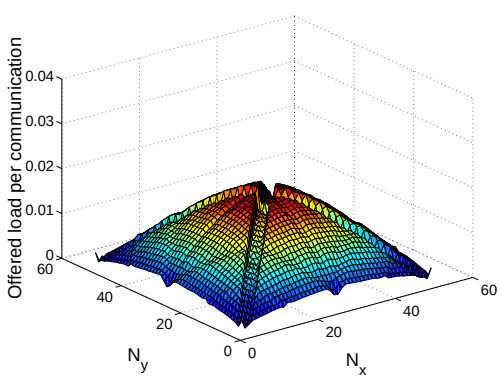

(a) Load distribution

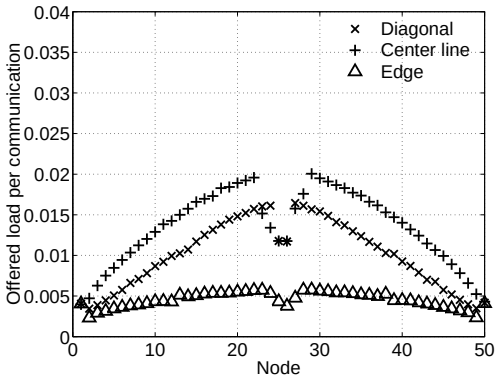

(b) Profiles

Figure 5.5. Simulation results of two-step strategy in a 50×50 ad hoc square network (8-neighbor case).

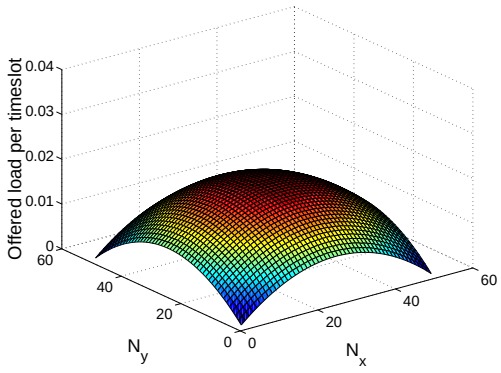

(a) Load distribution

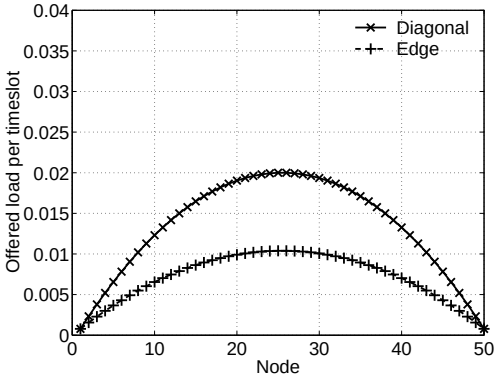

(b) Profiles

Figure 5.6. Analytically derived load distribution for Strategy 2 in a 50×50 ad hoc square network.

5.2.1 Strategy 1

4-neighbor case and improvement strategy. The load $L(x, y)$ at node (x, y) in a square regular grid network of size $m \times m$ where every node generates packets that are routed towards the common sink (m, m) with strategy 1 is

$$L(x,y) = \begin{cases} 2y - \frac{1}{2} & 1 \le x \le m-1, \quad 1 \le y \le x-1 \\ 2y - 1 & 1 \le x < m, \quad y = x \\ \frac{1}{2}y^2 + y & x = m, \quad 1 \le y < m \\ 0 & x = m, \quad y = m \quad \text{(sink node)} \end{cases} \tag{5.4}$$

for the lower triangular part of the network where $x \ge y$. The load in the upper triangle is symmetric. We can see for interior nodes, the load is a linear function of the coordinate, for nodes in the two edges near the destination node, the load is a quadratic function of the coordinate. The derivation is given in the Appendix to this chapter. We plot the load distribution for nodes of the whole network, the inside network, and one edge in Fig. 5.7.

Based on previous results on ad hoc networks, it is apparent that the one-step and two-step strategies can improve most of the load distribution over the nodes in the main diagonal. For sensor networks, let $N_{hv} = ||OB| - |BA||/d_0$ as shown in Fig. 5.1 (a), we route the packet along the horizontal or vertical direction over h_1 hops with h_1 a random number uniformly distributed in 0 and N_{hv}, then along the diagonal direction. We call this *random step strategy* and plot the simulation results in Fig. 5.8.

8-neighbor case and improvement strategy. Similar to the 4-neighbor case, the load $L(x, y)$ at node (x, y) in a square sensor network (8-neighbor) with strategy

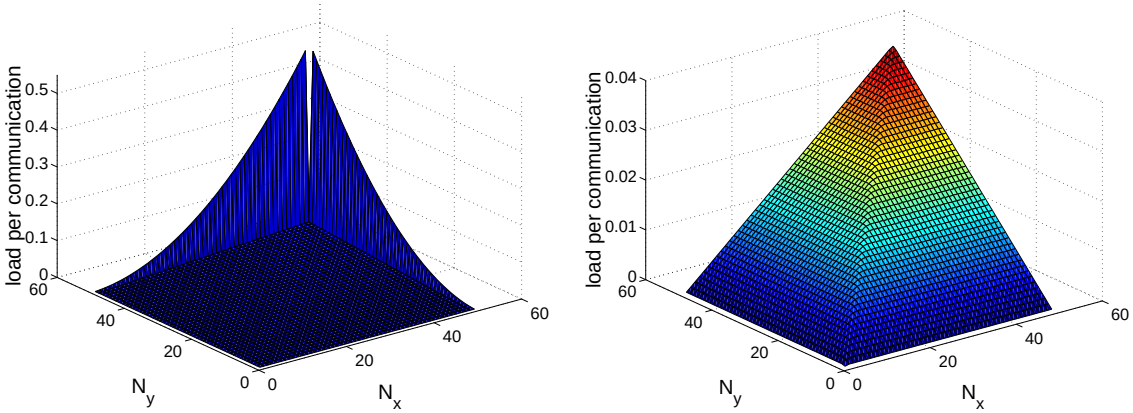

(a) (b)

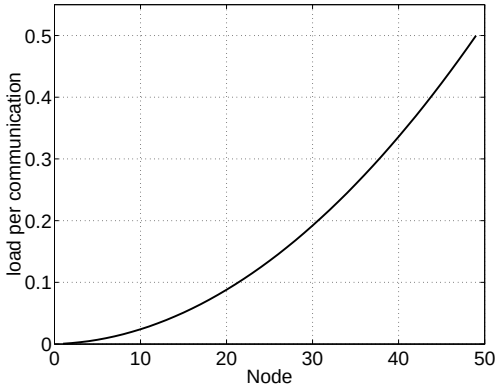

(c)

Figure 5.7. Analytically derived load distribution for Strategy 1 in a 50×50 square sensor network (4-neighbor case). (a) the whole network, (b) the interior of the network, and (c) one edge connected with the sink node.

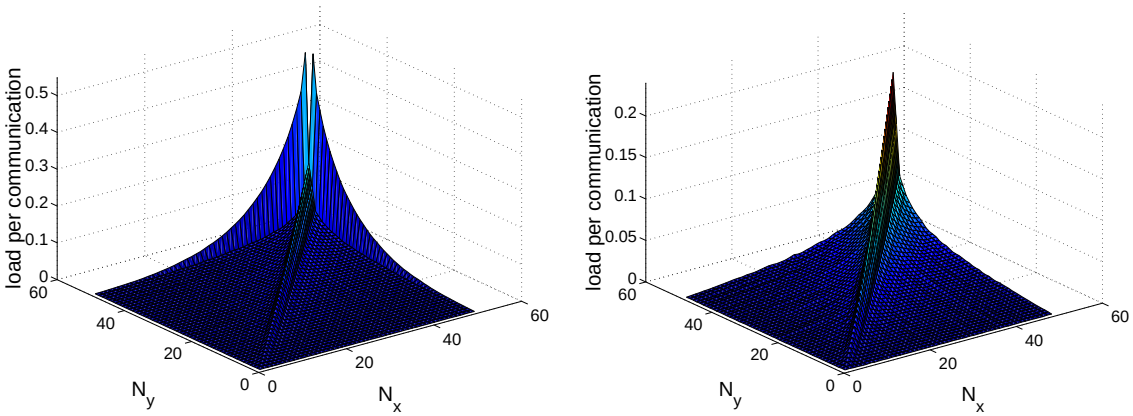

(a) (b)

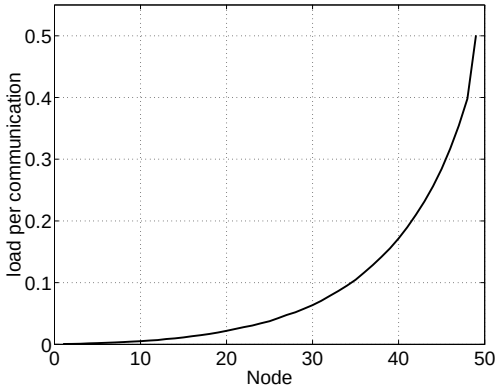

(c)

Figure 5.8. Simulation results of random step strategy in a 50×50 square sensor network (4-neighbor case). (a) the whole network, (b) the interior of the network, and (c) one edge connected with the sink node.

1 is

$$L(x,y) = \begin{cases} y & 2 \le x \le m-1, \quad 1 \le y \le x-1 \\ y & 1 \le x \le m, \quad y = x \\ \frac{1}{2}y^2 + \frac{1}{2}y & x = m, \quad 1 \le y \le m \\ 0 & x = m, \quad y = m \quad \text{(sink node)} \end{cases} \tag{5.5}$$

for the lower triangular part of the network where $x \ge y$. The load in the upper triangle is symmetric. The load distribution for nodes of the whole network, the interior of the network, and one edge is shown in Fig. 5.9. The simulation results for the random step strategy are shown in Fig. 5.10.

5.2.2 Strategy 2

Similar to Strategy 2 of ad hoc networks, for node (x, y) in a square sensor network (4-neighbor case), we find the load $L(x, y)$ to be

$$L(x,y) \;=\; \frac{1}{2}(x-1) + \frac{1}{2}(y-1), \tag{5.6}$$

since there are $(x-1)$ paths passing through node (x, y) with probability 0.5 of going vertical first and there are $(y-1)$ paths passing through node (x, y) with probability 0.5 of going horizontal first. The load distribution and corresponding profiles based on (5.6) are shown in Fig. 5.11.

5.3 Conclusions

For ad hoc networks, the analytic functions and simulation results of strategy 1 (nearest neighbor and shortest routing for square regular networks, starting diagonally) shows that the nodes in the center area carry significantly more traffic

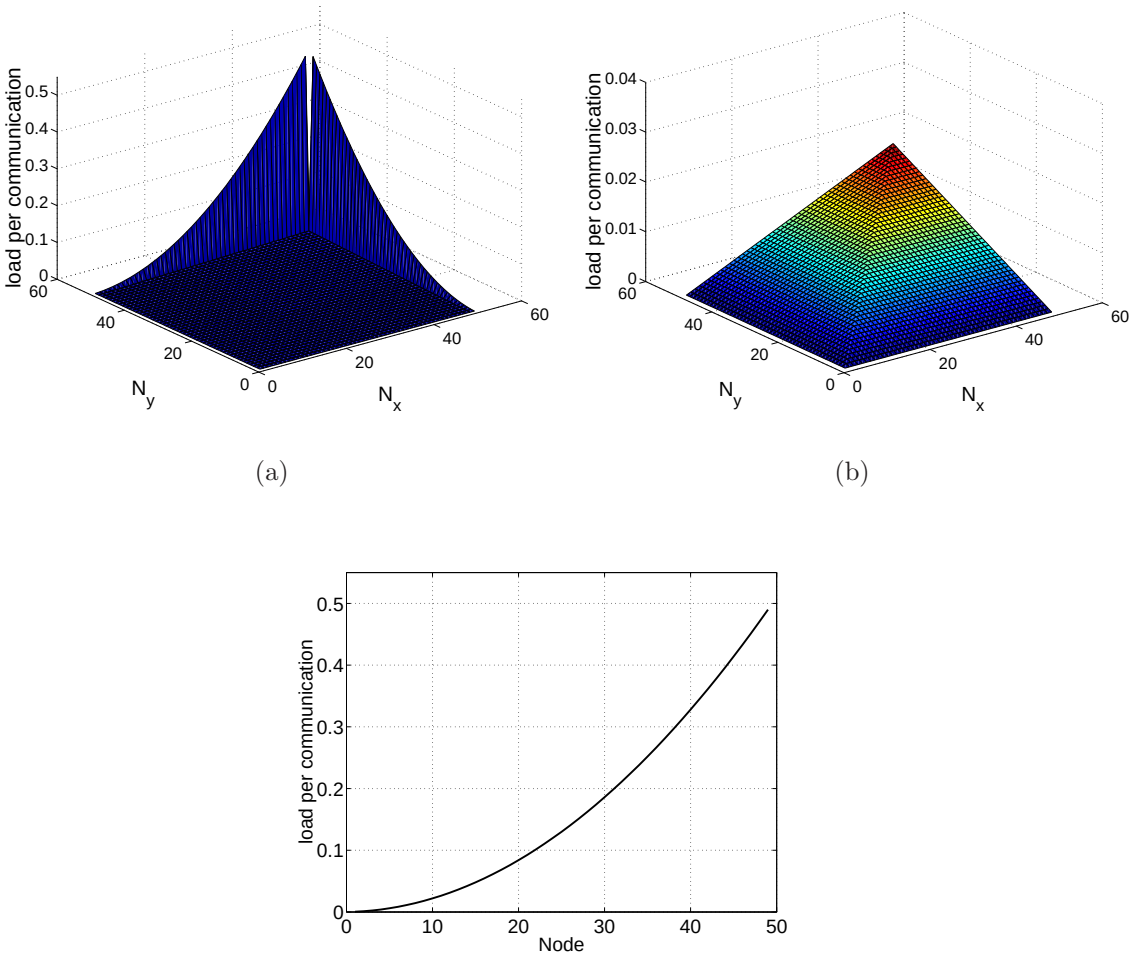

(a) (b)

(c)

Figure 5.9. Analytically derived load distribution for Strategy 1 in a 50×50 square sensor network (8-neighbor case). (a) the whole network, (b) the interior of the network, and (c) one edge connected with the sink node.

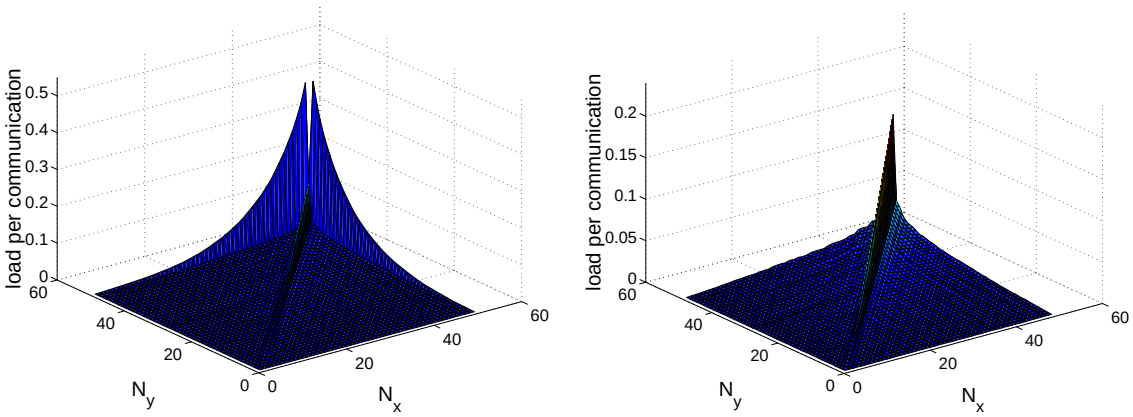

(a)

(b)

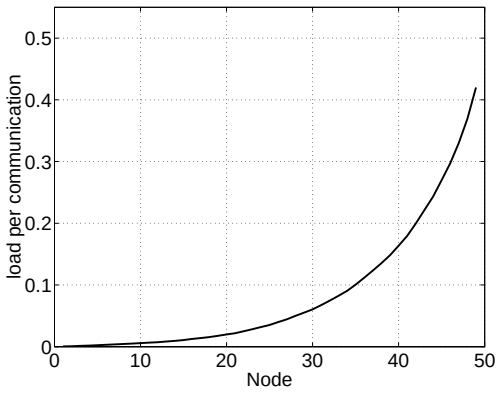

(c)

Figure 5.10. Simulation results of random step strategy in a 50×50 square sensor network (8-neighbor case). (a) the whole network, (b) the interior of the network, and (c) one edge connected with the sink node.

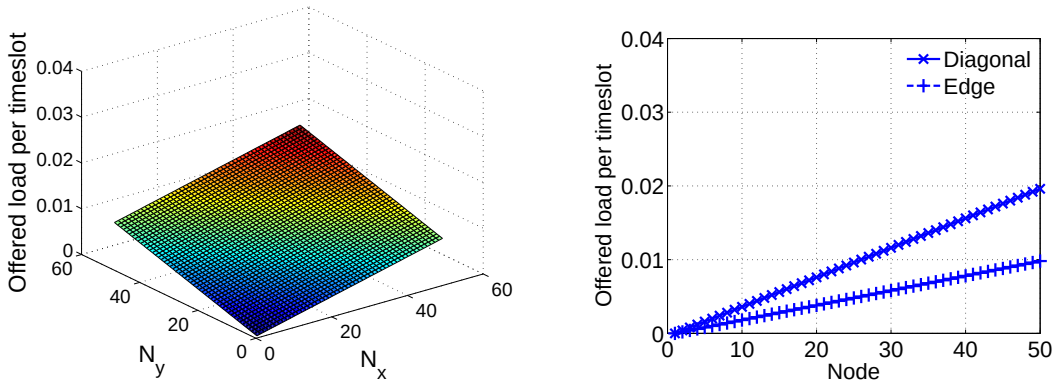

(a) Load distribution

(b) Profiles

Figure 5.11. Analytically derived load distribution for Strategy 2 in a 50×50 square sensor network.

than those at the edge. For sensor networks, the load increases linearly when approaching the sink node along the main diagonal and quadratically along the edge, hence the critical nodes are located near the sink node. Those nodes are the bottleneck for the network lifetime. To balance the load, we use a one-step and a two-step strategy for ad hoc networks and a random step strategy for sensor networks. It is shown that one- and two-step strategies can mainly balance the load of the nodes in the main diagonal. The random step strategy can move some of the load from the edge to the diagonal and interior area. However, it can not solve the high burden problem of the nodes which are neighbors of the corner destination. The APR (Alternate Path Routing) protocol [80] indirectly balances the load by distributing the traffic to a set of diverse paths for one source-destination connection. [76] uses an analytic model to show that multipath routing can improve the end-to-end reception probability and balance the load among nodes. However, the increased overhead traffic load might offset the benefits.

This multipath routing scheme works only for peer-to-peer traffic, not for sensor networks. For ad hoc and sensor networks, strategy 2 outperforms strategy 1 in terms of load balance.

5.4 Appendix: Derivation of Analytic Functions

Strategy 1. Consider the lower triangle, main diagonal, and bottom edge of the lattice square network as shown in Fig. 5.12(a), (b) and (c), respectively. For any node with coordinate (x,y) in an $m \times m$ (m is even) grid network, the possible source nodes whose packets will pass through node (x, y) are contained in a polygon (the solid polygon if the packet travels horizontally first, the dashed polygon if it travels vertically first). We denote the number of all the possible source nodes of node (x, y) located at the lower triangle, diagonal and bottom edge as n_1^h, n_2^h and n_3^h if the packet travels horizontally first, and n_1^v, n_2^v and n_3^v if the packet travels vertically first. We find

$$\begin{aligned} n_1^h &= 2(y-1)+1 = 2y-1, \\ n_2^h &= 2(y-1)+1 = 2y-1, \\ n_3^h &= \frac{y(y+1)}{2} = \frac{1}{2}(y^2+y). \end{aligned} \tag{5.7}$$

and

$$\begin{aligned} n_1^v &= 2(y-1)+1+1 = 2y, \\ n_2^v &= 2(y-1)+1 = 2y-1, \\ n_3^v &= \frac{(y+1)(y+2)-1}{2} = \frac{1}{2}(y^2+3y). \end{aligned} \tag{5.8}$$

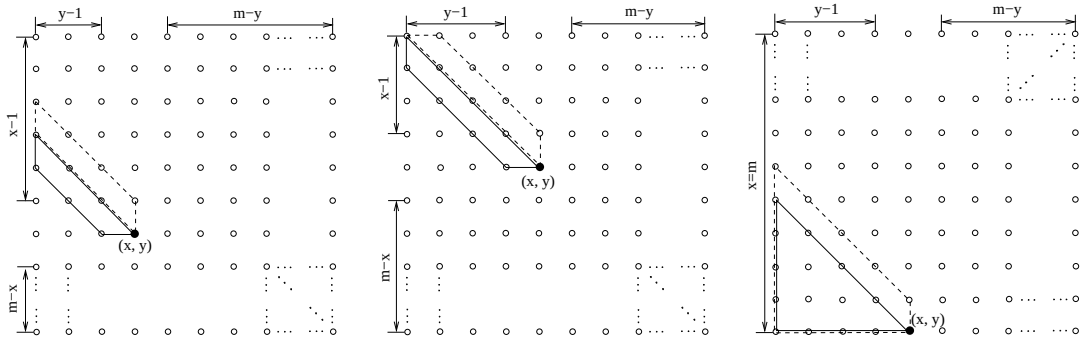

(a) (b) (c)

Figure 5.12. Set of source nodes of a packet traveling through node (x, y) for Strategy 2. (a) For a node inside the lower triangle. (b) For a node in the main diagonal. (c) For a node in the bottom edge.

Since the packet travels horizontally or vertically first with 50% probability, we get the expected number of transmissions of node (x, y) as

$$\begin{aligned} n_1 &= \frac{1}{2}n_1^h + \frac{1}{2}n_1^v = 2y - \frac{1}{2}, \\ n_2 &= \frac{1}{2}n_2^h + \frac{1}{2}n_2^v = 2y - 1, \\ n_3 &= \frac{1}{2}n_3^h + \frac{1}{2}n_3^v = \frac{1}{2}y^2 + y\,, \end{aligned} \tag{5.9}$$

from which (5.3) follows. For m is odd, the derivation is similar to the even case.

Strategy 2. As shown in Fig. 5.13, if the possible source nodes locate at the solid line left to the node (x, y), the possible destination nodes locate at the right plan of node (x, y) plus the vertical line passing through node (x, y). Since the probability of going horizontal is 0.5, the number of those paths is $0.5(y-1)[(m-y+1)m-1]$. If we switch the source nodes and destination nodes, we can get another $0.5(y-1)[(m-y+1)m-1]$ paths passing through node (x, y). Similarly, if the possible

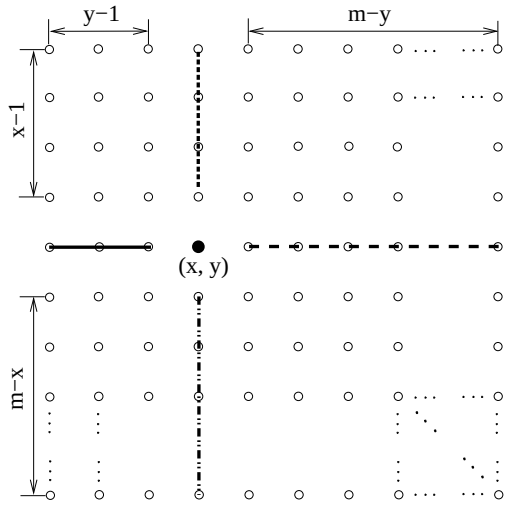

Figure 5.13. Derivation of the load distribution for Strategy 2 of ad hoc square networks (4-neighbor).

source or destination nodes locate at the dashed line right to node (x, y), there are $(m-y)(ym-1)$ paths passing through node (x, y). Because the paths from nodes in the left line to the nodes in right dashed line are counted twice, we subtract $(y-1)(m-y)$. Similarly, we add the path number when the possible source or destination nodes locate at the dotted line area or dash-dotted line. Finally we add m^2-1 because node (x, y) can be the source node transmitting to all the other nodes. The load $L(x, y)$ is

$$\begin{aligned} L(x,y) &= \frac{1}{2}(y-1)[(m-y+1)m-1]\cdot 2+\frac{1}{2}(m-y)(ym-1)\cdot 2 \\ &\quad -(y-1)(m-y)+\frac{1}{2}(x-1)[(m-x+1)m-1]\cdot 2 \\ &\quad +\frac{1}{2}(m-x)(xm-1)\cdot 2-(x-1)(m-x)-(m-x)(y-1) \\ &\quad -(y-1)(x-1)-(x-1)(m-y)-(m-y)(m-x)+m^2-1 \\ &= (-2m+1)(x^2+y^2)+(2m^2+m-1)(x+y)-2m^2. \end{aligned} \tag{5.10}$$

CHAPTER 6

COMPARISON OF REGULAR AND RANDOM NETWORKS

A uniformly random distribution is a widely accepted model for the location of the nodes in wireless sensor networks if nodes are deployed in large quantities and there is little control over where they are dropped. A typical scenario is a deployment from an airplane for environmental or battlefield monitoring. Current testbeds, however, often have regular topologies (equidistant nodes), and it may be assumed that their performance gives a good indication of how a random network would perform with the same set of protocols and algorithms. This chapter will show that this assumption is fundamentally wrong, i.e., that the performance of regular and random networks differs greatly, and that, consequently, different protocols are needed for random networks. In this chapter, we employ a Rayleigh fading link model assuming a transmission over an *effective distance* $d = \max\{1, R\}$ instead of R, where R is the Euclidean distance $\|x_i - x_j\|_2$. This way, the problem that the received power diverges for $R \to 0$ is avoided.

6.1 One-dimensional Networks

We study the performance of line networks first. It is assumed that the left end node is the source node and the right end node is the destination node. For every transmitting node, its next-hop receiver is its right neighbor. Although part of the results are derived in Chapter 3, we list them here for convenience. The

throughput and energy consumption of regular line networks and random line networks with adaptive transmit power are compared in the following.

6.1.1 Throughput

The average per-node throughput for regular and random line networks is plotted in Fig. 6.1. The regular line network has a higher throughput than the random line network, and the difference is higher for larger α.

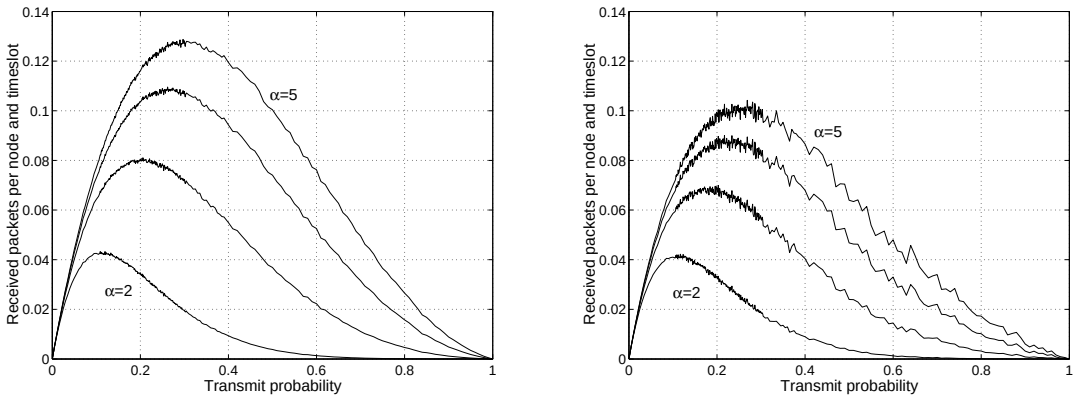

(a) (b)

Figure 6.1. (a) Simulation results of average per-node throughput for $\Theta = 10$ of a large regular line network based on the simple MAC scheme. (b) Simulation results of average per-node throughput for $\Theta = 10$ of a large random line network based on the simple MAC scheme.

6.1.2 Energy consumption

The analysis of the average energy consumption has been carried out in Section 3.2.1.1 (p. 20). Since the maximum energy consumption is related to the lifetime of a connection, we determine the expected maximum R^α in an h-hop connection,

TABLE 6.1

COMPARISON OF THROUGHPUT AND ENERGY CONSUMPTION FOR 20-HOP REGULAR AND RANDOM LINE NETWORK WITH SIMPLE MAC SCHEME.

	$\alpha = 2$	$\alpha = 3$	$\alpha = 4$	$\alpha = 5$
g_{ave} of regular line network	0.0538	0.0875	0.1138	0.1327
g_{ave} of random line network	0.0495	0.0811	0.1080	0.1266
g_{min} of regular line network	0.0576	0.0855	0.1078	0.1231
g_{min} of random line network	0.0352	0.0503	0.0614	0.0669
E_{ave} of regular line network	1	1	1	1
E_{ave} of random line network	2	6	24	120
E_{max} of regular line network	1	1	1	1
E_{max} of random line network	14.5	66.2	340.2	1974.5

e.g., $\mathbb{E}[R^{\alpha}_{max}|h] := \mathbb{E}[\max\{R^{\alpha}_1, R^{\alpha}_2, ...R^{\alpha}_h\}]$. The cumulative density function (cdf) of R^{α} is

$$F_{R^{\alpha}}(y) = \mathbb{P}[R^{\alpha} \leq y] = \mathbb{P}[R \leq y^{1/\alpha}] = \int_0^{y^{1/\alpha}} e^{-x} dx = 1 - e^{-y^{1/\alpha}}. \tag{6.1}$$

Thus we get

$$\mathbb{E}[R^{\alpha}_{max}|h] = \int_0^{\infty} [1 - (F_{R^{\alpha}}(y))^h] dy = \int_0^{\infty} 1 - (1 - e^{-y^{1/\alpha}})^h dy, \tag{6.2}$$

which is plotted in Fig. 6.5(c) for $\alpha = 4$.

6.1.3 Comparison

Let g_{ave} and g_{min} denote the average and end-to-end throughput[1], and E_{ave} and E_{max} the average and maximum energy consumption, respectively. We list the throughput and energy consumption (normalized by the corresponding energy consumption of the regular network) for 20-hop regular and random line networks for different α in Table 6.1 for the simple MAC (slotted ALOHA) scheme. We can see that with power adaptation, the random line network consumes one or two orders of magnitude more energy than the regular line network and has 2-25% smaller throughput. Moreover, the maximum energy consumption is drastically higher, and the penalty on the end-to-end throughput is more severe since the minimum throughput is typically about 40% lower than the average.

[1]As mentioned in the introduction, the end-to-end throughput over a multi-hop connection is the minimum of the throughput values of the nodes involved.

6.2 Two-dimensional Networks

In this section, we consider two-dimensional sensor networks and compare regular square grid networks with random networks. For the former, nodes are regularly placed in $A := [1/2, m + 1/2]^2$ at positions $A \cap \mathbb{Z}^2$, and the next hop receiver of each node is one of the four nearest neighbors. For random networks, nodes are uniformly randomly located in an area $m \times m$. The base station is assumed to be located at (m, m) for both networks, and the two networks have the same size and node densities. We assume that for each connection, no other nodes except the source node and relay nodes in that route are transmitting. So we just consider the intra-connection or intra-route interference, not the inter-connection or inter-route interference. To find an upper bound on the throughput, we employ the near-optimum scheduler in Chapter 3 to take advantage of spatial reuse and balance the per-node throughput. We assume that traffic is only generated at a single node (i, j), but let i and j vary over $1 \leq i, j \leq m$ so that all possible cases are considered. To compare the regular and random networks, we also study the simple MAC scheme for a single connection.

6.2.1 Regular square sensor networks

We consider regular square networks (4-neighbor case) such that the routing strategy is to select one of the four neighbors which is closer to the base station.

6.2.1.1 Throughput

For the connections originating at all the nodes, we determine the end-to-end throughput for a 15×15 square grid network. This throughput is plotted in Fig. 6.2 for $\alpha = 4$. Averaging the throughput over all the connections, the mean

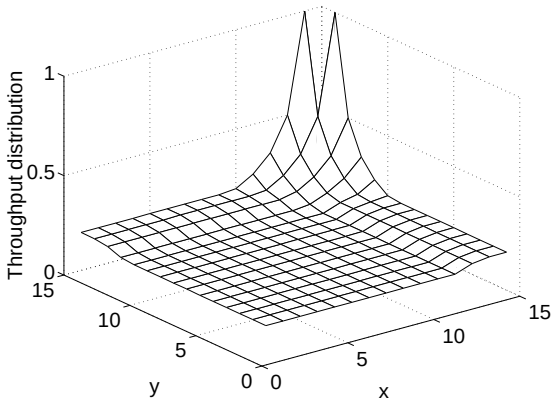

Figure 6.2. End-to-end throughput for traffic originating from the nodes at positions (x, y) in a 15×15 regular square grid network for $\alpha = 4$.

value is 0.1799, the variance is 0.0085.

6.2.1.2 Energy consumption

A packet originating at position (x, y) takes $m - x + m - y$ hops to be relayed to the base station (m, m). From Chapter 2, we know that if there are h hops with unit distance $d_0 = 1$, the transmit energy at each hop for an end-to-end reliability p_{EE} is $E_L = h\frac{d_0^\alpha \Theta N_0}{-\ln p_{EE}} = h\frac{\Theta N_0}{-\ln p_{EE}}$. The total energy consumption to deliver one packet to the base station is $hE_L = h^2\frac{\Theta N_0}{-\ln p_{EE}} = h^2 E_0$, where $h = 2m - x - y$ and $E_0 := \frac{\Theta N_0}{-\ln p_{EE}}$. Thus, we have

$$E_{tot} = \sum_{y=1}^{m}\sum_{x=1}^{m}(2m - x - y)^2 E_0 = \left(\frac{7}{6}m^4 - 2m^3 + \frac{5}{6}m^2\right) E_0. \tag{6.3}$$

6.2.2 Two-dimensional random networks

We adapt the transmit power to d^α to compensate for the path loss and employ the generic routing strategy from [21]: each node in the path sends packets to

its nearest neighbor that lies within a sector ϕ, i.e., within $\pm\phi/2$ of the source-destination direction, which results in the routing trees shown in Fig. 6.3.

6.2.2.1 Throughput

We expect the end-to-end throughput to increase with decreasing angle ϕ since the path follows a straight line more closely for smaller ϕ. For $\phi = \pi/6$ and $\phi = \pi/2$, Fig. 6.4 displays the throughput distribution for $\alpha = 4$. The average end-to-end throughput per connection is 0.2310 and 0.1595, with variance 0.0202 and 0.0067 for $\phi = \pi/6$ and $\phi = \pi/2$, respectively. As expected, routing within a smaller sector has better throughput performance. Note that for Fig. 6.3(a), there are 5 nodes with throughput 1 since they are directly connected to the base station, whereas for $\phi = \pi/2$, there is only a single node with throughput 1.

6.2.2.2 Energy consumption

Similar to one-dimensional case, we determine the expected value of R^α, where R has a Rayleigh distribution[2] [21], *i.e.*, $f_R(x) = x\phi e^{-x^2\phi/2}$.

$$\mathbb{E}[R^\alpha] = \int_0^\infty x^\alpha f_R(x)dx = \left(\frac{2}{\phi}\right)^{\alpha/2} \Gamma(1+\frac{\alpha}{2}), \tag{6.4}$$

shown in Fig. 6.5(a). The energy consumption is decreasing with increasing ϕ. For $\phi = \pi/2$ and $\alpha = 4$, $\mathbb{E}[R^\alpha] = 3.6393$, which is much smaller than in the one-dimensional case, $\Gamma(1+\alpha) = 24$. In terms of averages, the difference of energy consumption between 2-d random networks and square grid networks is not as big as in the one-dimensional case. How about the maximum energy consumption? Again, we need to determine $\mathbb{E}[R^\alpha_{max}|h] := \mathbb{E}[\max\{R^\alpha_1, R^\alpha_2, ...R^\alpha_h\}]$, where h is the

[2]For simplicity, we use the Euclidean distance R rather than the effective distance d, which yields a tight lower bound.

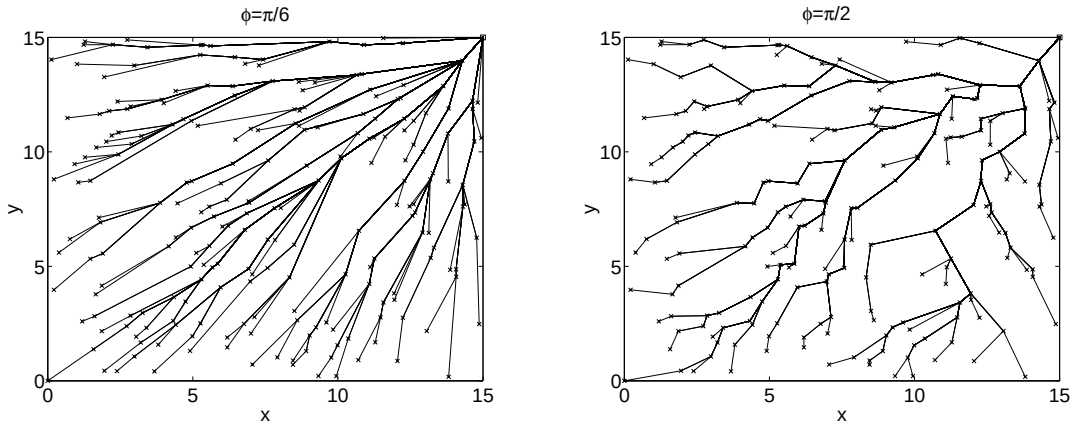

(a) (b)

Figure 6.3. Routing trees from all the nodes to the base station for a random network with area 15×15 and density 1. (a) Routing within sector $\phi = \pi/6$. (b) Routing within sector $\phi = \pi/2$.

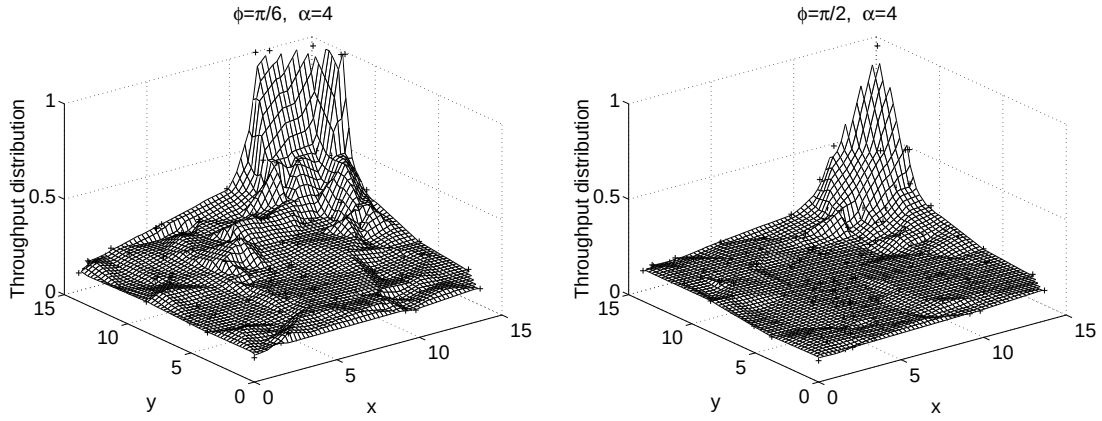

Figure 6.4. End-to-end throughput for traffic originating from all the nodes to the base station for a random network with area 15×15 and density 1 for $\alpha = 4$.

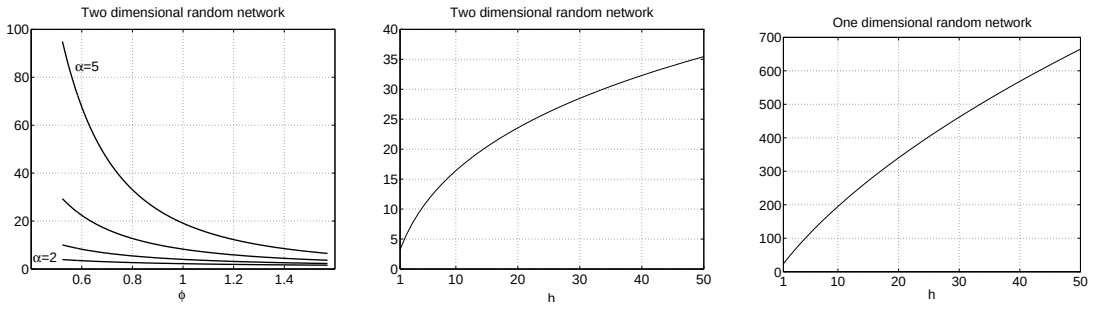

(a) $\mathbb{E}[R^\alpha]$ (2-d) (b) $\mathbb{E}[R^\alpha_{max}|h]$ (2-d) (c) $\mathbb{E}[R^\alpha_{max}|h]$ (1-d)

Figure 6.5. (a) $\mathbb{E}[R^\alpha]$ vs. ϕ for two-dimensional random network for $\alpha = 2$, 3, 4, 5. (b) $\mathbb{E}[R^\alpha_{max}|h]$ vs. h for two dimensional random networks for $\alpha = 4$ and $\phi = \pi/2$. (c) $\mathbb{E}[R^\alpha_{max}|h]$ vs. h for random line networks for $\alpha = 4$.

hop number. The cdf of R^α is

$$F_{R^\alpha}(y) = \mathbb{P}[R^\alpha \le y] = \int_0^{y^{1/\alpha}} x\phi e^{-\frac{x^2\phi}{2}} dx = 1 - e^{-\frac{y^{2/\alpha}\phi}{2}}. \tag{6.5}$$

and

$$\mathbb{E}[R^\alpha_{max}|h] = \int_0^\infty [1 - (F_{R^\alpha}(y))^h]dy = \int_0^\infty 1 - (1 - e^{-\frac{y^{2/\alpha}\phi}{2}})^h dy, \tag{6.6}$$

which is plotted in Fig. 6.5(b) for $\alpha = 4$ and $\phi = \pi/2$. Will the curves in Fig. 6.5(a) (b) have the relationship $a \log h + b$ with h? We can see that the maximum transmit energy increases with the number of hops for one connection in random networks. For example, for a two-dimensional random network with area 40×40 and density 1, the average number of hops per connection is about 34 using (6.20) with $\phi = \pi/2$. From Fig. 6.5(b), we can see $\mathbb{E}[R^4_{max}|h = 34]$ is about 30, indicating that the lifetime of a connection is only 1/30 of the lifetime

TABLE 6.2

COMPARISON OF TWO DIMENSIONAL REGULAR AND RANDOM NETWORKS ($\phi = \pi/2$) FOR A SINGLE CONNECTION WITH 10 HOPS AND 20 HOPS FOR $\alpha = 4$. g_{ave} AND g_{min} DENOTE THE AVERAGE PER-NODE THROUGHPUT AND END-TO-END THROUGHPUT.

	Regular network		Random network	
	10-hop	20-hop	10-hop	20-hop
g_{ave} of simple MAC	0.1296	0.1176	0.1124	0.1004
g_{min} of simple MAC	0.0960	0.0903	0.0762	0.0644
g_{ave} of opt. MAC	0.1802	0.1698	0.1575	0.1373
g_{min} of opt. MAC	0.1725	0.1611	0.1476	0.1256
$\mathbb{E}[R^{\alpha}]$	1	1	3.6	3.6
$\mathbb{E}[R^{\alpha}_{max}\|h]$	1	1	16.4	23.6

of a connection in a regular network, where $\mathbb{E}[d_0^{\alpha}] = 1$.

6.2.3 Comparisons

To fairly compare the two-dimensional regular and random networks (with adaptive power) in terms of path efficiency, we use a routing sector $\phi = \pi/2$ which is equivalent to nearest-neighbor routing in regular square grid networks. Table 6.2 compares the throughput and energy consumption (normalized) for single connections with 10 and 20 hops. For the random network, we can approximate the total energy consumption per connection as $\bar{h}^2\mathbb{E}[\frac{R^{\alpha}\Theta N_0}{-\ln p_{EE}}]$ using $\bar{h}$ from (6.20)

(see the Appendix of this chapter). We have

$$E_{tot} = (m^2-1)\bar{h}^2\mathbb{E}[R^\alpha]E_0 = (m^2-1)\left(\frac{0.769m}{\sqrt{\frac{\pi}{2\phi}}\frac{2}{\phi}\sin(\frac{\pi}{4})}\right)^2 \mathbb{E}[R^\alpha]E_0, \qquad (6.7)$$

where $E_0 = \frac{\Theta N_0}{-\ln p_{EE}}$. Using (6.3), (6.7) and simulation result, we compare the average end-to-end throughput and total energy consumption (normalized by E_0) in Table 6.3 for networks with area 15×15 and 30×30 (density 1).

6.3 Equal Transmit Power Strategy

Since strategies with equal transmit power are energy-balanced, we study schemes with and without retransmissions. Let the normalized SNR $\gamma_N := P_0/(\Theta N_0)$, from (2.5), resulting in a link reception probability $p_r^N = e^{-\frac{d^\alpha}{\gamma_N}}$.

6.3.1 Without retransmissions

For random line networks, the conditional link reception probability given $d = \max\{1, R\}$ is $p_r^N = e^{-\frac{d^\alpha}{\gamma_N}}$, since the internode distance R is exponentially distributed, the cumulative distribution function (cdf) is

$$F_{p_r^N}(y) = \begin{cases} e^{-(-\gamma_N \ln y)^{\frac{1}{\alpha}}}, & 0 \le y < y_{th}, \\ 1, & y \ge y_{th}, \end{cases}$$

where $y_{th} := e^{-\frac{1}{\gamma_N}}$ (see the Appendix for the proof).

TABLE 6.3

COMPARISON OF TWO DIMENSIONAL REGULAR AND RANDOM NETWORKS ($\phi = \pi/2$) FOR WHOLE NETWORK FOR THE NETWORKS WITH AREA 15×15 AND 30×30 AND DENSITY 1 FOR $\alpha = 4$.

	Regular network		Random network	
Area size	15×15	30×30	15×15	30×30
Average min. throughput	0.1799	0.1611	0.1595	0.1344
E_{tot} of analysis	52500	891750	$1.33 \cdot 10^5$	$2.14 \cdot 10^6$
E_{tot} of simulation			$1.26 \cdot 10^5$	$2.09 \cdot 10^6$

For $\alpha = \infty$,

$$F_{p_r^N}(y) = \begin{cases} e^{-1}, & 0 \leq y < y_{th}, \\ 1, & y \geq y_{th}. \end{cases} \tag{6.8}$$

This is of interest because it shows that for $\alpha \to \infty$, the model degenerates to a disk model. Fig. 6.6 (a) illustrates the cdf of the link reception probability for $\alpha = 4$ and $\gamma_N = 10$ in one-dimensional line networks. It is shown that with medium transmit power, very small link reception probabilities exists with a certain non-negligible probability. If $\gamma_N = 10$ and $\alpha = 4$, for example, the probability that p_r^N is below 10% is 0.11. Over an h-hop connection, the cdf of the minimum reception probability is

$$\mathbb{P}[\min\{p_{r1}^N, p_{r2}^N ... p_{rh}^N\} \leq y] = 1 - (\mathbb{P}[p_r^N > y])^h = 1 - (1 - F_{p_r^N}(y))^h. \tag{6.9}$$

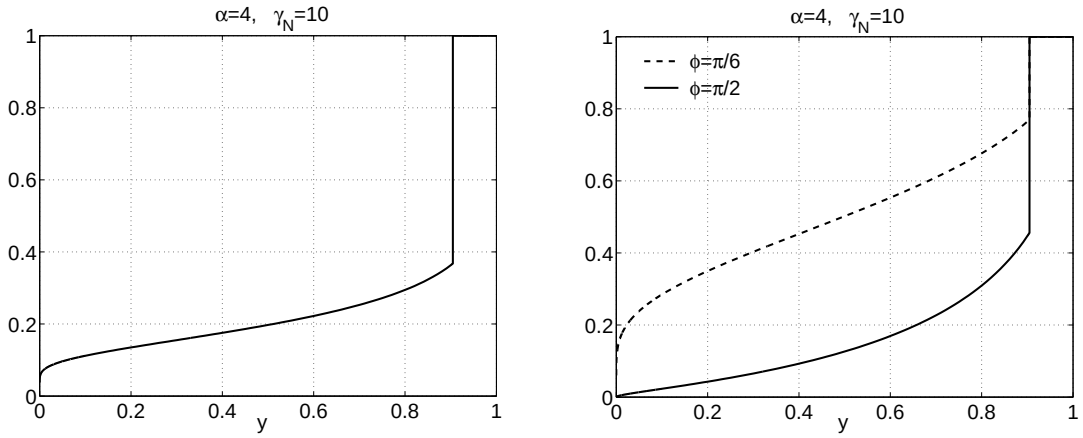

(a) (b)

Figure 6.6. Cdf of link reception probability p_r^N for (a) one-dimensional random networks and (b) two-dimensional random networks.

Therefore, for a 30-hop connection, even with $\gamma_N = 100$, corresponding to $p_r^N = 0.99$ for $d = 1$, there is a 25% chance that the minimum p_r^N is below 0.01 for $\alpha = 4$. This illustrates that strategies without power control will suffer from either very low end-to-end throughput or very high energy consumption (and interference) over short links.

For two-dimensional random networks, the distance between a node and its nearest neighbor in a sector ϕ is Rayleigh distributed [20]. Similar to the one-dimensional network, we obtain for the cdf of p_r^N

$$F_{p_r^N}(y) = \begin{cases} e^{-\frac{\phi}{2}(-\gamma_N \ln y)^{\frac{2}{\alpha}}}, & 0 \le y < y_{th}, \\ 1, & y \ge y_{th}, \end{cases}$$

where $y_{th} := e^{-\frac{1}{\gamma_N}}$. Fig. 6.6(b) illustrates the cdf of p_r^N for $\phi = \pi/6$ and $\phi = \pi/2$

for $\alpha = 4$ and $\gamma_N = 10$.

6.3.2 With retransmissions

The previous analysis indicates that the equal transmit power strategy may lead to very small p_r^N. Therefore, retransmissions are necessary. For an h-hop connection and desired end-to-end reliability p_{EE}, the desired link reliability should be $p_{EE}^{1/h}$. If $p_{EE}^{1/h} \leq p_r^N = e^{-\frac{d^\alpha}{\gamma_N}}$, no retransmission is needed. So, if $d > (\frac{-\gamma_N \ln p_{EE}}{h})^{1/\alpha}$, the number of transmissions for one hop is given by

$$n_t = \frac{\log(1 - p_{EE}^{1/h})}{\log(1 - p_r^N)} = \frac{\log(1 - p_{EE}^{1/h})}{\log(1 - e^{-\frac{d^\alpha}{\gamma_N}})}. \tag{6.10}$$

Combining the above expressions, we find

$$n_t = \begin{cases} 1, & d \leq D \\ \frac{\log(1-p_{EE}^{1/h})}{\log(1-e^{-\frac{d^\alpha}{\gamma_N}})}, & d > D. \end{cases} \tag{6.11}$$

where $D := (\frac{-\gamma_N \ln p_{EE}}{h})^{1/\alpha}$. Fig. 6.7(a) displays the mean transmission number per hop, $\mathbb{E}[n_t]$, and the average maximum transmission number $\mathbb{E}[n_{tmax}|h = 40]$ for 40-hop connections in two-dimensional random networks. The average energy consumption per hop for the retransmission strategy is $E_{retr} = \mathbb{E}[n_t]\gamma_N \Theta N_0$; for the adaptive power strategy it is $E_{adp} = \mathbb{E}[\frac{d^\alpha \Theta N_0}{-\ln p_{EE}{}^{1/h}}]$. Let β_E denote the energy ratio

$$\beta_E = \frac{E_{retr}}{E_{adp}} = \frac{-\gamma_N \ln p_{EE} \mathbb{E}[n_t]}{h\mathbb{E}[d^\alpha]}. \tag{6.12}$$

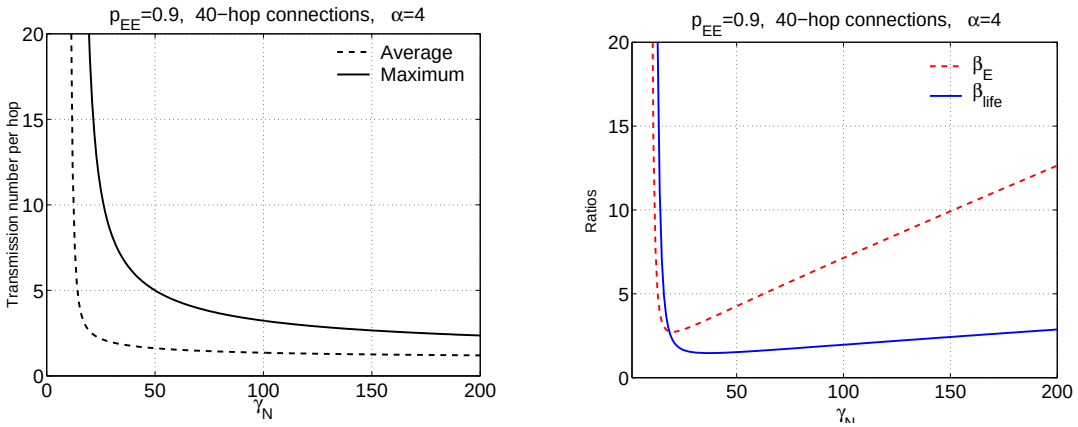

(a) (b)

Figure 6.7. Investigation of retransmission strategy for 40-hop connections in two dimensional random networks at $\alpha = 4$. (a) $\mathbb{E}[n_t]$ vs. γ_N and $\mathbb{E}[n_{tmax}|h = 40]$ vs. γ_N. (b) Energy ratio β_E vs. γ_N and lifetime ratio β_{life} vs. γ_N of the retransmissions strategy to the adaptive power strategy.

Since the maximum energy consumption determines the lifetime of the connections, we define the lifetime ratio for an h-hop connection as

$$\beta_{\text{life}} = \frac{-\gamma_N \ln p_{EE} \mathbb{E}[n_{tmax}|h]}{h\mathbb{E}[d^{\alpha}_{max}|h]}. \tag{6.13}$$

The energy ratio and lifetime ratio versus different γ_N are plotted in Fig. 6.7(b) for 40-hop connections in two dimensional random networks for $\alpha = 4$. It is shown that for the retransmission strategy, the minimum lifetime ratio can be achieved at $\gamma_N = 35$, $\beta_{\text{life}} = 1.5$; however the energy consumption is 3.4 times higher than for the of adaptive power strategy. The minimum energy ratio can be achieved at $\gamma_N = 20$, $\beta_E = 2.7$, but the average maximum transmission number is 20 and the average transmission number per hop is 2.6, which means for a 40-hop connection, 104 transmissions are needed on average.

6.4 Conclusions

The comparison of networks with regular and random topology shows that regular networks outperform random ones in terms of achievable throughput and, more significantly, in terms of energy consumption. The difference is bigger in 1-d networks than in 2-d networks due to the bigger variance of the distance distribution (exponential vs. Rayleigh). If we focus on a single multi-hop connection (2-d) and compare the maximum node energy consumption (that determines the lifetime of the connection) and the minimum per-node throughput (that determines the end-to-end throughput), the difference is even more prominent: for a path loss exponent of 4 and a connection of 10-20 hops, the lifetime of a connection in a random network is about 20× smaller, and the end-to-end throughput penalty is 25-30%, depending on the MAC scheme.

This analysis assumed that nodes adapt their transmit power according to the hop distance to keep the link reception probability p_r^N constant. Strategies with constant power would better balance the energy consumption among the nodes, but they are impractical since the connections would suffer from very low reception probabilities or intolerably high delay due to the many retransmissions that would become necessary. Clearly, the cause of these problems is the variance in the distances over which the nodes transmit. The only solution is to abandon the principle of nearest-neighbor routing and have every node transmit over a similar distance. For low latency, nodes should always transmit as far as possible, i.e., as far as the maximum available power permits. In so doing, the nodes chosen as relays approximately form a regular subnetwork, thereby emulating a regular topology. It has been shown in [18] that this "distance equalization" scheme also solves the problem of power amplifier inefficiencies, since it avoids power control

over a large dynamic range and, in turn, the use of the amplifiers at operating points with low efficiency (low power).

In terms of deployment, these results suggest that one should aim at a regular node spacing whenever possible. So, uniform coverage and efficient communication go hand in hand. This is addressed in Chapter 8.

6.5 Appendix

Pdf, cdf of link reception probability in random line networks. For random line networks where nodes are uniformly randomly placed in a line with density 1, the internode distance R is exponentially distributed with mean 1, which is $f_R(x) = e^{-x}u(x)$. The link reception probability over a distance d is

$$p_r^N = g(d) = e^{-\frac{d^\alpha}{\gamma_N}}, \qquad d = \max\{1, R\}. \tag{6.14}$$

where d is the effective internode distance, R is the Euclidean internode distance, and $\gamma_N := P_0/(\Theta N_0)$ is the normalized SNR. For $R \geq 1$, we can calculate the cdf as

$$\begin{aligned} F_{p_r^N}(y) &= \mathbb{P}[p_r^N \leq y] = \mathbb{P}[e^{-\frac{x^\alpha}{\gamma_N}} \leq y] = \mathbb{P}[x \geq (-\gamma_N \ln y)^{\frac{1}{\alpha}}] \\ &= \int_{(-\gamma_N \ln y)^{\frac{1}{\alpha}}}^{\infty} e^{-x} \mathrm{d}x = e^{-(-\gamma_N \ln y)^{\frac{1}{\alpha}}}, \qquad 0 \leq y < e^{-\frac{1}{\gamma_N}}. \end{aligned} \tag{6.15}$$

And the pdf as

$$f_{p_r^N}(y) = \frac{\mathrm{d}}{\mathrm{d}y}[F_{p_r^N}(y)] = -\frac{(-\gamma_N \ln y)^{\frac{1}{\alpha}} e^{-(-\gamma_N \ln y)^{\frac{1}{\alpha}}}}{\alpha y \ln y}, \qquad 0 \leq y < e^{-\frac{1}{\gamma_N}}. \tag{6.16}$$

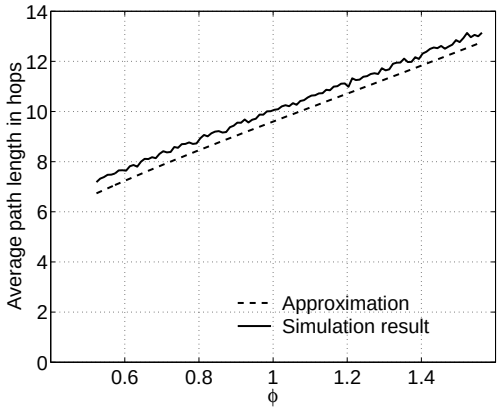

Figure 6.8. The approximation and simulation results of average path length in hops for two dimensional random network with area 15×15 and density 1.

For $R < 1$, $p_r^N = g(d) = e^{-\frac{1}{\gamma_N}}$, we have the cdf and pdf as

$$\begin{aligned} F_{p_r^N}(y) &= 1, && y \geq e^{-\frac{1}{\gamma_N}} \\ f_{p_r^N}(y) &= (1 - e^{-1})\delta(y - e^{-\frac{1}{\gamma_N}}), && y \geq e^{-\frac{1}{\gamma_N}} \end{aligned} \tag{6.17}$$

Average path length in hops for 2*-d random networks.* For two-dimensional random sensor networks (area $m \times m$, density 1, routing within sector ϕ, base station at (m, m)), we can approximate the average path length in hops from [8]

$$\bar{h} = \frac{\bar{r}}{\bar{R}\eta}. \tag{6.18}$$

where $\bar{r}$ denotes the expected distance between the source-destination pair, $\bar{R}$ the expected internode distance and η the expected path efficiency, where the path efficiency is the ratio between the Euclidean distance and the travelled distance.

From [45, Exercise 2.4.5], it is known that

$$\bar{r} = \left[\frac{\sqrt{2}}{3} + \frac{1}{3}\text{arctanh}(\frac{1}{\sqrt{2}})\right] m \approx 0.769m,$$
$$\bar{R} = \sqrt{\frac{\pi}{2\phi}}, \qquad \eta = \frac{2}{\phi}\sin(\frac{\phi}{2}). \tag{6.19}$$

So we have

$$\bar{h} \approx \frac{0.769m}{\sqrt{\frac{\pi}{2\phi}}\frac{2}{\phi}\sin(\frac{\phi}{2})}. \tag{6.20}$$

For $m = 15$, The approximation and simulation result of the expected number of hops are plotted in Fig. 6.8. Therefore, we can see that the average number of hops in one connection is increasing with the network size and sector angle ϕ.

CHAPTER 7

THROUGHPUT ANALYSIS OF FADING SENSOR NETWORKS WITH REGULAR AND RANDOM TOPOLOGIES

In previous chapters, the throughput of large networks with different topologies is obtained from simulation results. In this chapter, we present closed-form expressions of the average link throughput for sensor networks with a slotted ALOHA MAC protocol in Rayleigh fading channels. We compare networks with three regular topologies in terms of throughput, transmit efficiency, and transport capacity. In particular, for square lattice networks, we present a sensitivity analysis of the maximum throughput and the optimum transmit probability with respect to the signal-to-interference ratio threshold. For random networks with nodes distributed according to a two-dimensional Poisson point process, the average throughput is analytically characterized and numerically evaluated. It turns out that although regular networks have an only slightly higher average link throughput than random networks for the same link distance, regular topologies have a significant benefit when the end-to-end throughput in multihop connections is considered.

We define the (per-link) throughput as the expected number of successful packet transmissions of a given link per timeslot. The *end-to-end* throughput over a multihop connection, defined as the minimum of the throughput values of the links involved, is a performance measure of a route and the MAC scheme.

7.1 Slotted ALOHA MAC Scheme

We consider a variant of the slotted ALOHA channel access scheme, originally devised in [1], that takes advantage of spatial reuse. It is assumed, as in [6, 50, 65, 73], that in every timeslot, each node transmits independently with a certain fixed probability p. While often a "heavy traffic" model is used [50, 65], where nodes always have packets to transmit and p only reflects the channel access probability, we do not restrict ourselves to this "MAC-centric" case. Rather, we consider p to be composed of two factors, *i.e.*, $p = p_q p_t$, where p_q is the probability that there is a packet in a node's queue awaiting transmission, and p_t is the probability of transmission conditioned on having a packet in the queue (the channel access probability). So, p_q is given by the traffic model, p_t is the actual slotted ALOHA channel access probability, and p is the unconditioned probability of transmission. The heavy traffic case mentioned above corresponds to $p_q = 1$, $p_t = p$, and the other extreme case is $p_q = p$, $p_t = 1$, where Bernoulli traffic is generated with probability p_q and each node with a packet to transmit has immediate access to the channel. Since there is no need for a MAC scheme in this case, we may denote it as "traffic-centric". Hence the decomposition of p shows that the throughput analysis and optimization with respect to p in fact includes a range of traffic intensities and channel access probabilities. The Bernoulli traffic model is well justified by the following three observations: (1) In [73], it was shown that the traffic from a slotted ALOHA population of nodes can indeed be modeled as Bernoulli; (2) in [7, p. 278] it is pointed out that the re-transmission traffic is usually Bernoulli (since an unsuccessfully transmitted packet re-enters the queue); and (3) the Bernoulli traffic model is memoryless and thus the discrete-time counterpart of the ubiquitous Poisson model.

The traffic distribution in a sensor networks is usually spatially and temporally bursty, *i.e.*, busy periods alternate temporally and busy areas alternate spatially with periods and areas with little or no traffic. It may therefore be impractical to employ reservation-based MAC schemes such as TDMA and FDMA that require a substantial amount of coordination traffic and cannot be implemented efficiently and in a fully distributed fashion[1]. In any case, the slotted ALOHA scheme is the simplest meaningful MAC scheme and therefore provides a lower bound on the performance for more elaborate schemes. Since areas of the network or periods with little or no traffic pose no problems, our analysis focuses on and applies to busy areas and busy periods of the network where collisions are unavoidable and the throughput is interference-limited. During such a burst of traffic, we assume that the parameters p, p_q, and p_t remain constant. An important example of a busy area is certainly the critical area around the base station or fusion center, where traffic accumulation due to the many-to-one transmission scheme often results in heavy traffic [17] (see also Chapter 5).

7.2 The Rayleigh Fading Link Model with slotted ALOHA

The following theorem is an extension of Theorem 1 to slotted ALOHA.

Theorem 2 *In a Rayleigh fading network with slotted ALOHA, where nodes transmit at equal power levels with probability p, the success probability of a transmission given a desired transmitter-receiver distance d_0 and n other nodes at distances d_i $(i = 1, \ldots, n)$ is*

$$P_{s|d_0,\ldots,d_n} = \exp\Big(-\frac{\Theta N_0}{P_0 d_0^{-\alpha}}\Big) \cdot \prod_{i=1}^{n} \Big(1 - \frac{\Theta p}{\Big(\frac{d_i}{d_0}\Big)^{\alpha} + \Theta}\Big) \tag{7.1}$$

[1] In general this problem is NP-hard.

where P_0 is the transmit power, N_0 the noise power, and Θ the SINR threshold.

Proof: Let Q_0 denote the received power from the desired transmitter and Q_i, $i = 1, \ldots, n$, the received power from n potential interferers. All the received powers are exponentially distributed, *i.e.*, $p_{Q_i}(q_i) = 1/\bar{Q}_i e^{-q_i/\bar{Q}_i}$, where $\bar{Q}_i$ denotes the average received power $\bar{Q}_i = P_i d_i^{-\alpha}$. The cumulated interference power at the receiver is

$$I = \sum_{i=1}^{n} S_i Q_i,$$

where S_i is a sequence of iid Bernoulli random variables with $\mathbb{P}(S_i = 1) = p$ and $\mathbb{P}(S_i = 0) = 1 - p$. The success probability of a transmission is[2]

$$\begin{aligned}
P_{s|d_0,d_1,\ldots,d_n} &= \mathbb{E}_I\Big[\mathbb{P}[Q_0 \geqslant \Theta(I + N_0) \mid I\,]\Big] \\
&= \mathbb{E}_{Q,S}\Big[\exp\Big(-\frac{\Theta(\sum_{i=1}^{n} S_i Q_i + N_0)}{\bar{Q}_0}\Big)\Big] \\
&= \exp\Big(-\frac{\Theta N_0}{\bar{Q}_0}\Big)\mathbb{E}_{Q,S}\Big[\prod_{i=1}^{n}\exp\Big(-\frac{\Theta(S_i Q_i)}{\bar{Q}_0}\Big)\Big] \\
&= \exp\Big(-\frac{\Theta N_0}{P_0 d_0^{-\alpha}}\Big)\prod_{i=1}^{n}\Big\{P(S_i = 1)\cdot\int_0^{\infty}\exp\Big(-\frac{\Theta q_i}{\bar{Q}_0}\Big)p_{Q_i}(q_i)\mathrm{d}q_i + P(S_i = 0)\Big\} \\
&= \exp\Big(-\frac{\Theta N_0}{P_0 d_0^{-\alpha}}\Big)\prod_{i=1}^{n}\Big(\frac{p}{1 + \Theta\big(\frac{d_0}{d_i}\big)^{\alpha}} + 1 - p\Big) \\
&= \exp\Big(-\frac{\Theta N_0}{P_0 d_0^{-\alpha}}\Big)\prod_{i=1}^{n}\Big(1 - \frac{\Theta p}{\Big(\frac{d_i}{d_0}\Big)^{\alpha} + \Theta}\Big) \qquad (7.2)
\end{aligned}$$

□

Since the throughput in large sensor networks is limited by the interference, in the following, we focus on the interference part (the second factor of (7.2),

[2]A similar calculation has been carried out in Theorem 1 for the case where in every timeslot it is known exactly who is transmitting. In contrast, Theorem 2 incorporates the uncertainty at the MAC level: we only assume we know the probability of a transmission, but not exactly who is transmitting in every timeslot.

assuming $N_0 = 0$) to determine bounds that are fundamental in the sense that they cannot be exceeded even if the transmit power is not constrained. The first exponential term is easily evaluated if $N_0 \neq 0$.

Corollary 2.1 *Under the same assumptions as in Theorem 2 but with $N_0 = 0$ and unit transmit power $P_i = 1$, the success probability given a desired link of normalized distance $r_0 = d_0/d_0 = 1$ and n other nodes at normalized distances $r_i = d_i/d_0$ is:*

$$P_{s|r_0,r_1,\ldots,r_n} = \prod_{i=1}^{n} \Big(1 - \frac{p}{1 + {r_i}^{\alpha}/\Theta}\Big) = \mathcal{L}_I(\Theta), \tag{7.3}$$

which is the Laplace transform of the interference power I evaluated at the SIR threshold Θ.

Proof: With unit transmit power, the mean power from the i-th interferer at distance r_i is $1/r_i^{\alpha}$. The Laplace transform of the exponential distribution with mean $1/\mu$ is $\mu/(\mu + s)$, thus the Laplace transform of I is [46]:

$$\mathcal{L}_I(s) = \prod_{i=1}^{n} \Big(\frac{p r_i^{\alpha}}{r_i^{\alpha} + s} + 1 - p\Big) = \prod_{i=1}^{n} \Big(1 - \frac{p}{1 + r_i^{\alpha}/s}\Big) \tag{7.4}$$

From (7.2) and with $r_i = d_i/d_0$ (normalized distances), if $N_0 = 0$,

$$P_{s|r_0,r_1,\ldots,r_n} = \prod_{i=1}^{n} \Big(1 - \frac{p}{1 + {r_i}^{\alpha}/\Theta}\Big) \tag{7.5}$$

we get (7.3). □

7.3 Regular Networks

In this section, we investigate networks with three regular topologies (square, triangle, hexagon) in which every node has the same number of nearest neighbors

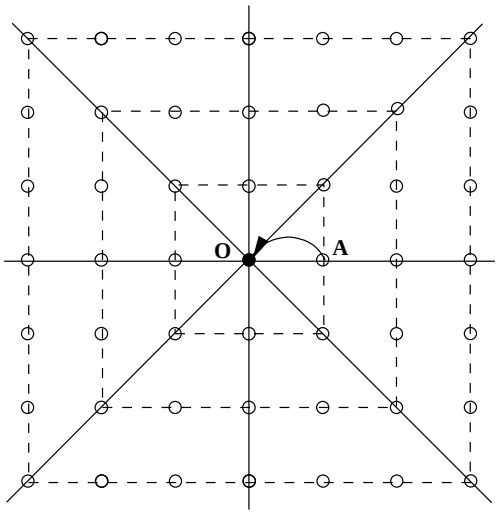

Figure 7.1. The topology of a square network. Node O is the receiver and node A is the desired transmitter such that the link distance $d_0 = |OA| = 1$.

and the same distance to all nearest neighbors.

7.3.1 Square networks

We first analyze square networks with N nodes placed in the vertices of a square grid with distance 1 between all pairs of nearest nodes (density 1). The next-hop receiver of each packet is one of the four nearest neighbor nodes of the transmitter, so the transmitter-receiver distance $d_0 = 1$. If the receiver node O is located in the center of the network as shown in Fig. 7.1 and node A is the desired transmitter, the success probability for node O based on (7.5) can be written as:

$$P_s(p) = \left(1 - \frac{\Theta p}{1^\alpha + \Theta}\right)^3 \cdot \left(1 - \frac{\Theta p}{(\sqrt{2})^\alpha + \Theta}\right)^4 \times \prod_{i=2}^{\sqrt{N}/2} \left\{\left(1 - \frac{\Theta p}{i^\alpha + \Theta}\right)^4 \cdot \left(1 - \frac{\Theta p}{(\sqrt{2i^2})^\alpha + \Theta}\right)^4 \cdot \prod_{j=1}^{i-1} \left(1 - \frac{\Theta p}{(\sqrt{i^2 + j^2})^\alpha + \Theta}\right)^8\right\}. \tag{7.6}$$

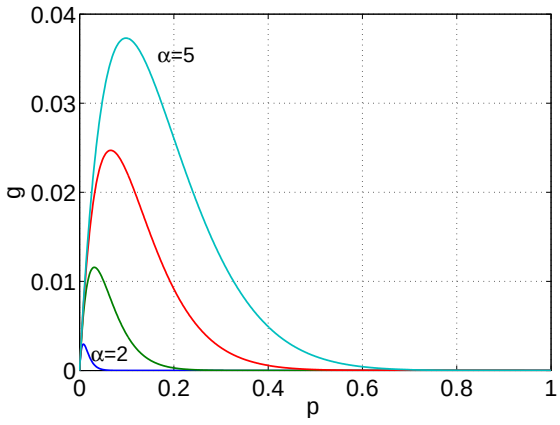

Figure 7.2. The analytic throughput $g(p)$ based on equation (7.6) for a square network with 40×40 nodes, with $\Theta = 10$.

The first term in (7.6) accounts for the other three nearest neighbor nodes of the receiver; the second term for the 4 diagonal nodes at distance $\sqrt{2}$; all the other terms from the nodes located on the dashed squares with edge ≥ 2 in Fig. 7.1. The throughput[3] is given by

$$g(p) = p(1-p)P_s(p), \tag{7.7}$$

where p is the probability that A transmits and $1-p$ is the probability that O does not transmit in the same timeslot. Note that g is the throughput achievable with a simple ARQ scheme (with error-free feedback) [3]. The analytic throughput $g(p)$ based on (7.6) and (7.7) for a regular square network with 40×40 nodes with node density $\lambda = 1$ is displayed in Fig. 7.2. For $\alpha = 4$, the maximum throughput $g_{\max} = 0.0247$ is achieved at an optimal transmit probability $p_{\text{opt}} = 0.066$. The transmit efficiency, defined as $T_{\text{eff}} = g_{\max}/p_{\text{opt}}$, is 37.4%.

For the *sensitivity* analysis of the throughput with respect to Θ, we need to

[3]The throughput is calculated as the throughput of the center link of the busy area under consideration. This is the worst case since most other nodes experience a lower interference. In the case of infinite networks, the interference distribution is the same at every node.

determine $p_{\text{opt}}(\Theta)$ and $g_{\max}(\Theta)$. We use three analytic approximations for $p_{\text{opt}}(\Theta)$ and $g_{\max}(\Theta)$. From (7.5), g can be written as

$$g = p(1-p)\prod_{i=1}^{n}\Big(1 - \frac{p}{1+r_i^{\alpha}/\Theta}\Big), \tag{7.8}$$

where $r_i = d_i/d_0$.

Since $p_{\text{opt}} = \arg\max_p g(p) = \arg\max_p \log\big(g(p)\big)$, we maximize

$$\log(g) = \log(p) + \log(1-p) + \sum_{i=1}^{n}\log\Big(1 - \frac{p}{1+r_i^{\alpha}/\Theta}\Big), \tag{7.9}$$

using $\log(1+x) \approx x$ for small x,[4] yielding

$$p_{\text{opt}}^2 - p_{\text{opt}}(1+2s) + s = 0, \tag{7.10}$$

with

$$s = \frac{1}{\sum_{i=1}^{n}\frac{1}{1+r_i^{\alpha}/\Theta}}. \tag{7.11}$$

Note $r_i = d_i$ for $d_0 = 1$. So, p_{opt} is given by

$$p_{\text{opt}} = s + \frac{1}{2}\Big(1 - \sqrt{1+4s^2}\Big). \tag{7.12}$$

$g_{\max}$ can be obtained by $g_{\max} = p_{\text{opt}}(1-p_{\text{opt}})P_s(p_{\text{opt}})$, where $P_s(p_{\text{opt}})$ is obtained by plugging p_{opt} into (7.6). This method is called *Analytic 1.*

For $\alpha = 4$, we use i^2 to approximate d_i^4 for the nodes located in one quadrant. As shown in Fig. 7.3, the distance of node i ($i = 1, \ldots, 8$) in the first quadrant to

[4]The approximation is accurate for p in the range of interest, *i.e.*, $0 < p < 0.3$.

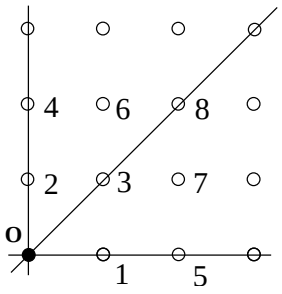

Figure 7.3. Node numbering scheme pertaining to Table 7.1 for nodes in the first quadrant of a square network. O is the receiver.

TABLE 7.1

COMPARISON OF d_i^4 AND i^2.

i	1	2	3	4	5	6	7	8
d_i^4	1	1	4	16	16	25	25	64
i^2	1	4	9	16	25	36	49	64

the receiver node O is d_i.

Table 7.1 compares d_i^4 and i^2 for $i = 1, \ldots, 8$. By Euler's summation formula, $d_i^4 \approx i^2$ allows a simplification (the node at distance 1 is the desired transmitter):

$$\sum_{i=2}^{k+1} \frac{1}{1 + i^2/\Theta} \approx \sqrt{\Theta}\Big(\arctan \frac{k + 3/2}{\sqrt{\Theta}} - \arctan \frac{3}{2\sqrt{\Theta}} \Big). \tag{7.13}$$

For $k \to \infty$,

$$s \approx \frac{1}{4\sqrt{\Theta}\Big(\frac{\pi}{2} - \arctan \frac{3}{2\sqrt{\Theta}} \Big)}, \tag{7.14}$$

where the factor 4 in (7.14) comes from the fact that nodes are located in 4

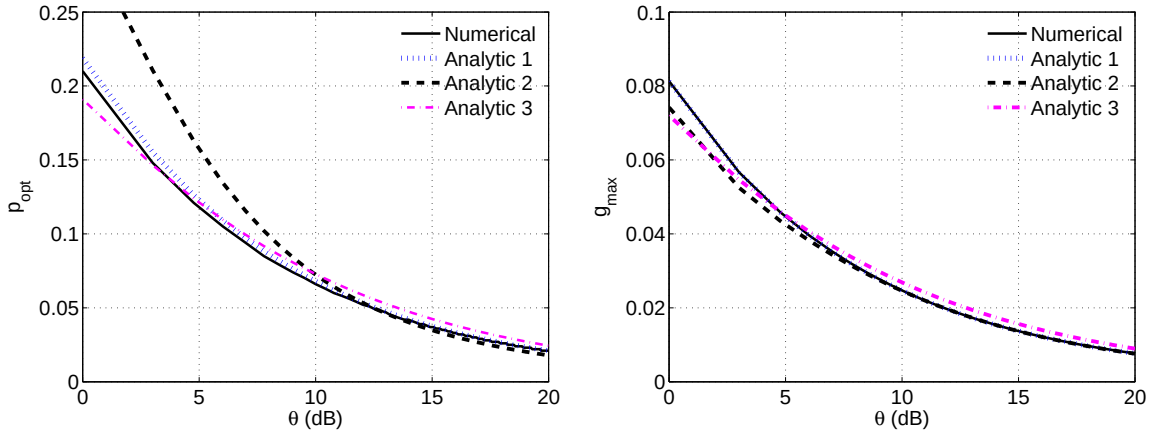

(a) (b)

Figure 7.4. For a square network with 40×40 nodes and $\alpha = 4$, the numerical results and analytic results from *Analytic 1, Analytic 2* and *Analytic 3* for (a) the relationship between p_{opt} and Θ; (b) the relationship between $g_{\max}$ and Θ.

quadrants. Plugging (7.14) into (7.12) is our method *Analytic 2*.

In method *Analytic 3*, we use the approximation $s \approx 1/(4\sqrt{\Theta})$, which is within $\mp 20\%$ for the practical range $9/(2\cot(0.8))^2 \approx 2.4 < \Theta < 9/(2\cot(1.2))^2 \approx 14.9$, and substitute it into (7.12), which yields

$$p_{\text{opt}} = \frac{1}{4\sqrt{\Theta}} + \frac{1}{2}\Big(1 - \sqrt{1 + \frac{1}{4\Theta}}\ \Big). \tag{7.15}$$

Based on (7.9) and (7.11), $g_{\max}$ is given by

$$g_{\max} = p_{\text{opt}}(1 - p_{\text{opt}})\ e^{-p_{\text{opt}}/s}. \tag{7.16}$$

The numerical result obtained by direct maximization of (7.6) for different Θ is compared with the results from the three analytical approximations in Fig. 7.4. In *Analytic 2*, approximating interfering nodes at distance d_i by the larger distance

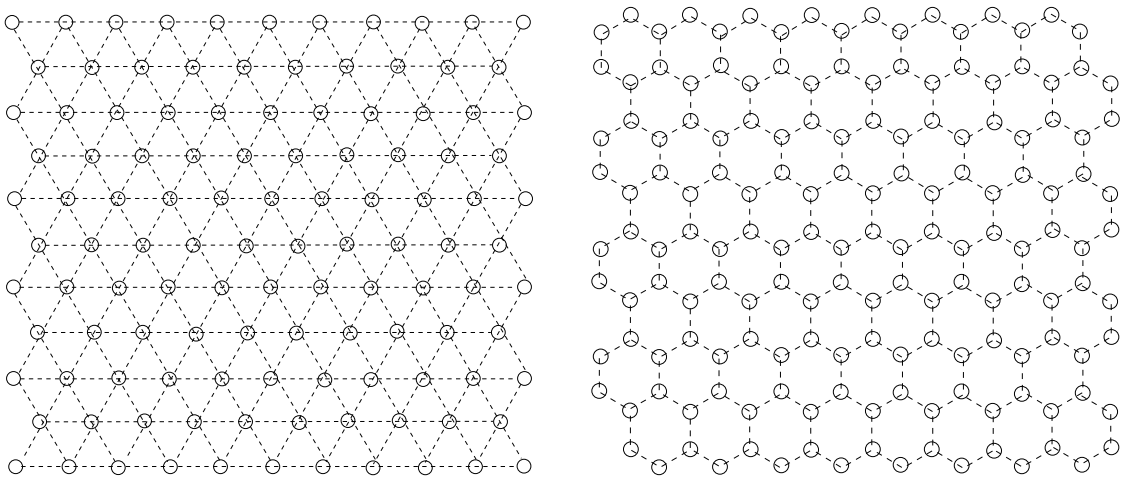

Figure 7.5. The topology of (a) triangle network and (b) hexagon network

$i^{1/2}$ (shown in Table 7.1) results in lower interference. The interference has a more significant impact on the throughput (and p_{opt}) for small Θ (see (7.13)). Thus for small Θ, this lower interference leads to a higher p_{opt} than for *Analytic 1.* The transmit efficiency is $T_{\text{eff}} = g_{\max}/p_{\text{opt}} = (1 - p_{\text{opt}})e^{-p_{\text{opt}}/s}$, which is monotonically increasing from $\lim_{s\to 0} T_{\text{eff}} = e^{-1} \approx 0.37$ to $\lim_{s\to\infty} T_{\text{eff}} = 1/2$. The upper bound is achieved if the interference goes to zero, in which case $p_{\text{opt}} = 1/2$ and $g_{\max} = 1/4$. For the lower bound, as $s \to 0$, we have $p_{\text{opt}} \to 0$ and $g_{\max} \to 0$, and T_{eff} converges to e^{-1}. Hence s is a measure for spatial reuse. Indeed for $s \to 0$, which happens for $\alpha \to 0$ [5] or $\Theta \to \infty$, the network does not permit any spatial reuse. In this case, the transmit efficiency reduces to the efficiency of conventional slotted ALOHA [1], where for a network with N nodes, $p_{opt} = 1/N$ and $T_{\text{eff}} = \lim_{N\to\infty}(1-1/N)^{N-1} = e^{-1}$, as pointed out earlier [65]. The fact that our limit coincides with the limit for conventional slotted ALOHA further validates our approximations.

[5] In fact, $\alpha \to 2$ is sufficient for infinite networks.

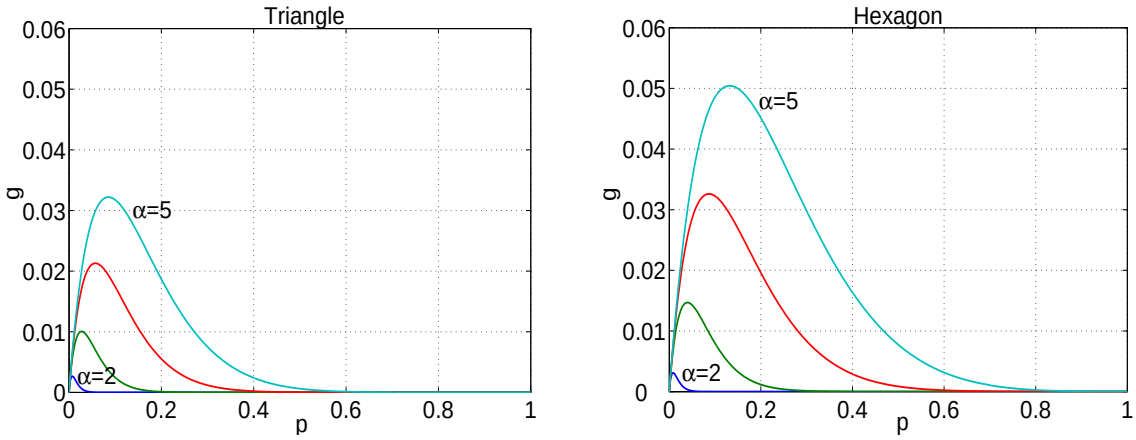

Figure 7.6. The analytic throughput $g(p)$ vs. p for two-dimensional networks with (a) triangle topology and (b) hexagon topology, where $\Theta = 10$ and $N = 1600$ nodes.

7.3.2 Triangle networks and hexagon networks

Other regular topologies of interest are the triangle topology and its dual, the hexagon topology (Fig. 7.5). For each triangle, there are three vertices and six nearest neighbors for each vertex, while for the hexagon, there are six vertices for each hexagon and three nearest neighbors for each vertex. Again, the next-hop receiver of each packet is one of the nearest neighbor nodes of the transmitter, so the transmitter-receiver distance d_0 is equal to the side length of the regular polygon. In the triangle network, each node is located in a hexagon with area $(\sqrt{3}d_0^2)/2$. For node density is 1, $d_0^2 = 2/\sqrt{3}$. Similarly, for hexagon networks, $d_0^2 = 4/(3\sqrt{3})$.

Similar to the calculation of square lattice networks as in (7.6), we obtain the relationship between the throughput g and the transmit probability p and compare the performance of triangle and hexagon networks in Fig. 7.6. For a fair comparison, we introduce the *transport capacity* which can be defined as

TABLE 7.2

COMPARISON OF SQUARE, TRIANGLE AND HEXAGON NETWORKS FOR $\alpha = 4$ AND $\Theta = 10$, WHERE p_{opt}, $g_{\max}$ AND T_{eff} DENOTE THE OPTIMUM TRANSMIT PROBABILITY, MAXIMUM THROUGHPUT AND TRANSMIT EFFICIENCY.

	p_{opt}	$g_{\max}$	T_{eff}	d_0	$g_{\max} d_0$
Square	0.0660	0.0247	0.37	1.0	0.0247
Triangle	0.0570	0.0213	0.37	1.0746	0.0229
Hexagon	0.0870	0.0326	0.37	0.8774	0.0286

$Z := g_{max} d_0$. The results for square, triangle, and hexagon networks for $\alpha = 4$ are shown in Table 7.2. The performance difference among the three topologies can be explained by the distance and number of the potential interfering nodes. Note that the transmit efficiency T_{eff} is very close to the one of conventional slotted ALOHA and does not depend on the topology.

7.4 Random Networks

Here, we assume that the positions of the nodes constitute a Poisson point process[6]. In the following, we will investigate the throughput averaged over network realizations when the transmitter-receiver distance d_0 is fixed (Section 7.4.1) and not fixed (Section 7.4.2).

[6]For large networks, this is equivalent to a uniformly random distribution for all practical purposes.

7.4.1 Average throughput for fixed d_0

In this case, we assume the distance between the desired transmitter and receiver is fixed and there are N other nodes constituting a two-dimensional Poisson point process. Although (7.5) gives the success probability conditioned on node distances, we still need to find the joint density of d_1, $d_2, \ldots$, d_N (ordered distances). It is well known that for one-dimensional Poisson point processes with density λ, the ordered distance from nodes to the desired receiver form the arrival times of a Poisson process [46]. The inter-arrival intervals are iid exponential with parameter λ:

$$f_{d_i - d_{i-1}}(x_i - x_{i-1}) = \lambda e^{-\lambda(x_i - x_{i-1})} \tag{7.17}$$

So for the ordered distance $0 \le d_1 \le \cdots \le d_N$, the joint density function of the inter-arrival intervals is

$$\begin{aligned} & f_{d_1, d_2, \cdots, d_N}(x_1, x_2, \cdots, x_N) \\ =& f_{d_1, \cdots, d_N - d_{N-1}}(x_1, x_2 - x_1, \cdots, x_N - x_{N-1}) \\ =& \left(\lambda e^{-\lambda x_1}\right)\left(\lambda e^{-\lambda(x_2 - x_1)}\right) \cdots \left(\lambda e^{-\lambda(x_N - x_{N-1})}\right) \\ =& \lambda^N e^{-\lambda x_N}, \qquad 0 \le x_1 \le x_2 \le \cdots \le x_N. \end{aligned} \tag{7.18}$$

When nodes are distributed according to a two-dimensional Poisson point process with density λ, the squared ordered distances from the desired receiver have the same distribution as the arrival times of a Poisson process with density $\lambda\pi$ [46].

The squared ordered distances have a joint distribution with density

$$f_{d_1^2,\cdots,d_N^2}(x_1,\cdots,x_N) = (\lambda\pi)^N e^{-\lambda\pi x_N},$$
$$0 \le x_1 \le x_2 \le \cdots \le x_N, \tag{7.19}$$

because from [26], we have

$$f_{d_i^2 - d_{i-1}^2}(x_i - x_{i-1}) = \lambda\pi e^{-\lambda\pi(x_i - x_{i-1})}. \tag{7.20}$$

The conditional success probability can be written as (see (7.5))

$$P_{s|d_0,d_1,\cdots,d_N} = \prod_{i=1}^{N} \frac{(d_i^2)^{\frac{\alpha}{2}} + (1-p)\Theta d_0^{\alpha}}{(d_i^2)^{\frac{\alpha}{2}} + \Theta d_0^{\alpha}}. \tag{7.21}$$

Integrating (7.21) with respect to the joint density (7.19), and in particular, evaluating it for $\alpha = 4$, we obtain

$$P_{s|d_0} = \int_0^{\infty} (\lambda\pi)^N e^{-\lambda\pi x_N} \Big\{ \int_0^{x_N} \cdots \int_0^{x_2} \prod_{i=1}^{N} \frac{x_i^2 + (1-p)\Theta d_0^4}{x_i^2 + \Theta d_0^4} \mathrm{d}x_1 \cdots \mathrm{d}x_{N-1} \Big\} \mathrm{d}x_N. \tag{7.22}$$

By applying a similar inductive technique as in [46], it can be shown that

$$\int_0^{x_N} \cdots \int_0^{x_2} \prod_{i=1}^{N-1} \frac{x_i^2 + (1-p)\Theta d_0^4}{x_i^2 + \Theta d_0^4} \mathrm{d}x_1 \cdots \mathrm{d}x_{N-1}$$
$$= \frac{1}{(N-1)!} \Big(x_N - p\sqrt{\Theta d_0^4} \arctan\big(\frac{x_N}{\sqrt{\Theta d_0^4}}\big) \Big)^{N-1}. \tag{7.23}$$

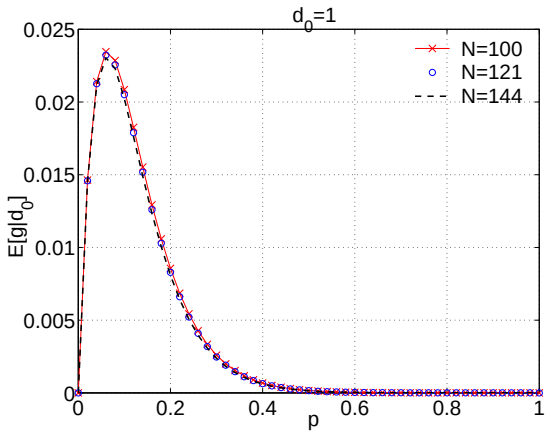

Figure 7.7. For $\alpha = 4$ and $\Theta = 10$, the analytical average throughput $\mathbb{E}[g|d_0 = 1]$ based on equation (7.24) for networks with node number $N = 100$, 121 and 144.

Combining (7.22) and (7.23), we have

$$P_{s|d_0} = \int_0^\infty \frac{(\lambda\pi)^N}{(N-1)!} e^{-\lambda\pi x} \frac{x^2 + (1-p)\Theta d_0^4}{x^2 + \Theta d_0^4} \Big(x - p\sqrt{\Theta d_0^4} \arctan\big(\frac{x}{\sqrt{\Theta d_0^4}}\big)\Big)^{N-1} \mathrm{d}x. \tag{7.24}$$

Based on (7.24), we numerically evaluate the average throughput $\mathbb{E}[g|d_0] = p(1-p)P_{s|d_0}$ (averaged over all network realizations) and plot it as a function of p in Fig. 7.7 for a network with node numbers $N = 100$, 121 and 144, where $d_0 = 1$. It is shown that they are very close, indicating that only a portion of the nodes interfere at the receiver and nodes further away have little impact on the transmission.

7.4.2 Average throughput for variable d_0

In the previous analysis, we assumed that the transmitter-receiver distance d_0 is fixed and there are N potential interfering nodes uniformly distributed. Now we assume that the receiver located at the center selects its nearest neighbor

node as its desired transmitter. Then there are $N-1$ nodes further away than the desired transmitter. The distance to the nearest neighbor has the Rayleigh density function (as shown in [21]):

$$f_{d_0}(x) = 2\pi x e^{-\pi x^2}. \tag{7.25}$$

Since d_0 is the nearest distance, d_i^2 in (7.21) can be varying from d_0^2 to d_{i+1}^2. So we integrate x_i from d_0^2 to x_{i+1}:

$$\begin{aligned} P_{s|d_0} = &\int_{d_0^2}^{\infty} f_{d_1^2,\ldots,d_{N-1}^2|d_0^2}(x_1,\ldots,x_{N-1}|d_0^2)\Big\{\int_{d_0^2}^{x_{N-1}} \\ &\cdots\int_{d_0^2}^{x_2}\prod_{i=1}^{N-1}\frac{x_i^2+(1-p)\Theta d_0^4}{x_i^2+\Theta d_0^4}\mathrm{d}x_1\ldots\mathrm{d}x_{N-2}\Big\}\mathrm{d}x_{N-1} \end{aligned} \tag{7.26}$$

and

$$\begin{aligned} &f_{d_1^2,\ldots,d_{N-1}^2|d_0^2}(x_1,\ldots,x_{N-1}|d_0^2) = (\lambda\pi)^{N-1}e^{-\lambda\pi(x_{N-1}-d_0^2)}, \\ &\qquad \text{where}\ \ 0\le d_0^2\le x_1\le\cdots\le x_{N-1}. \end{aligned} \tag{7.27}$$

By induction, it can be shown that

$$\begin{aligned} &\int_{d_0^2}^{x_{N-1}}\cdots\int_{d_0^2}^{x_2}\prod_{i=1}^{N-2}\frac{x_i^2+(1-p)\Theta d_0^4}{x_i^2+\Theta d_0^4}\mathrm{d}x_1\ldots\mathrm{d}x_{N-2} \\ =&\frac{1}{(N-2)!}\Big\{x_{N-1}-d_0^2-p\sqrt{\Theta d_0^4}\cdot\Big[\arctan\big(\frac{x_{N-1}}{\sqrt{\Theta d_0^4}}\big)-\arctan\big(\frac{d_0^2}{\sqrt{\Theta d_0^4}}\big)\Big]\Big\}^{N-2}. \end{aligned} \tag{7.28}$$

The success probability is $P_{s|d_0}$ averaged over d_0:

$$P_s = \int_0^{\infty} f_{d_0}(x)P_{s|d_0}\mathrm{d}x \tag{7.29}$$

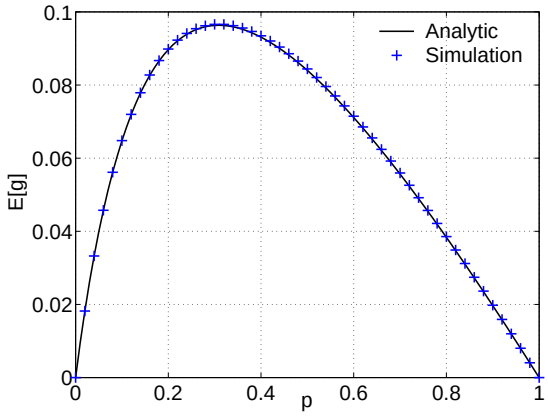

Figure 7.8. For $\alpha = 4$ and $\Theta = 10$, $\mathbb{E}[g]$ vs. p for random network with $N = 144$. The analytic result from (7.26) and (7.29) is displayed by solid line; the simulation result over 10000 runs by + mark.

Substituting (7.27) and (7.28) into (7.26) and evaluating (7.29) with (7.25), we obtain the relationship between $\mathbb{E}[g] = p(1-p)P_s$ and p, which is plotted in Fig. 7.8. It is shown that the analytic (solid line) and simulation result (marked by +) match perfectly.

Fig. 7.8 implies that random networks have better average throughput for local data exchange than regular networks. This can be explained by d_0, the transmitter-receiver distance. In random networks, a variable d_0 leads to a variable throughput. Fig. 7.9 (a) displays $\mathbb{E}[g|d_0]$ vs. p for d_0 from 0.5 to 1.5. Fig. 7.9 (b) shows the relationship for $d_0 = 0.1$, 0.5, 1.0 and 1.5. Not surprisingly, smaller d_0 results in higher throughput. For the variable d_0 case, it is assumed that the desired transmitter is the nearest neighbor of the receiver. With the pdf of (7.25), the probability that d_0 is greater than 1 (the transmitter-receiver distance in the square lattice network) is $\mathbb{P}[d_0 > 1] = e^{-\pi} = 0.043$. So for most nodes, the received signal power from the desired transmitter is greater than that in regular networks. In Fig. 7.9 (b), for $d_0 = 0.1$, it is shown that the strong signal power resulting from

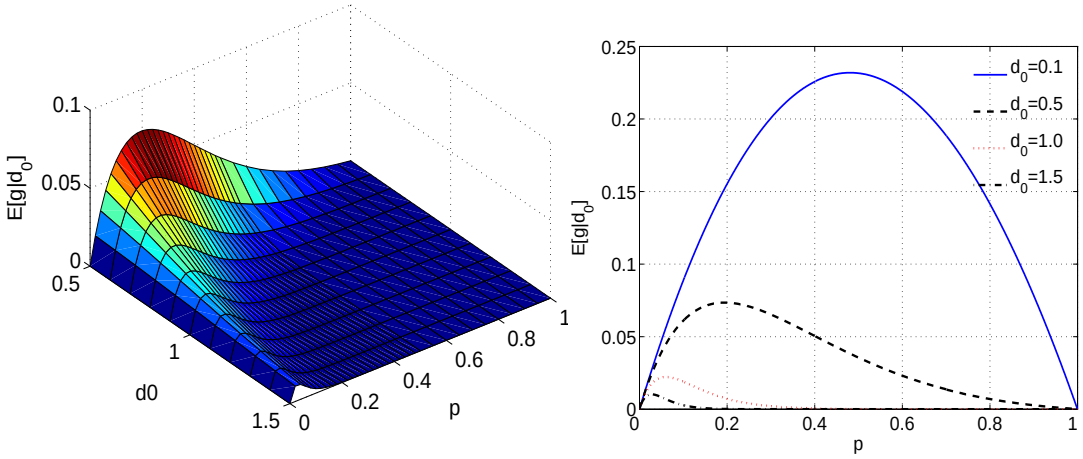

Figure 7.9. For $\alpha = 4$ and $\Theta = 10$, average throughput (a) $\mathbb{E}[g|d_0]$ vs. p for d_0 from 0.5 to 1.5. (b) $\mathbb{E}[g|d_0]$ vs. p for $d_0 = 0.1$, 0.5, 1.0 and 1.5.

very small d_0 offsets the impact of interference even for high transmit probabilities p.

Now consider the generic routing strategy from [21]: each node in the path sends packets to its nearest neighbor that lies within a sector ϕ, i.e., within $\pm\phi/2$ of the source-destination direction. The previous scheme where d_0 is obtained as the distance to the nearest neighbor makes no progress in the source-destination direction. Such a choice of d_0 would correspond to routing within $\phi = 2\pi$, clearly an inefficient choice of ϕ. More sensible is $\phi \leq \pi$. Let d_0 be the distance to the nearest neighbor within sector ϕ. The probability density of d_0 is given by [21]:

$$f_{d_0}(x) = x\phi e^{-x^2\phi/2}. \tag{7.30}$$

If the routing sector $\phi = \pi/2$, then $\mathbb{E}[d_0] = 1$. For $d_0 = 1$, Fig. 7.10 displays the throughput for square network and random network with $N = 1600$. It turns out that for the same transmitter-receiver distance, square networks have a slightly

higher average throughput than random networks.

We compare the transport capacity $g_{\max}d_0$ of regular and random networks. Fig. 7.11 (a) shows $g_{\max}$ vs. d_0 and p_{opt} vs. d_0 for a random network. Fig. 7.11 (b) compares the transport capacity of random and regular networks. It is shown that at a specific transmitter-receiver distance d_0, regular networks slightly outperform random networks in terms of transport capacity.

7.4.3 End-to-end throughput g_{EE} in a random network

In wireless sensor networks with multihop communication, the end-to-end throughput (the minimum of the throughput values of the links involved) of a route with an average number of hops is a better performance indicator than the average throughput. For two-dimensional random sensor networks (busy area $m \times m$, density 1, routing within sector ϕ) with uniformly randomly selected source and fixed destination located at the corner[7], As mentioned in the Appendix of Chapter 6, we can approximate the average path length in hops $\bar{h}$ by plugging (6.19) into:

$$\bar{h} \approx \frac{\bar{r}}{\bar{R}\eta}. \tag{7.31}$$

where $\bar{r}$ denotes the expected distance between the source and the destination, $\bar{R}$ the expected hop length and η the expected path efficiency, where the path efficiency is the ratio between the Euclidean distance and the travelled distance of a path. To evaluate the end-to-end throughput of a route with $\bar{h}$ hops, we use a semi-analytic approach by generating an $\bar{h}$-hop path with each hop length obtained as a realization of R according to the pdf in (7.30), and evaluate the throughput of each hop based on Fig. 7.9 (a). The average end-to-end throughput

[7]For the many-to-one traffic typical in sensor networks, we assume the data sink for all connections to be in one of the corners of the (square) network.

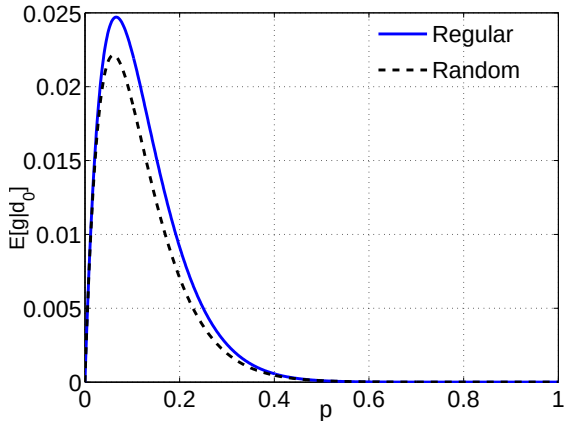

Figure 7.10. Comparison of the average throughput of regular square network and random network. For both networks, $N = 1600$, $d_0 = 1$, $\alpha = 4$ and $\Theta = 10$.

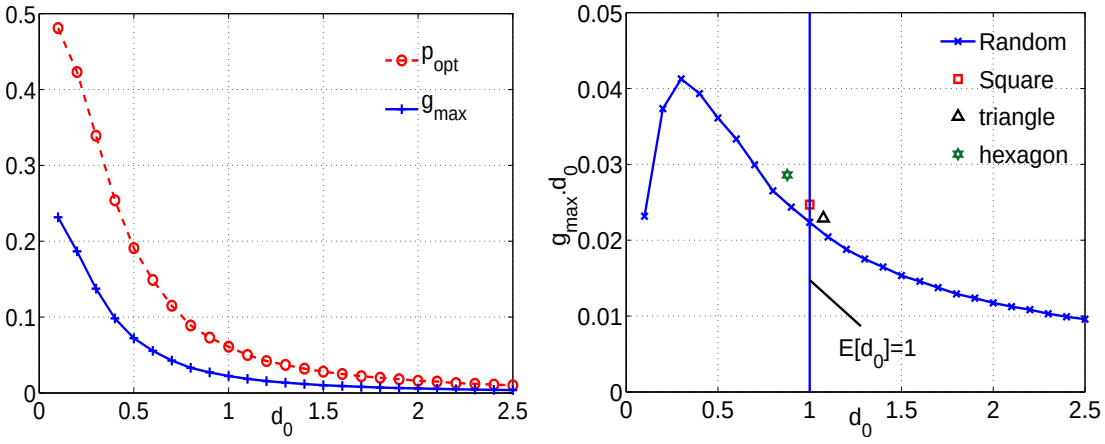

(a) (b)

Figure 7.11. With $N = 1600$, $\alpha = 4$ and $\Theta = 10$, (a) $g_{\max}$ vs. d_0 and p_{opt} vs. d_0 for a random network, (b) transport capacity $g_{\max} d_0$ for random and regular networks with the same size and node density. For random networks, $\mathbb{E}[d_0] = 1$ for $\phi = \pi/2$.

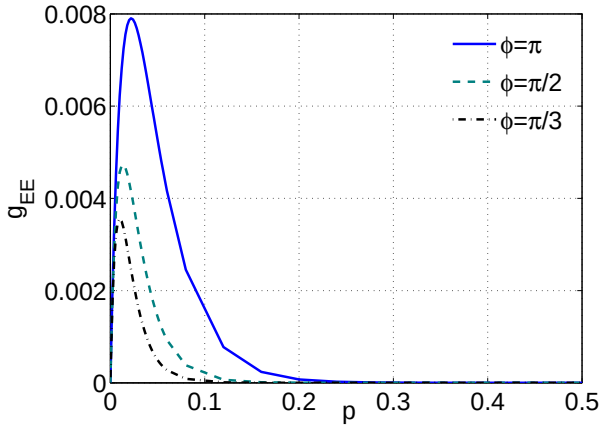

Figure 7.12. The average end-to-end throughput of random networks for different routing sectors ϕ, where $\alpha = 4$ and $\Theta = 10$.

is then obtained by taking the minimum of each path and averaging the minimum over the number of realizations of the simulated routes. It is shown in Fig. 7.12 that the maximum end-to-end throughput g_{EE} is 0.0086, 0.0053 and 0.0039 for $\phi = \pi$, $\pi/2$ and $\pi/3$.

What is the end-to-end throughput for regular networks? It can be directly obtained from Fig. 7.2 (a) and Fig. 7.6, which is 0.0247, 0.0213 and 0.0326 for square, triangle and hexagon networks. For regular networks, every hop has the same length, and the throughput is calculated for a link in the center of the network, which is the worst case, so the end-to-end throughput is the throughput of the center link of the busy area. In terms of the end-to-end throughput for multi-hop communication, regular networks significantly outperform random networks. For larger networks, the benefit is larger since larger m results in longer paths.

7.5 Conclusions

We have shown that for a noiseless Rayleigh fading network with slotted ALOHA, the success probability of a transmission is the Laplace transform of the

interference evaluated at the SIR threshold Θ. We assume that in every timeslot, each node transmits independently with a certain fixed probability $p = p_q p_t$, where p_q is the intensity of the Bernoulli traffic and p_t is the channel access probability. This decomposition of p shows that the throughput analysis and optimization with respect to p includes a range of traffic intensities and channel access probabilities.

Among the three regular networks (square, triangle, hexagon), the hexagon network provides the highest throughput since every node has only three nearest neighbors which is the smallest among the three networks. The sensitivity analysis of the maximum throughput $g_{\max}$ and optimum transmit probability p_{opt} with respect to Θ for square networks explains why the transmit efficiency $T_{\text{eff}} = g_{\max}/p_{\text{opt}}$ is approximately 37%. These results hold quantitatively for the other two regular networks — triangle and hexagon networks.

For random networks, two scenarios are considered — fixed and variable transmitter-receiver distance d_0. If d_0 is the same for regular and random networks, regular networks slightly outperform random networks in terms of throughput and transport capacity. In the case of variable d_0 where the receiver selects the nearest neighbor node as its desired transmitter, the average throughput of random networks is better than that of regular ones. This is because strong signal powers resulting from very small d_0 offset the impact of interference even for high transmit probabilities. This result, however, only pertains to local data exchange. When multihop communication and routing is taken into account, regular topologies have a significant advantage in terms of end-to-end throughput. The reason for the inferior end-to-end performance of random networks is the large variance in the node distances.

CHAPTER 8

TOWARDS QUASI-REGULAR SENSOR NETWORKS: TOPOLOGY CONTROL ALGORITHMS

So far, we focused on networks with uniformly random and completely regular topologies. Uniformly random and completely regular topologies are the two extreme cases. For some applications, a model that incorporates some uncertainty into a regular distribution may be more realistic, as it may not be possible to deploy nodes completely regularly.

The idea to partition the network area into regular square grid cells has been explored for energy-saving purposes. [79] comes up with virtual grids which are defined such that the nodes in one square cell can communicate with all the nodes in the neighboring cell. In that way, nodes in one cell are considered equivalent for routing. So only one node needs to be active in each cell, while the other nodes can sleep to save energy. The problems with this model is that there may be empty cells, that active nodes may still be very close, and that nodes need to be able to transmit reliably over distances larger than twice the length of the cell.

Due to the large variance in the inter-node distances, it is very difficult to efficiently communicate and balance the energy consumption in a network with uniformly random distribution, as was shown in Chapter 5. Hence it is highly desirable to make the node distribution more regular by selecting an appropriate subset of random nodes. We describe and analyze a basic localized algorithm and

three modifications for topology control that achieve this objective of regularizing the topology for improved energy efficiency while maintaining the coverage properties. The basic algorithm produces *quasi-regular networks*, where only nodes that are approximately evenly spaced to emulate a regular grid network are active and other nodes are put to sleep to save energy. After nodes remain active for a period of time, the virtual grid is shifted and nodes closest to the shifted grid points are active for the same period of time (or phase). We analyze the network lifetime of quasi-regular networks in two operating modes, a *monitoring mode* where a subset of nodes is active, acting as sentries, and a *reporting mode*, where an event of interest has been detected and a set of nodes forming a route to a base station is relaying messages. It is shown that quasi-regular networks substantially outperform random networks in both modes.

8.1 A Topology Control Algorithm for Sensor Networks

In regular networks, the nodes are placed on the vertices of a regular grid. Here, we focus on square grids (square lattices). In (purely) random networks, the position of the nodes constitute a Poisson point process with density λ. Note that λ does not affect the *relative* distances, since all the distances are simply scaled by $1/\sqrt{\lambda}$ compared with the network with $\lambda = 1$. *Quasi-regular* networks are networks that are more regular than the Poisson point process but not perfectly regular. We offer two definitions for quasi-regular networks. To be concise and avoid tedious border effects, we focus on infinite networks. Let R be the distance to the nearest neighbor of a node that lies within a sector $\pi/2$ of a desired direction (the source-destination axis). For a fair comparison, the network has to be normalized such that $\mathbb{E}[R] = 1$. In the Poisson case, this corresponds to a net-

work with density 1. Both definitions are based on a measure of the uncertainty in R.

(1) A *quasi-regular network* is a network where the differential entropy $h(R)$ [10] (expressed in nats) satisfies $-\infty < h(R) < 1 + \frac{\gamma_{em} - \log \pi}{2}$, where γ_{em} is the Euler-Mascheroni constant. The upper bound is the differential entropy of the Rayleigh distribution with mean 1, which is the distribution of R in a Poisson point process [21].

(2) A *quasi-regular network* is a network with $0 < \mathrm{Var}[R] < 4/\pi - 1$. Again, the upper bound is the variance of the Rayleigh distribution with mean 1.

The closer a network is to the lower bounds, the more regular it is. The two definitions seem equivalent in the sense that they order networks in the same way, since the relationship $h(R) \propto \mathrm{Var}[R]$ holds for other distributions than the Rayleigh distribution [10, p. 225].

We will focus on a particular type of quasi-regular networks, namely the ones that can be obtained by *thinning* a random network. The resulting sub-network only activates nodes as sentries and relays that are approximately evenly spaced, thereby emulating a regular topology. For example, as shown in Fig. 8.1, a network with uniformly randomly distributed nodes (marked by circles) can emulate a regular square network by appropriately selecting a subset of random nodes. In the first phase, the nodes closest to the integer grid points (marked by squares) are selected to be active and all the other node are put to sleep. In the second phase, the original grid points are shifted and a new set of nearest nodes to the shifted grid points (marked by up-triangles) are selected. In each phase, the grid that the selected nodes are closest to is called the *active grid*. For example, in Fig. 8.1, in the 1st, 2nd, 3rd, and 4th phase, the active grid points are marked by

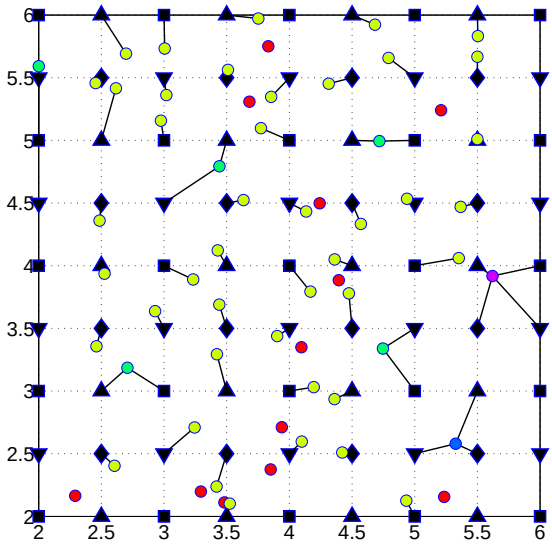

Figure 8.1. A part of a network where nodes are uniformly distributed in an area 100×100. The circles denote the random nodes. The squares, up-triangles, diamonds, and down-triangles denote the active grids in the 1st, 2nd, 3rd, and 4th phase and all of them constitute the dense grid.

squares, up-triangles, diamonds, down-triangles, respectively. The density of the active grid in each phase is one, without loss of generality due to scale-invariance. The grid consisting of all the original integer grid points and all the shifted grid points is denoted as *dense grid*. The active grid is always a subset of the dense grid. In this way, we can construct a quasi-regular network. Next we formally define two specific infinite quasi-regular networks:

Quasi-regular network of type A: Gaussian distribution. For each grid point $(x_i, y_i) \in \mathbb{Z}^2$, place a node in the plane with coordinates (X_i, Y_i) with $X_i \sim \mathcal{N}(x_i, \sigma^2)$, $Y_i \sim \mathcal{N}(y_i, \sigma^2)$, where $\sigma^2 < 1/(2\pi)$.

Quasi-regular network of type B: Subset of Poisson point process. Denote the set of vertices of a Poisson point process in $\mathbb{R}^2$ with density $\lambda > 1$ by P. Network B consists of the smallest subset $S \subset P$ of nodes as follows: For each $p \in P \backslash S$ and

any grid point, there is a node $s \in S$ such that s is closer to that grid point than p, *i.e.*, for all $s \in S$, $\exists\ z_i \in \mathbb{Z}^2$ s.t. $s = \arg\min_{p \in P} \|C(p) - z_i\|$, where $C(p) \in \mathbb{R}^2$ are the coordinates of point p. Note that for each lattice point, there is a unique (with probability one) nearest neighbor in the Poisson point process.

The uncertainty in the nearest-neighbor distance is reduced since the probability that it is very small or very large is substantially smaller than for a purely random network. So both type A and B networks are indeed quasi-regular[1].

This definition of quasi-regular network of type B implies a *basic* local topology control algorithm to achieve quasi-regularity (of type B): by exchanging position information with its neighbors, each node determines whether it is closest to a virtual integer grid point.

Basic algorithm:

1. Perform synchronization and localization of the network nodes.

2. Calculate distances to the nearest grid points, exchange this information with neighboring nodes, and decide whether to enter sleep mode or stay active as a sentry.

3. After a certain period, wake up all nodes, shift the virtual grid by a certain amount. Go back to step 2 unless the desired number of periods has passed.

Note that this is a local algorithm since it is fully distributed and only requires local data exchange. Many distributed synchronization and localization algorithms have been proposed for sensor networks, see, *e.g.*, [31, 69] and references therein. The outcome of the localization step is that all the nodes know their position with

[1]For a detailed analysis, please refer to Theorem 3 (page 119), Theorem 4 (page 137) and Subsection 8.4.2.

respect to a common coordinate system, *i.e.*, a joint grid, which is exactly what is required for step 2 in the algorithm. The number of neighbors with which each node needs to share its distance information is limited; it does not exceed the average number of nodes within a finite radius that is of the order of the grid distance. This algorithm will be analyzed in detail in Section 8.3, and three modifications will be suggested in Section 8.5 to overcome its shortcomings.

Note that switching periods or phases incurs a substantial expenditure of energy, since all nodes need to woken up first before steps 2 and 3 of the basic algorithm can be carried out. Therefore it is normally preferred to perform phase shifts only if necessary, *i.e.*, when the currently active set of nodes is about to run out of energy. Also, phase shifts should only happen during monitoring mode. The detection of an event of interest by a sentry is assumed to cause the network to switch from monitoring to reporting mode. In reporting mode, the active set of nodes should not be changed to not perturb the ongoing transmission and avoid re-routing. Furthermore, if fresh nodes are being added to the network, they can be naturally integrated at the beginning of the next phase. As the phase shifts, the new nodes are considered part of the network, and after localization and synchronization, they may be selected as active nodes in the next phase.

8.2 Properties of Quasi-Regular Networks

Theorem 3 *The distributions of quasi-regular networks of type A and B are equivalent if* $2\pi\sigma^2 < 1$ *and*

$$\lambda = \frac{1}{2\pi\sigma^2}. \tag{8.1}$$

By equivalence, we mean that the distances between the integer grid point and its nearest neighbor node are identically distributed.

Proof: For network type A, the distance $D = \sqrt{(X_i - x_i)^2 + (Y_i - y_i)^2}$ from node (X_i, Y_i) to the grid point (x_i, y_i) is Rayleigh distributed with mean $\mathbb{E}[D] = \sigma\sqrt{\pi/2}$ since the square root of the square summation of two Gaussian random variables is Rayleigh distributed. For network type B, the distance from an arbitrarily chosen point to its nearest node is also Rayleigh distributed with mean $1/(2\sqrt{\lambda})$ [21]. In particular, this is true if the arbitrarily chosen point is a grid point. So for $\lambda = 1/(2\pi\sigma^2)$, the two distributions are identical. □

In practice, we may consider finite areas and uniformly random distributions rather than Poisson point processes. We expect Theorem 3 to hold with good accuracy if the number of nodes is large, in which case the uniform distribution is equivalent to the Poisson process for all practical purposes[2]. For example, for a network of type A, consider an area $[-\frac{1}{2}, \frac{19}{2}]^2$ and place 100 nodes close to the integer square grid points with $\sigma = 1/\sqrt{2\pi \cdot 16} \approx 0.0997$ in X and Y. This yields a grid with Gaussian uncertainty. Manual placement (with some Gaussian uncertainty) as for networks of type A may be costly and impractical, so we focus on type B, where we start with a Poisson point process and apply thinning to make it more regular. This thinning procedure is exactly the topology control algorithm described in the previous section. In the subsequent analysis, we therefore focus on networks of type B. So, for the network of type B, place N nodes uniformly randomly in the same area and pick the 100 nodes closest to the 100 active grid points. Due to the localization (step 1 in the basic algorithm), the nodes can easily determine whether they are closest to an active grid point. Since the area is 100, $N = 1600$. So for each phase, almost $1 - 100/1600 \approx 94\%$ nodes can be put to sleep. They will be activated later when the grid is shifted. For the quasi-regular

[2]Note that, conditioned on the number of nodes in an area, the distribution of points in a Poisson process is uniformly random.

network to emulate a square regular network in all phases, the phase number n_p and the shift interval δ are related by $n_p = 1/\delta^2$. The shift interval and the density λ can, in principle, be chosen independently. However, the case where the number of dense grid points equals the number of points in the Poisson point process is of particular importance and will henceforth be referred to as the *natural choice*. For the previous example, if the active grid has density one, the shift interval δ should be $\delta = 1/\sqrt{\lambda}$ so that the total number of selected nodes in all the phases is approximately the total number of random nodes. In this case, the total number of phases is $n_p = 1/\delta^2 = \lambda$, which implies that for the natural choice the number of phases equals the density, *i.e.*, $n_p = \lambda$.[3] The grid shift selection scheme of the natural choice for $\lambda = 16$ is shown in Fig. 8.2(b), where A, B, C, D are the original grid points in the active grid for the 1st phase. The 16 circles within the dashed box except A are the 15 shifted grid points of the original grid point A. The shift interval is $\delta = 1/\sqrt{\lambda} = 1/4$. Since a particular node may be closest to both an original grid point and the shifted grid points, the node could be selected several times (see Fig. 8.1). The *usage number* U of a node in a quasi-regular network of type B is defined as the number of dense grid points a node is closest to. For the natural choice, the mean usage number is one because

$$\mathbb{E}[U] = \sum_{i=0}^{\infty} i \cdot U_i = \frac{\text{density of dense grid}}{\text{density of Poisson points}} = 1, \tag{8.2}$$

where U_i denotes the probability mass function (pmf) of U, *i.e.*, $U_i = \mathbb{P}[U = i]$ with $0 \leq i < \infty$, which means the probability that a node is selected by i dense grid points.

[3]For non-integer density λ, $n_p = [\text{round}(\sqrt{\lambda})]^2$, where rounding is used to obtain an integer that is close to the natural choice.

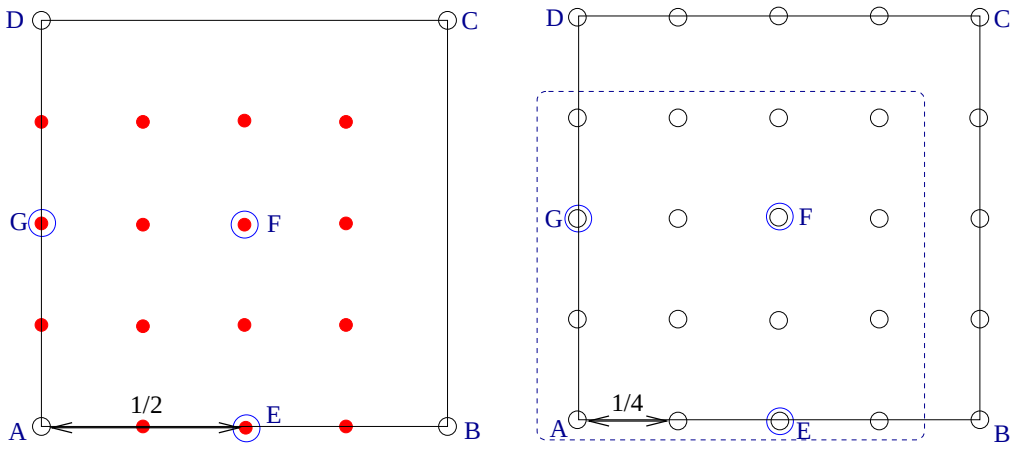

(a) $\lambda = 4$, $n_p = 4$ or 16

(b) $\lambda = 16$, $n_p = 4$, or 16

Figure 8.2. Shift assignment of quasi-regular network of type B. where A, B, C, D are the original square grid points with density one. (a) $\lambda = 4$, natural choice has 4 phases and $\delta = 1/2$, where for original grid point A (1st phase), the shifted grid points are E, F and G (2nd, 3rd, and 4th phases). For the 16−phase case, the 15 filled circles consist of the 15 shifted grid points of the original grid point A. (b) $\lambda = 16$, natural choice has 16 phases and $\delta = 1/4$, where the 16 circles within the dashed box except A are the 15 shifted grid points of the original grid point A. For the 4−phase case, E, F, G are the 3 shifted grid points of the original grid point A.

We focus on a specific network with node density $\lambda = 4$. The phase number for the natural choice is 4. The grid shift selection scheme is shown in Fig. 8.2(a), where A, B, C, D are the original grid points in the active grid for the 1st phase. For the natural choice with 4 phases, for original grid point A (1st phase), the shifted grid points are E, F and G (2nd, 3rd, and 4th phases). The dense grid consists of the original grid points and the shifted grid points. The shift interval is $\delta = 1/\sqrt{\lambda} = 1/2$. In the next section, a detailed analysis on the node usage number U will be provided.

8.3 Analysis of Node Usage

8.3.1 Numerical investigation

To determine how often a node is selected, we simulated 10^9 points of the Poisson process. For $\lambda = 4$, in addition to the natural choice, we also consider another shift value by increasing the phase number from 4 to 16. As shown in Fig. 8.2(a), for the 16−phase case, the 15 filled circles consist of the 15 shifted grid points of the original grid point A. The normalized histograms (probability mass functions or pmfs) of the usage numbers for the natural choice and the 16−phase case are illustrated in Fig. 8.3(a) and (b).

For node density $\lambda = 16$, the natural choice has 16 phases. We also study the case with 4 phases. As shown in Fig. 8.2(b), for the 4−phase case, E, F, G are the 3 shifted grid points of the original grid point A. The normalized histograms of the node usage numbers for the natural choice and the 4−phase case are shown in Fig. 8.3(c) and (d).

An interesting observation from comparing Fig. 8.3(a) and (c) is that the normalized histograms of the node usage number with natural choice are similar,

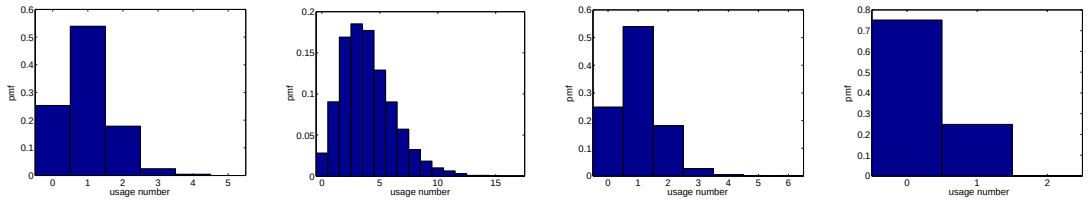

(a) $\lambda = 4$, 4-phase (b) $\lambda = 4$, 16-phase (c) $\lambda = 16$, 16-phase (d) $\lambda = 16$, 4-phase

Figure 8.3. Normalized histogram (pmf) of node usage numbers for $\lambda = 4, 16$ and different phase numbers. (a) and (c) are natural choices.

e.g., the probability that a node is not active is approximately 25% in Fig. 8.3(a) and (c). Furthermore, we can see that employing more phases than the natural choice decreases the number of nodes that are not active, as expected.

8.3.2 Asymptotic behavior

If the shift interval δ gets smaller and smaller, the number of phases increases. In the limiting case, there is an infinite number of shift phases so that the usage number of a node will be proportional to the area of the Voronoi cell of that node. Fig. 8.4 (a) plots the normalized histogram of the usage numbers for 64 phases as $\lambda = 4$. Fig. 8.4 (b) displays the normalized histogram of the Poisson Voronoi cell area (solid curve) which match the generalized gamma distribution (dashed curve):

$$f(x|a,b,c) = \frac{ab^{c/a}}{\Gamma(c/a)} x^{c-1} \exp(-bx^a) \qquad (a,b,c > 0), \tag{8.3}$$

where $a = 1.07950$, $b = 3.03226$ and $c = 3.31122$ are from [72].

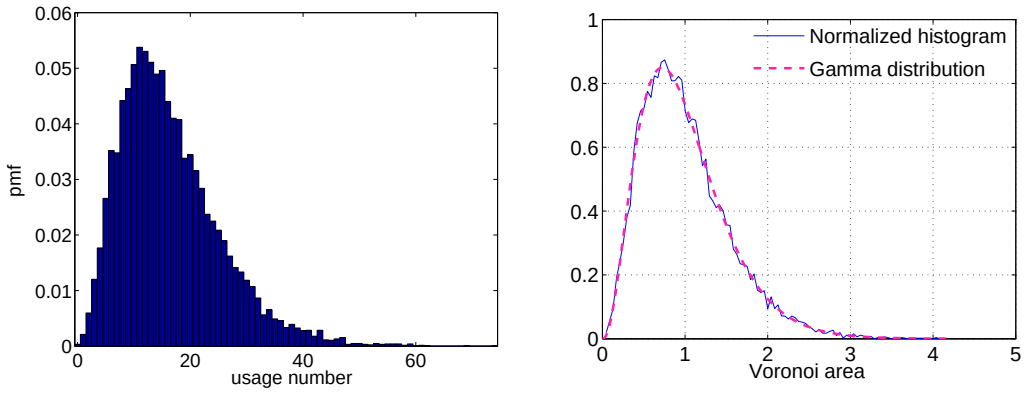

(a) (b)

Figure 8.4. (a) Normalized histogram (pmf) of usage numbers of nodes for 64 phases for $\lambda = 4$. (b) Normalized histogram (pmf) of Voronoi cells area (solid curve) and the generalized gamma distribution in eqn (8.3) (dashed curve).

8.3.3 Analytic bounds

The natural choice for the density of the underlying Poisson process for networks of type B is appealing since it provides a good tradeoff between regularity and hardware cost. An exact and complete analysis of the usage numbers for this case is elusive. It is, however, possible to derive sharp bounds.

8.3.3.1 Probability that a node is not active

Here we determine the lower bound of the probability that a node is not active. The exact probability calculation is given in the appendix. If a node is not active, it is not the nearest neighbor of any grid point. In particular, it is not the nearest neighbor of its 4 neighbor grid points. In addition, it is not the nearest neighbor of any more distant grid points. We consider the probability that a node at (X, Y)

is not the nearest neighbor of its 4 neighbor grid points A, B, C, D[4] (shown in Fig. 8.5(a)) because this is the most likely event. Note here the grid points are A and its shifted versions B, C, D. We have

$$\begin{aligned}&\mathbb{P}[\text{node}(X,Y) \text{ is not the nearest neighbor of A,B,C,D}] \geq \hat{p}\\ =&\mathbb{E}[(1-e^{-\lambda\pi r_1^2})(1-e^{-\lambda\pi r_2^2})(1-e^{-\lambda\pi r_3^2})(1-e^{-\lambda\pi r_4^2})].\end{aligned} \tag{8.4}$$

$\hat{p}$ is the lower bound since (8.4) does not consider the overlaps between the circles (the shaded areas in Fig. 8.5(b)). It is assumed that we need four different other nodes that are closer to the four cell corner grid points, although two or three nodes may be sufficient if one or more lies in the intersection of any two circles. The probability that a node is not active by its four nearest neighbor grid points but is active by more distant grid points is rather small and neglected here. Plugging the coordinate of A, B, C, D $(0, \frac{1}{\sqrt{\lambda}})$, $(\frac{1}{\sqrt{\lambda}}, \frac{1}{\sqrt{\lambda}})$, $(\frac{1}{\sqrt{\lambda}}, 0)$, $(0,0)$ into (8.4), and considering the uniform distribution of X and Y, we obtain

$$\begin{aligned}\hat{p} =&1-\text{erf}^2(\sqrt{\pi})+\text{erf}(\frac{\sqrt{2\pi}}{2})\,\text{erf}\,\sqrt{2\pi}e^{-\frac{\pi}{2}}+\text{erf}^2(\frac{\sqrt{2\pi}}{2})e^{-\pi}\\ &-\frac{1}{3}e^{-\frac{4\pi}{3}}[\text{erf}(2\sqrt{\frac{\pi}{3}})+\text{erf}(\sqrt{\frac{\pi}{3}})]^2+\frac{1}{4}e^{-2\pi}\,\text{erf}^2(\sqrt{\pi})\approx 0.2362.\end{aligned} \tag{8.5}$$

For $\lambda = 4$, the fraction of never active nodes is 24.68% (see Fig. 8.3(a)), which confirms the above lower bound.

[4]Here the points A, B, C, D are different from the integer grid points A, B, C, D in Fig. 8.2.

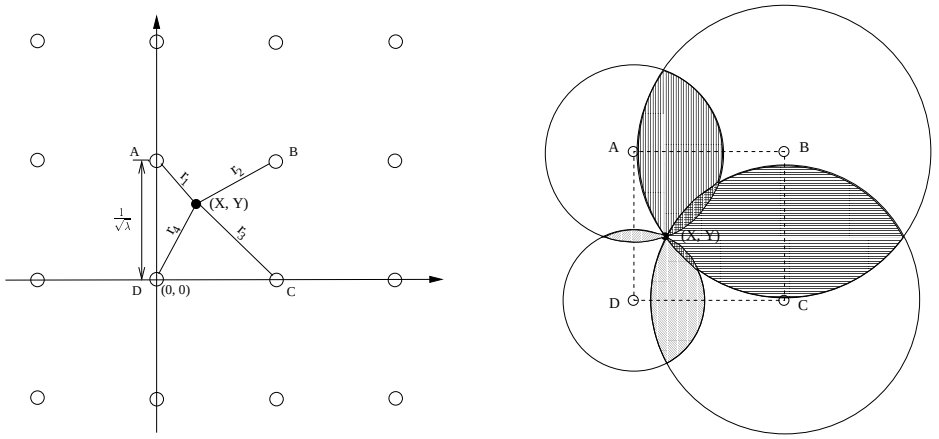

(a) (b)

Figure 8.5. In a quasi-regular network, node (X, Y) and its 4 nearest neighbor grid points A, B, C, D. The distance from node (X, Y) to A, B, C,D is r_1, r_2, r_3, r_4. The shift interval for the natural choice is $\delta = \frac{1}{\sqrt{\lambda}}$, so the coordinates of A, B, C, D are $(0, \frac{1}{\sqrt{\lambda}})$, $(\frac{1}{\sqrt{\lambda}}, \frac{1}{\sqrt{\lambda}})$, $(\frac{1}{\sqrt{\lambda}}, 0)$, $(0, 0)$.

8.3.3.2 Probability that a node is active

The probability that a node is activated by its nearest grid point is

$$p = 4\lambda \int_0^{\frac{1}{2\sqrt{\lambda}}} \int_0^{\frac{1}{2\sqrt{\lambda}}} e^{-\lambda\pi(x^2+y^2)} dxdy = \mathrm{erf}(\frac{\sqrt{\pi}}{2})^2 \approx 0.624, \tag{8.6}$$

which is a lower bound of the probability that a node is active.

8.3.3.3 Probability that a node is selected 4 times

As shown in Fig. 8.5(b), the area covered by the 4 circles is smallest if the random node (X, Y) is in the center of the square. In this case, the area is

$\frac{1}{\lambda}(2+\pi)$, so the probability that the area has no other random nodes is

$$p = e^{-\lambda \frac{1}{\lambda}(2+\pi)} \approx 0.58\%. \tag{8.7}$$

which is an upper bound of the probability that a node is selected 4 times, which is, from the simulation, about 0.36%.

8.3.3.4 Approximation of usage numbers

Since the usage number approaches the generalized gamma function (appropriately re-scaled) as $\delta^2\lambda$ gets small, the usage number can be approximated as follows: Let $F(x)$ be the cdf and $n_e := 1 + 4/(\delta^2\lambda)$ be an estimate for the number of essentially non-zero values of the pmf of U. Now, with $c := 7/(2n_e)$ the first order difference of F evaluated at ck is an approximation of U_k, i.e.: $U_k \approx F(c(k+1)) - F(ck)$. This approximation is better for n_e not too small.

8.3.3.5 Decay of the usage numbers U_i for large i

Since the probability that a node is used n times is related to the probability that a certain area around a node is empty, we can give a simple logarithmic approximation of these usage numbers. The solid line in Fig. 8.6 shows the approximation for larger usage numbers. The proportionality to n is intuitively clear, since the probability that no node is in an area A is e^{-4A}, since $\lambda = 4$. The area that needs to be empty is proportional to n, and can be assumed circular, therefore the factor π. Now the exact expression $(n-3)\pi - 2$ comes from (8.7) – the approximation is "calibrated" to obtain an approximation of (8.7) for U_4.

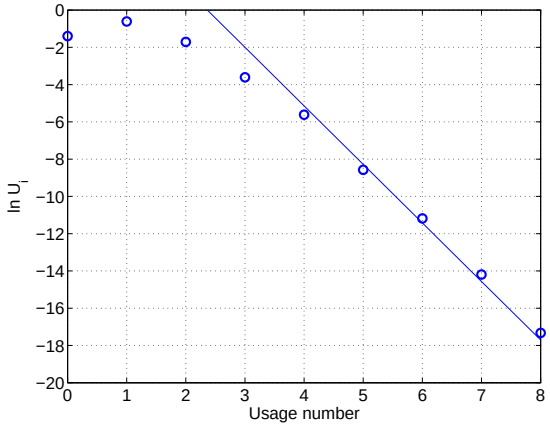

Figure 8.6. The approximation of how the usage numbers U_i decay for i larger than the natural number of cases. The circles indicate the logarithmic of usage numbers. The solid line shows the approximation for larger usage numbers.

8.3.4 Reliability analysis for different phases

In this subsection, we assume that the network is in monitoring mode, *i.e.*, that most of the nodes' energy is consumed to stay awake for surveillance. So we define the node lifetime L as the duration of a node being continuously active (awake), which is identical for every node. The lifetime of network type B is defined as the time during which in each phase at least a threshold ratio η of the selected subset is alive. So in the following, we will determine the fraction of live nodes in each phase. Again, we first consider the important natural choice with $\lambda = 4$ for the reliability analysis. Again, at first, we use the natural choice case of $\lambda = 4$ as an example for the reliability analysis. For network type B, we define the subset S_i ($i \in \mathbb{N}$), to be the set of selected nodes in the $i-$th phase. We extend this notation by introducing S_0 — the set of nodes that are never used. Fig. 8.1 displays the active grid points and active nodes in one phase. The subset in that phase is the set of nodes marked by $\times$. The subset of nodes that are selected

in different phases are not disjoint, *i.e.*, nodes may be selected repeatedly. As shown in Fig. 8.1, some nodes are selected in several phases, which means they are the nearest neighbor of several dense grid points (connected to two, three, or four dense grid points by black lines). It is important to find the probability that a node belongs to multiple S_i, *i.e.*, is selected in several phases. To this end, we introduce a *probability measure* $\mu(\cdot)$ as follows: $\mu(\cdot) : \mathcal{S} \to [0, 1]$ is the probability that a node of the original Poisson point process belongs to a set $S \in \mathcal{S}$, where $\mathcal{S}$ is the σ-algebra of the Poisson point set[5] and therefore constitutes a measurable space with $\mu(S_0 \cup S_1 \cup S_2 \cup \ldots) = 1$, so $\mu(\cdot)$ is a probability measure. With U_i the pmf of the usage number U (the fraction of nodes that are selected i times), we have $\mu(S_1 \cup S_2 \cup \ldots) = 1 - U_0$. Moreover, as shown in Fig. 8.5(b), the probabilities that a node is selected in phase 1 and/or 2 and/or 3 and/or 4 (nearest neighbor of D and/or C and/or B and/or A) satisfy the following equalities due to the homogeneity of the Poisson point process:

$$\begin{aligned}
\mu(S_1) = \mu(S_2) = \mu(S_3) = \mu(S_4) &=: \mu_1 \\
\mu(S_1 \cap S_2) = \mu(S_2 \cap S_3) = \mu(S_3 \cap S_4) = \mu(S_4 \cap S_1) &=: \mu_{2n} \\
\mu(S_1 \cap S_3) = \mu(S_2 \cap S_4) &=: \mu_{2d} \\
\mu(S_1 \cap S_2 \cap S_3) = \mu(S_1 \cap S_2 \cap S_4) = \mu(S_1 \cap S_3 \cap S_4) = \mu(S_2 \cap S_3 \cap S_4) &=: \mu_3 \\
\mu(S_1 \cap S_2 \cap S_3 \cap S_4) &=: \mu_4
\end{aligned} \tag{8.8}$$

So we denote μ_1 as the probability that a node belongs to S_i with $i > 0$; μ_{2n} as the probability that a node is selected by two nearest-neighbor dense grid points, *e.g.* $\mu(S_1 \cap S_2)$ (selected by D and C in Fig. 8.5(b)); μ_{2d} as the probability that

[5]So, in particular, $\mathcal{S}$ includes all the possible unions and intersections of the sets S_i.

a node is selected by two diagonal dense grid points, *e.g.* $\mu(S_2 \cap S_4)$ (selected by C and A in Fig. 8.5(b)); μ_3 as the probability that a node belongs to the intersection of three of these sets, etc. Our simulation considering 10^9 points (as shown in Fig. 8.3(a)) indicates $U_0 = 24.6829\%$, $U_1 = 54.1292\%$, $U_2 = 18.0906\%$, $U_3 = 2.7125\%$, $U_4 = 0.3644\%$, $U_5 = 0.0189\%$. $U_5 > 0$ shows that there is a small fraction of nodes that actually are selected by two points in the active grid in the same phase. For higher i, U_i becomes too small to be seen in the figure. Since the U_i values are very small for $i > 4$ (and exponentially decreasing) as shown in Subsection 8.3.3.5, we can safely ignore them and assume that only U_0 through U_4 are non-zero. In terms of probabilities, this means that we are looking at nodes that are selected at most four times only. Analogously to μ_{2n} and μ_{2d}, there are two different probabilities that a node is selected by two dense grid points, we denote them as U_{2n} (nearest neighbor) and U_{2d} (diagonal), so $U_2 = U_{2n} + U_{2d}$. From the simulation, we obtain $U_{2n} = 16.7661\%$, $U_{2d} = 1.3245\%$. Note that there are 5 μ values and 5 U values and there is a one-to-one relationship between them. For example, the probability that a node is only selected in phase 1 (but not selected in phase 2, 3, 4) can be expressed as:

$$\begin{aligned}\mu\big(S_1 \backslash (S_2 \cup S_3 \cup S_4)\big) =& U_1/4 = \mu(S_1) - \mu(S_1 \cap S_2) - \mu(S_1 \cap S_4) - \mu(S_1 \cap S_3) \\ &+ \mu(S_1 \cap S_2 \cap S_3) + \mu(S_1 \cap S_2 \cap S_4) + \mu(S_1 \cap S_3 \cap S_4) \\ &- \mu(S_1 \cap S_2 \cap S_3 \cap S_4) \\ =& \mu_1 - 2\mu_{2n} - \mu_{2d} + 3\mu_3 - \mu_4, \end{aligned} \tag{8.9}$$

Since the intersections of two and more sets have to be added and subtracted appropriately to yield the measure for $S_1 \backslash (S_2 \cup S_3 \cup S_4)$. Carrying this out for

all values of U_i, the relationship between the pmf of the usage number and the measures μ_i can be summarized as follows:

$$\begin{bmatrix} U_1 \\ U_{2n} \\ U_{2d} \\ U_3 \\ U_4 \end{bmatrix} = \mathbf{T} \begin{bmatrix} \mu_1 \\ \mu_{2n} \\ \mu_{2d} \\ \mu_3 \\ \mu_4 \end{bmatrix} = \begin{bmatrix} 4 & -8 & -4 & 12 & -4 \\ 0 & 4 & 0 & -8 & 4 \\ 0 & 0 & 2 & -4 & 2 \\ 0 & 0 & 0 & 4 & -4 \\ 0 & 0 & 0 & 0 & 1 \end{bmatrix} \begin{bmatrix} \mu_1 \\ \mu_{2n} \\ \mu_{2d} \\ \mu_3 \\ \mu_4 \end{bmatrix}. \tag{8.10}$$

Since the matrix T is upper triangular it is very easily invertible. The μ_i values are given by

$$\begin{bmatrix} \mu_1 \\ \mu_{2n} \\ \mu_{2d} \\ \mu_3 \\ \mu_4 \end{bmatrix} = \mathbf{T^{-1}} \begin{bmatrix} U_1 \\ U_{2n} \\ U_{2d} \\ U_3 \\ U_4 \end{bmatrix} = \begin{bmatrix} 0.25 & 0.5 & 0.5 & 0.75 & 1 \\ 0 & 0.25 & 0 & 0.5 & 1 \\ 0 & 0 & 0.5 & 0.5 & 1 \\ 0 & 0 & 0 & 0.25 & 1 \\ 0 & 0 & 0 & 0 & 1 \end{bmatrix} \begin{bmatrix} U_1 \\ U_{2n} \\ U_{2d} \\ U_3 \\ U_4 \end{bmatrix} = \begin{bmatrix} 0.2498 \\ 0.0591 \\ 0.0238 \\ 0.0104 \\ 0.0036 \end{bmatrix}. \tag{8.11}$$

For the natural choice, the duration of a phase is assumed to be equal to the lifetime of the nodes. Because shifting the grid and activating a different set of nodes causes overhead, there is no reason to do this before the current set of nodes expires. In each phase, $1/\lambda = 1/4 = 25\%$ of all nodes are selected. Then, after phase 1, 25% of the nodes are dead. Let f_i denote the fraction of live nodes in phase i. $f_1 = 1$ and, since a fraction $\mu(S_1 \cap S_2)$ of the nodes are in $S_1 \cap S_2$, in phase 2 there are only $f_2 = 1 - \frac{\mu(S_1 \cap S_2)}{1/\lambda} = 1 - 4\mu_{2n}$ of the nodes in S_2 alive. Taking into account the fraction of nodes that have been active already in previous phases,

TABLE 8.1

LIFETIME COMPARISON OF TWO QUASI-REGULAR NETWORKS OF TYPE B WITH DIFFERENT PHASE NUMBER n_p AND DENSITY λ. THE NETWORK LIFETIME IS DEFINED AS THE TIME DURING WHICH IN EACH PHASE AT LEAST A FRACTION η OF THE SELECTED SUBSET IS ALIVE.

	$\lambda = 4$		$\lambda = 9$	$\lambda = 16$		$\lambda = 25$
Phase number n_p	4 (natural)	16	9 (natural)	4	16 (natural)	25 (natural)
Lifetime ($\eta = 0.75$)	$2L$	L	$4L$	$4L$	$6L$	$9L$
Lifetime ($\eta = 0.5$)	$4L$	$2L$	$9L$	$4L$	$16L$	$25L$

we obtain for phases 3 and 4:

$$f_3 = 1 - \frac{1}{1/\lambda}\big(\mu(S_2 \cap S_3) + \mu(S_1 \cap S_3) - \mu(S_1 \cap S_2 \cap S_3)\big) = 1 - 4\big(\mu_{2n} + \mu_{2d} - \mu_3\big)$$

$$\begin{aligned} f_4 &= 1 - 4\big(\mu(S_1 \cap S_4) + \mu(S_2 \cap S_4) + \mu(S_3 \cap S_4) - \mu(S_1 \cap S_2 \cap S_4) \\ &\qquad - \mu(S_1 \cap S_3 \cap S_4) - \mu(S_2 \cap S_3 \cap S_4) + \mu(S_1 \cap S_2 \cap S_3 \cap S_4)\big) \\ &= 1 - 4\big(2\mu_{2n} + \mu_{2d} - 3\mu_3 + \mu_4\big) \end{aligned} \tag{8.12}$$

From the above analysis and (8.11), we have $f_1 = 1$, $f_2 = 0.7635$, $f_3 = 0.7099$, $f_4 = 0.5422$. So by simple inspection of f_1, f_2, f_3, and f_4, it is straightforward to obtain the first column of Table 8.1 (which is the natural choice for $\lambda = 4$): For the threshold $\eta = 0.75$, only f_1 and f_2 are greater than η, so there are two phases that have an alive node percentage greater than $\eta = 0.75$, which results in a lifetime of $2L$. We also consider the natural cases for $\lambda = 9$, 16, and 25 and

include the results in Table 8.1. For all the natural cases, we can proceed as in (8.12) to obtain the f_i values. For $\lambda = 4$ and 16, we also consider non-natural cases, see Table 8.1. For the case $\lambda = 4$, $n_p = 16$, one may also assume to switch phases after $L/4$, so that the maximum duration of the entire network is $4L$, as in the natural case $\lambda = n_p = 4$. The resulting lifetime is $2.5L$ for $\eta = 0.75$ and $3.75L$ for $\eta = 0.5$. Although this is slightly better for $\eta = 0.75$ than the natural case, the energy consumption to switch phases needs to be considered, too, and is likely to offset the benefit of choosing a larger n_p. In conclusion, the natural choice best enhances the lifetime of quasi-regular networks. Note that for a regular network with unity density, the lifetime is L. This analysis confirms that emulating a regular network from a random one indeed increases the network lifetime, at the price of more nodes deployed in the network. As can be seen from the four natural cases considered in Table 8.1, increasing the node density results in longer lifetime, so there is a tradeoff between hardware cost and lifetime.

If the node density λ is not exactly i^2 for some $i \in \mathbb{N}$, the phase number has to be chosen as $n_p = [\text{round}(\sqrt{\lambda})]^2$ to ensure that each node is used approximately once, *i.e.*, to get close to the natural case. If $n_p > \lambda$, nodes will be selected more than once on average, and if $n_p < \lambda$, some nodes will never be used. The above choice of n_p best balances these two problems of shortened lifetime and waste of nodes.

8.4 Comparison of the Route Lifetime for Different Networks

In this section, we assume the network operates in reporting mode, *i.e.*, there is a phenomenon of interest detected in the network, causing heavy traffic along at least one route. In this case, the lifetime of this route is determined by the

transmit (and possibly receive) energy consumption. We will focus on the former.

8.4.1 Regular and random networks

The lifetime of a route is determined by the maximum energy consumption among the nodes in the route. In regular networks, we assume the nodes are placed on an integer square grid over an area $m \times m$, and the next-hop receiver of each node is one of the four nearest neighbors. For random networks, the Poisson point process has density one, and the nodes are distributed in the same area. So, random networks have the same size and node densities as regular networks.

8.4.1.1 Random networks

With power control. We adapt the transmit power to d^α to compensate for the path loss and employ the generic routing strategy from [21]: each node in the path sends packets to its nearest neighbor that lies within a sector ϕ, *i.e.*, within $\pm\phi/2$ of the source-destination direction. The maximum energy consumption has been calculated in Subsection 6.2.2.2. As was derived in [19], for $\alpha \geq 2$

$$\begin{aligned} \mathbb{E}[\max\{R_1, R_2, ..., R_h\}^\alpha] &\geq (\mathbb{E}[\max\{R_1^2, R_2^2, ..., R_h^2\}])^{\frac{\alpha}{2}} \\ &> \mathbb{E}[R^2](\ln h + \gamma_{em})^{\alpha/2}, \end{aligned} \tag{8.13}$$

where $\gamma_{em} \approx 0.5772$ is the Euler-Mascheroni constant. Thus for $\alpha \geq 2$, the maximum energy consumption is at least logarithmically increasing with the hop number h. For example, for a 30-hop route, $\mathbb{E}[R_{max}^4 | h = 30]$ is about 28, indicating that the lifetime of this route is only 1/28 of that of a regular network, where $\mathbb{E}[R^\alpha] = 1$.

In a square regular network with unit density, the energy consumption is the

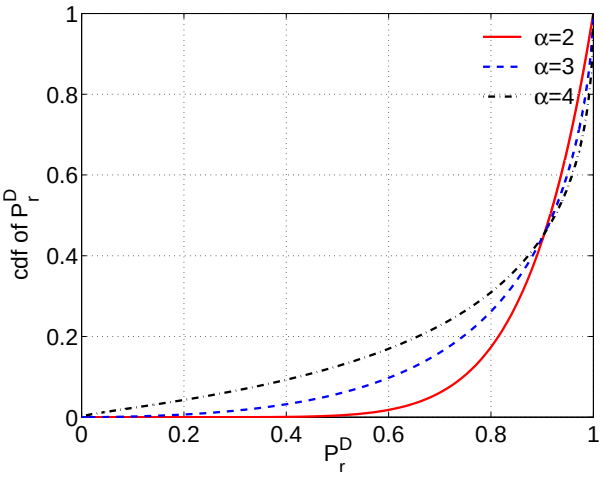

Figure 8.7. Cdf of P_r^D for random networks with $\gamma_N = 10$.

same for all nodes in a route, *i.e.*, the normalized energy consumption is $\mathbb{E}[R^\alpha] = \mathbb{E}[R_{max}^\alpha|h] = 1$ for any h. In a random network (with $\phi = \pi/2$ and $\alpha = 4$), however, we obtain $\mathbb{E}[R^\alpha] = 3.6$ and $\mathbb{E}[R_{max}^\alpha|h = 10] = 16.4$ for a 10-hop route and $\mathbb{E}[R_{max}^\alpha|h = 20] = 23.6$ for a 20-hop route, respectively. So the lifetime of the routes in random networks is considerably shorter.

Without power control. Strategies with equal transmit power which are energy balanced, are already studied in Section 6.3.1. Let the normalized SNR $\gamma_N := P_0/(\Theta N_0)$ from (2.5), resulting in a link reception probability $p_r^N = e^{-\frac{d^\alpha}{\gamma_N}}$. Considering the link distance d a random variable, then $P_r^D = e^{-\frac{d^\alpha}{\gamma_N}}$ is a transformation of the random variable d. Fig. 8.7 illustrates the cdf of P_r^D for $\alpha = 2, 3, 4$ and $\gamma_N = 10$ in random networks. It is shown that with medium transmit power, very small link reception probabilities exist with a certain probability.

8.4.2 Quasi-regular networks

By comparing the energy consumption for random and regular networks, we demonstrated that random distributions incur substantially higher energy expenditures. The large variance in the link distances necessitates power control with a large dynamic range, which, in turn, entails a proportional variance in the nodes' lifetime. The only way to avoid these fundamental problems is to abandon the principle of nearest-neighbor routing and only use nodes as relays that are approximately evenly spaced.

Theorem 4 *In quasi-regular networks (of type A or B), the node distance between nearest neighbors (inter-node distance) follows a Ricean distribution.*

Proof: The distances in the $x-$ and $y-$ axes of a node to the ideal grid point are Gaussian random variables. As shown in Fig. 8.8, we assume the ideal grid points are $(0,0)$ and $(0,1)$, and the real location of the two nodes is (X_1, Y_1) and (X_2, Y_2). Thus $X_1 \sim \mathcal{N}(0, \sigma^2)$, $X_2 \sim \mathcal{N}(1, \sigma^2)$ and $Y_1 \sim \mathcal{N}(0, \sigma^2)$, $Y_2 \sim \mathcal{N}(0, \sigma^2)$. We have

$$\Delta X = X_2 - X_1 \sim \mathcal{N}(1, 2\sigma^2), \qquad \Delta Y = Y_2 - Y_1 \sim \mathcal{N}(0, 2\sigma^2). \tag{8.14}$$

The inter-node distance $R = \sqrt{\Delta X^2 + \Delta Y^2}$ is Ricean distributed with pdf

$$p_R(r) = \frac{r}{2\sigma^2} \exp\big(-\frac{1+r^2}{4\sigma^2}\big) I_0(\frac{r}{2\sigma^2}), \qquad r \geq 0, \tag{8.15}$$

where $I_0(\cdot)$ is the zero-order modified Bessel function of the first kind [54]. □

Therefore, quasi-regular networks turn the Rayleigh inter-node distance distribution of Poisson random networks into Ricean distribution. This is analogical to

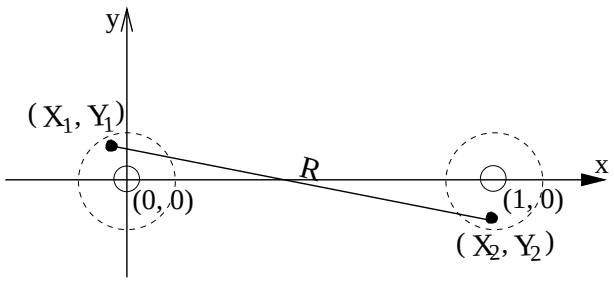

Figure 8.8. Inter-node distance in a quasi-regular network.

turning the Rayleigh fading channel into a Ricean channel by adding a strong line of sight (LOS) component.

Now we study the differential entropy and variance of the inter-node distance R to see if they meet the requirement of the two definitions of quasi-regular networks. Because the variance of R comes from the variance of ΔX and ΔY, under the condition that $2\pi\sigma^2 < 1$ (see Theorem 3), it is reasonable to assume that the variance is dominated by the distance along the axis that has $\mathcal{N}(1, 2\sigma^2)$ distribution. So the variance of R can be approximated by the variance of ΔX, namely, $2\sigma^2$. Consider the $4-$phase natural choice, where $\lambda = 4$ and $\sigma \approx 0.1995$ (see Theorem 3), the variance of R is $2\sigma^2 = 1/(4\pi)$, which is less than the upper bound $4/\pi - 1$ given by definition (2) of quasi-regular networks. With $2\sigma^2$ as the variance of the approximated Gaussian inter-node distance, we have $h(R) = 1/2 \cdot \log(2\pi e 2\sigma^2)$ [10]. So in the case $\lambda = 4$, we obtain $h(R) = 1/2 \cdot \log(2e/4) \approx 0.15$, which is less than the 0.72 upper bound given by definition (1) of quasi-regular networks.

Next we will determine the lifetime benefit that results from Ricean distances rather than Rayleigh distances. The simulation results of average maximum R^α for an $h-$hop route $\mathbb{E}[R^\alpha_{max}|h]$ is plotted in Fig. 8.9 for $\alpha = 2$, 3, 4 by solid lines. The dashed line is $\mathbb{E}[R^\alpha_{max}|h]$ for random network for $\alpha = 4$. Obviously,

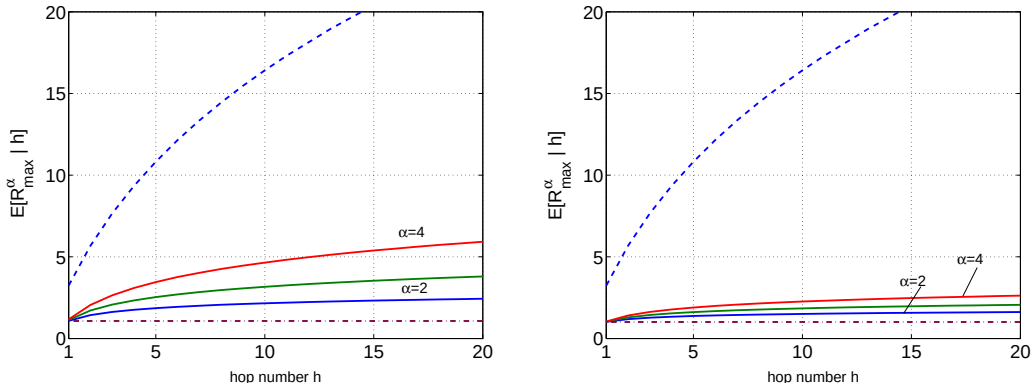

(a) $\lambda = 4$ (b) $\lambda = 16$

Figure 8.9. $\mathbb{E}[R^{\alpha}_{max}|h]$ vs. h for (a) $\lambda = 4$ and (b) $\lambda = 16$. The solid lines are for quasi-regular networks for various α. The dashed line is for random networks for $\alpha = 4$. The dash-dotted line is for a square regular network with unit density, where $\mathbb{E}[R^{\alpha}] = \mathbb{E}[R^{\alpha}_{max}|h] = 1$.

the maximum energy consumption in a route for quasi-regular networks is much smaller than that of random networks.

8.5 Modified Algorithms for Extended Lifetime

In the basic topology control algorithm introduced in Section 8.1, there is a fraction of nodes that is never used, and there are more and more nodes missing in the quasi-regular topology with increasing phase numbers. To alleviate this problem, we suggest three improvements over the basic algorithm which make better use of the nodes. The numerical results presented in this section are obtained from simulations with area 100×100.

8.5.1 Modification I

From the previous analysis, we know that for the natural choice, approximately 25% (Figs. 8.3(a) and (c)) of the nodes are never activated. However, they can be turned on in an additional phase at the end. By doing so, the modified algorithm I extends the network lifetime by one more phase duration L. So the network has *original phases* (the ones already present in the basic algorithm) and an *additional phase*. The distribution of the distance between a grid point and its nearest node in this additional phase may be approximated by the distribution of the distance between nearest neighbors in a Poisson point process with density $\lambda/4$, which is simply Rayleigh with mean $1/\sqrt{\lambda}$ [21]. The difference stems from the fact that the selected nodes in previous phases are not chosen independently. Fig. 8.10 (a) displays the comparison of such two distance distributions in the additional phase for $\lambda = 4$. Note that in previous phases, the distance between a grid point and its nearest node has Rayleigh distribution with mean $1/(2\sqrt{\lambda})$. The disadvantage of this modified algorithm is that certain nodes are still selected in multiple phases.

8.5.2 Modification II

To avoid the problem that certain nodes are selected in multiple phases, Modification II lets each node be picked only once, which means once a node has been selected by one grid point, it can not be selected again even it is also the nearest node of other grid points. The advantage of Modification II is that every node is selected exactly once, which increases the lifetime in the original phases in monitoring mode compared to Modification I. The disadvantage is that the distances between the grid points and their nearest nodes grow larger at later phases (as shown in Fig. 8.10(b), (c)). The analysis in Subsection 8.4.1 shows that larger

distances from the grid points imply a higher variance in the inter-node distance, which results in higher energy consumption for a route in a reporting mode.

8.5.3 Modification III

The problem of smaller reliability in later phases and very large distance in the final phase can be solved by the third proposed modification, which is a tradeoff between Modification I and II. In each phase, pick the closest node to the active grid point from the nodes that are alive. The simulation result ($\lambda = 4$) shows that the fraction of live nodes in Modification III for phases 2, 3, and 4 are 0.9879, 0.9195 and 0.7059, which are better than 0.7635, 0.7099 and 0.5422 of Modification I, but there are still 10.1% of the total number of nodes never activated. The difference to Modification II is that in Modification III, the same node may be picked by two active grid points in the same phase so that there is less than 100% of the nodes alive in phase 2. The normalized distance histograms of four phases (Fig. 8.11 (a)) can be approximated by the Rayleigh distributions (Fig. 8.11 (b)) with mean $1/\left(2\sqrt{\lambda(1-f)}\right)$, where f is the fraction of nodes that has been selected in the previous phase(s). The advantage of Modification III is that it decreases the fraction of nodes that are selected multiple times, which increases the lifetime in the original phases in monitoring mode compared to Modification I, and it has smaller distances in higher phases than Modification II (by comparing Fig. 8.10(c) and Fig. 8.11(a)).

8.6 Conclusions

We proposed and analyzed topology control algorithms for improved energy efficiency. The basic algorithm turns a random network into a quasi-regular network

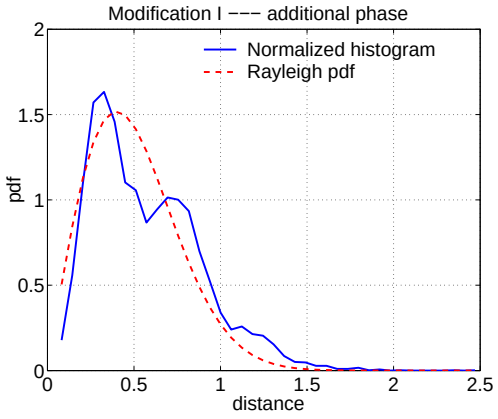

(a)

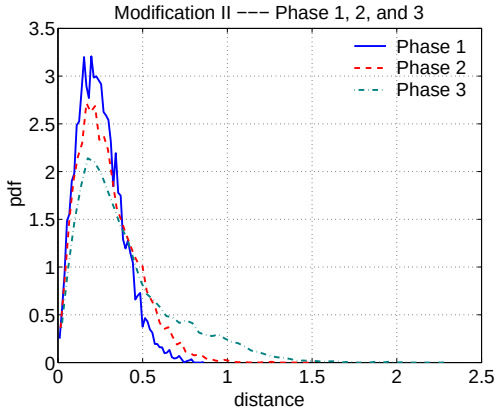

(b)

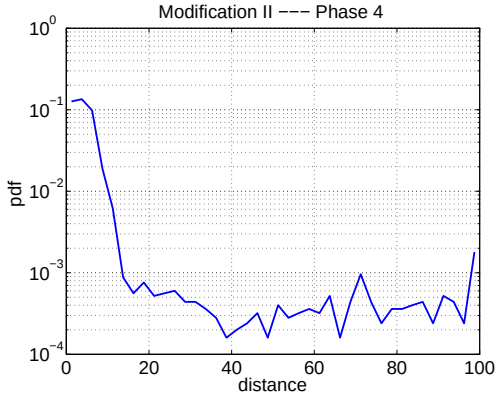

(c)

Figure 8.10. For $\lambda = 4$, for Modification I, (a) comparison of the distribution of distance in the additional phase with the Rayleigh distribution with mean $1/\sqrt{\lambda} = 1/2$. For Modification II, (b) normalized distance histograms of phase 1, 2, and 3, and (c) of phase 4. Note that a logarithmic scale is used for (c) to better visualize the small but non-zero probabilities of large distances.

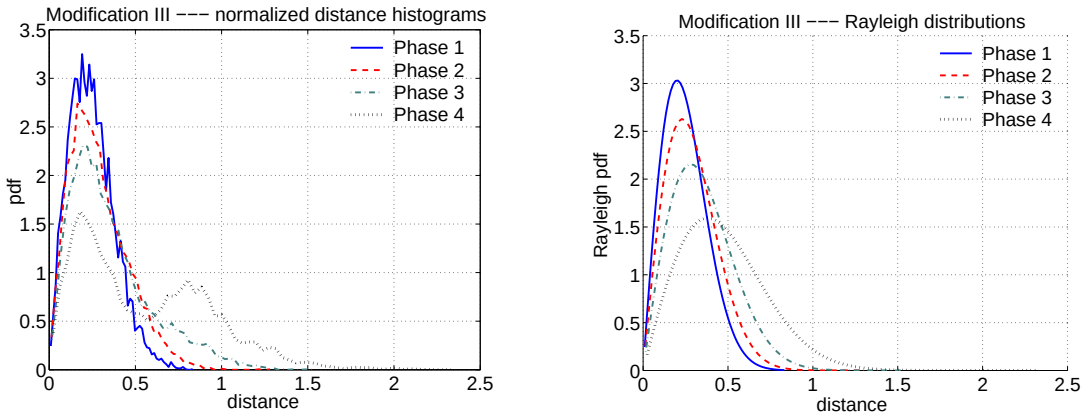

(a) (b)

Figure 8.11. For $\lambda = 4$, for Modification III, (a) normalized distance histograms of different phases, (b) Rayleigh distributions with mean 0.2500, 0.2886, 0.3523, 0.4780.

of type B, which is equivalent to the Gaussian quasi-regular network of type A. It abandons the principle of nearest-neighbor routing and has every node transmit over a similar distance. This way, the nodes chosen as sentries and relays approximately form a regular subnetwork, emulating a regular topology. We suggest *differential entropy* and *variance* of the nearest-neighbor distance as measures for regularity. If the variance of the nearest-neighbor distances goes to zero, the network is completely regular. Similarly, since differential entropy is a measure for the *uncertainty* of a random variable, the higher it is for the nearest-neighbor distances, the "more random" the network topology is. The two measures are closely related and both capture the (ir)regularity of a node distribution.

We have analyzed the network lifetime of regular, random, and quasi-regular networks in two operating modes, a *monitoring mode* and a *reporting mode*. In both cases, quasi-regular networks have substantial advantages over purely ran-

dom ones.

Monitoring mode: Compared with regular networks (that have λ times less nodes), the lifetime of quasi-regular networks of type B is extended, *i.e.*, the quasi-regular network can to some extent exploit the higher number of nodes. For the natural choice in quasi-regular networks of type B, where the number of nodes corresponds to the total number of dense grid points, approximately 25% of the nodes are never activated. An improved algorithm (Modification I) extends the network lifetime by activating all the unused nodes in an additional phase (but does not solve the problem that nodes may be selected repeatedly in previous phases). Modification II lets each node be selected exactly once, with the disadvantage that the distances between a grid point and its nearest live node grow large for the later phases. Modification III presents a tradeoff between I and II, selecting the closest node to the active grid point from nodes that are still alive. However, there are still some nodes never activated.

Reporting mode: The comparison of the maximum node energy consumption (that determines the lifetime of the route) of a single route in networks with regular and random topology shows that regular networks drastically outperform random ones: for a path loss exponent of 4 and a route of 10-20 hops, the lifetime of a route in a random network is about 20$\times$ smaller. This analysis assumes that nodes adapt their transmit power according to the hop distance to keep the link reception probability p_r^N constant. Equal power strategies would better balance the energy consumption among the nodes but the routes would suffer from very low reception probabilities. Clearly, the cause of these problems is the variance in the transmission distances. It is shown that quasi-regular networks of type B provide a solution to the energy consumption problem in random networks. Based on the

premise that route longevity implies network longevity, quasi-regular networks of type B outlive random networks although the number of nodes is the same.

The proposed "distance equalization" scheme also solves the problem of power amplifier inefficiencies addressed in [18], since it avoids power control over a large dynamic range and, in turn, permits the amplifiers to use operating points with high efficiency. In terms of deployment, these results suggest that one should aim at a regular node spacing whenever possible. For sensor networks, more regular topologies also have an obvious advantage in terms of coverage [47]. By turning random into quasi-regular networks by means of the proposed algorithm, we expect little or no loss in coverage, since isolated nodes will still be active. Clearly, by thinning, it is not possible to improve the coverage, but if it is done in a clever way as suggested, there is no significant loss in coverage.

8.7 Appendix: the probability that a node is not active for the natural choice

A node is not activated means it is not closest to any dense grid points. Denote p as the probability that node (X, Y) is not the nearest neighbor of dense grid point A,B,C,D (shown in Fig. 8.5). We have

$$p = 1 - p_1 + p_2 - p_3 + p_4, \tag{8.16}$$

where $p_1 = 4\mu_1$ is the probability that node (X, Y) is closest to any one grid point of A, B, C, D; $p_2 = 4\mu_{2n} + 2\mu_{2d}$ is the probability that node (X, Y) is closest to any two grid points; $p_3 = 4\mu_3$ is the probability that node (X, Y) is closest to any three grid points; $p_4 = \mu_4$ is the probability that node (X, Y) is closest to the four grid points. We denote the area of circle centered at A as M_A, the area covered by the overlap between circles centered at A, B as $M_{A\cap B}$, the area covered by circles

centered at A, B is $M_{A\cup B}$, and so on. So,

$$
\begin{aligned}
p_1 &= \mathbb{E}[e^{-\lambda M_A} + e^{-\lambda\pi M_B} + e^{-\lambda M_C} + e^{-\lambda\pi M_D}] = \mathbb{E}[e^{-\lambda\pi r_1^2} + e^{-\lambda\pi r_2^2} + e^{-\lambda\pi r_3^2} + e^{-\lambda\pi r_4^2}],\\
p_2 &= \mathbb{E}[e^{-\lambda M_{A\cup B}} + e^{-\lambda M_{B\cup C}} + e^{-\lambda M_{C\cup D}} + e^{-\lambda M_{D\cup A}} + e^{-\lambda M_{A\cup C}} + e^{-\lambda M_{B\cup D}}],\\
p_3 &= \mathbb{E}[e^{-\lambda M_{A\cup B\cup C}} + e^{-\lambda M_{B\cup C\cup D}} + e^{-\lambda M_{C\cup D\cup A}} + e^{-\lambda M_{D\cup A\cup B}}],\\
p_4 &= \mathbb{E}[e^{-\lambda M_{A\cup B\cup C\cup D}}].
\end{aligned}
\tag{8.17}
$$

When calculate p_3, we neglect the area where three circles overlaps, shown by the area filled by dense square grids in Fig. 8.5(b), since for some node locations, this area should be added, whereas in others, it should be deducted. We obtain

$$
\begin{aligned}
M_{A\cup B\cup C\cup D} &= \pi r_1^2 + \pi r_2^2 + \pi r_3^2 + \pi r_4^2 - M_{A\cap B} - M_{B\cap C} - M_{C\cap D} - M_{D\cap A}\\
&\quad + M_{B\cap D} + M_{A\cap C};\\
M_{A\cup B\cup C} &= \pi r_1^2 + \pi r_2^2 + \pi r_3^2 - M_{A\cap B} - M_{B\cap C} - \text{sign}(X + Y - \frac{1}{\sqrt{\lambda}})M_{A\cap C};\\
M_{A\cup B} &= \pi r_1^2 + \pi r_2^2 - M_{A\cap B}.
\end{aligned}
\tag{8.18}
$$

The area covered by circles centered at A, B, C is the sum of the area of circles centered at A, B, C minus the overlap area of $M_{A\cap B} + M_{B\cap C}$ and minus $\text{sign}(X+Y-\frac{1}{\sqrt{\lambda}})M_{A\cap C}$. The terms of $\text{sign}(X+Y-\frac{1}{\sqrt{\lambda}})$ comes from the fact that if the node is in the left-lower triangle, the area of $M_{A\cap C}$ should be added, if the

node is in the right-upper triangle, the area of $M_{A\cap C}$ should be subtracted.

$$
\begin{aligned}
M_{A\cap B} &= r_1^2 \arcsin \frac{1/\sqrt{\lambda} - Y}{r_1} + r_2^2 \arcsin \frac{1/\sqrt{\lambda} - Y}{r_2} - (\frac{1}{\sqrt{\lambda}} - Y)\frac{1}{\sqrt{\lambda}}. \\
M_{A\cap C} &= r_1^2 \arcsin \frac{Y'}{r_1} + r_3^2 \arcsin \frac{Y'}{r_3} - Y'\frac{\sqrt{2}}{\sqrt{\lambda}}\,, \\
Y' &= r_1 \Big| \sin\big(\frac{\pi}{4} - \arctan \frac{X}{\frac{1}{\sqrt{\lambda}} - Y}\big)\Big|. \\
M_{B\cap D} &= r_2^2 \arcsin \frac{Y''}{r_2} + r_4^2 \arcsin \frac{Y''}{r_4} - Y''\frac{\sqrt{2}}{\sqrt{\lambda}}\,, \\
Y'' &= r_4 \Big| \sin\big(\arctan \frac{Y}{X} - \frac{\pi}{4}\big)\Big|.
\end{aligned} \tag{8.19}
$$

Note although $M_{A\cap C}$ is different from $M_{B\cap D}$ for a specific point, their average values after integration are the same. Using MATLAB's `dblquad` function, p is 0.2479 which does not depend on λ. The simulation shows that the probability that a node is not active is 0.2468 (Fig. 8.3(a)).

CHAPTER 9

CONCLUDING REMARKS

9.1 Conclusions

This thesis presents our work on the performance analysis of large ad hoc networks, especially sensor networks based on a Rayleigh fading channel model. A typical sensor network consists of a large number of sensor nodes which are placed inside or near a phenomenon. Uniformly random or Poisson distributions are widely accepted models for the location of the nodes in wireless sensor networks, if nodes are deployed in large quantities and there is little control over where they are dropped. A typical scenario is a deployment from an airplane for battlefield monitoring. On the other hand, depending on the application, it may also be possible to place sensors in a regular topology, for example in a square grid. By completely regular node deployment, we expect benefits both in coverage and efficiency of communication.

To measure the performance of networks with different topologies, we use a set of well-known metrics — throughput, energy consumption, delay, end-to-end reliability. For one-dimensional networks, by comparing two (extreme) MAC schemes, we have shown that the regular networks outperform random networks in terms of throughput and energy consumption (thus lifetime). Power control is crucial for random networks since low link reception probabilities are unavoidable

at low to medium (common) power levels, and energy waste and interference are substantial at high (common) power levels. For regular two-dimensional networks, three topologies are studied. In the noise analysis, the triangle network gives the best performance due to its smallest energy consumption, delay and highest path efficiency. In the interference analysis, the hexagon network exhibits the highest transmit probability, throughput and effective transport capacity. For regular networks with peer-to-peer and many-to-one traffic model, we present the load distribution and study several load balancing strategies. The comparison of the random two-dimensional networks with adaptive transmit power and regular two-dimensional networks demonstrates that the regular ones has higher throughput at smaller energy consumption. For noiseless Rayleigh fading sensor networks with slotted ALOHA at equal transmit power levels, we present closed-form expressions of the average link throughput. For random networks, strategies with constant transmit power would better balance the energy consumption among the nodes, but the connections would suffer from very low reception probability (thus end-to-end throughput) or intolerably high delay. A tradeoff between the cost of regular deployment and communication efficiency is a quasi-regular network that incorporates some uncertainty into a regular distribution. Our topology control algorithms can achieve the goal of higher energy efficiency.

9.2 Important Future Work

9.2.1 Channel Models

Shadowing. Random signal variations due to large obstructing objects are called shadowing. The power of a received signal measured in dB subject to shadow fading follows a normal distribution, with the mean determined by the large scale

path loss. When the shadow fading distribution for the average received power in dB is normal, we call this log-normal shadowing. In [24, 25], the authors use a log-normal shadowing model and show the relationship between the link reception probability and distance is not a simple step function, similar to our Rayleigh fading channel model.

Shadowing and Rayleigh fading could be combined for the performance analysis. Also, for some applications and environments, the fading process is more accurately modeled by the Ricean distribution. However, the Ricean model comes with the drawback of reduced analytical tractability.

Pure AWGN channel. [83, 84] showed that the threshold model with fading (which corresponding to our Rayleigh fading model) at the bit level is accurate. We can evaluate the accuracy of the threshold model with fading for the non-fading AWGN channel.

The impact of the threshold Θ. So far, we have assumed Θ to be a constant. Actually the threshold depends on bit rate, modulation, channel code, and packet length. How to select Θ and what is minimum Θ? For example, from information theory view, the maximum transmit rate is $R = \frac{1}{2}\log(1 + \text{SNR})$. So if we want to communicate reliably at rate R, we need an SNR of at least $2^{2R} - 1$. In the future, we need to study the role and impact of the threshold Θ.

9.2.2 *Energy Consumption*

Use more refined consumption models. For the energy consumption, until now we just considered the transmit power. In the future, the receive and standby power consumption can be added.

9.2.3 Throughput Analysis

An *outage* is said to occur if the the S(I)NR is lower than a threshold [35]. Hence the probability of an outage event for the Rayleigh fading link model can be interpreted as the probability of a link failure. Information theory uses the outage event probability for non-ergodic channels. We can borrow the idea in our throughput analysis for the Rayleigh fading channel model.

In [23], the authors use a regular lattice to model the possible location of nodes and shows it allows to calculate an upper bound of the expected SIR. By using a simple power law model for path loss, they derive the expected SIR as a function of network size, network density, and traffic per node. Finally they use Shannon's capacity formula to find an upper bound on the throughput. [5] developed a SIR threshold model, combining Poisson statistics of the offered data traffic with Rayleigh statistics for the fading channel. One of the benefits of the SIR threshold model is that it allows spatial reuse. The results indicate a throughput improvement with Rayleigh fading channel. It will be a starting point for our further investigations. The SIR threshold model can be refined which has been done by [58] for fast fading.

9.2.4 Load Balancing

There are important problems related to critical nodes left unsolved in Chapter 5. For square sensor networks (4-neighbor case), there are only two neighbor nodes of the corner destination, so each of them will carry 1/2 of the load. For the 8-neighbor case, there are three neighbor nodes of the destination and we can do some improvement to evenly distribute 1/3 load to them. All these considerations show that simple routing can not effectively balance the load distribution. A

balanced load keeps individual nodes from being overloaded and thus ensures longer network lifetime.

The APR (Alternate Path Routing) protocol [80] indirectly balances the load by distributing the traffic to a set of diverse paths for one source-destination connection. [76] uses an analytic model to show that their multipath routing can improve the end-to-end reception probability and balance the load among nodes. However, the increased overhead traffic load might offset the benefits. This multipath routing scheme works only for peer-to-peer traffic, not for sensor networks. Hence, an effective load balance strategy for sensor networks should be devised.

One solution is to increase the number of the neighbors of destination which means some nodes have to transmit further. Also, the critical nodes may have to carry a bigger battery.

9.2.5 Opportunistic Scheduling

Opportunistic scheduling [36, 37] is a way to improve performance by exploiting time-varying channel conditions. In a one-hop wireless communication system, *e.g.* multi-cell system, every user in a cell communicates with the base station. Every user has different channel gain due to different distances to the base station, fading, *etc.* The time-varying channel condition results in difference performance levels of the users. Throughput could be the main performance metric. The scheduler decides which user should take the timeslot based on the performance values of all the users. It cannot always select the user who has the best channel condition, which would yield a greedy scheduler, since the users with worse channel condition will never transmit. Thus, it has to introduce fairness constraints

into the scheduling scheme. Under such constraints, the scheduler cannot always select the best user, rather it selects the "relatively-best" user in each timeslot to maintain a certain level of QoS for each user.

[37] investigates scheduling problems involving two fairness requirements — temporal fairness and utilitarian fairness — and a minimum-performance requirement. In the temporal fairness scheme, each user shares at least a certain part of the entire resource, *i.e.,* time. In the utilitarian fairness scheduling scheme, each user shares a certain portion of the overall performance. The minimum-performance guarantee scheduling scheme provides each user a direct QoS assurance, but brings the additional complication of feasibility. They confirm their work by simulations. In the simulation, they adopt a path loss and log-normal shadowing model and define the performance value of each user as a function of its SINR. Similarly, the link reception probability p_r^I in our Rayleigh fading link model is a function of the SIR. The work in [37] does not consider multihop connections but focuses on the last-hop wireless link. The interference power comes from neighboring cell and the signal power comes from the base station located at the center of the user's cell. It is quite different from our multihop networks.

We can employ the idea of opportunistic scheduling in our system, too. For example, the nodes who have better channel can be given a higher transmit probability instead of the common transmit probability. How to combine opportunistic scheduling and multihop routing with our Rayleigh fading link model is another research direction.

BIBLIOGRAPHY

1. N. Abramson, The Aloha System - Another Alternative for Computer Communications. *Proceedings of Fall Joint Computer Conference, AFIPS Conference* (1970).

2. P. Agrawal, Energy Efficient Protocols for Wireless Systems. In *Proc. IEEE Intl. Symp. Personal, Indoor, Mobile Radio Commun.*, pages 564–569 (September 1998).

3. N. Ahmed and R. G. Baraniuk, Throughput Measures for Delay-Constrained Communications in Fading Channels. In *Allerton Conference on Communication, Control and Computing*, Monticello, IL (October 2003).

4. I. F. Akyildiz, W. Su, Y. Sankarasubramaniam and E. Cayirci, Wireless sensor networks: a survey. *Computer Networks*, 38(4): 393–422 (March 2002).

5. J. C. Arnbak and W. V. Blitterswijk, Capacity of Slotted ALOHA in Rayleigh-Fading Channels. *IEEE Journal on Selected Areas in Communications*, SAC-5(2): 261–269 (February 1987).

6. F. Baccelli, B. Blaszczyszyn and P. Mühlethaler, An ALOHA Protocol for Multihop Mobile Wireless Networks. *IEEE Transactions on Information Theory*, 52(2): 421–436 (February 2006).

7. D. P. Bertsekas and R. Gallager, *Data Networks*. Prentice Hall (1991), ISBN 0132009161.

8. P. Billingsley, *Probability and Measure*. Wiley Series in Probability and Mathematical Statistics (1995).

9. L. Booth, J. Bruck and M. Cook, Ad hoc wireless networks with noisy links. In *IEEE Information Theory Symposium (ISIT '03)*, Yokohama, Japan (2003).

10. T. M. Cover and J. A. Thomas, *Elements of Information Theory*. John Wiley & Sons, Inc., New York (1991).

11. A. Ephremides, Energy Concerns in Wireless Networks. *IEEE Wireless Communications*, 9(4): 48–59 (August 2002).

12. G. Y. Akavia, Hierarchical organization of distributed packet-switching communication systems (1978), Ph.D. dissertation, Dep. Comput. Sci., Univ. California, Los Angeles.

13. D. Ganesan, B. Krishnamachari, A. Woo, D. Culler, D. Estrin and S. Wicker, An Empirical Study of Epidemic Algorithms in Large Scale Multihop Wireless Networks (2002), Intel Research Report IRB-TR-02-003.

14. A. J. Goldsmith and S. B. Wicker, Design Challenges for Energy-Constrained Ad Hoc Wireless Networks. *IEEE Wireless Communications*, 9(4): 8–27 (August 2002).

15. M. Grossglauser and D. Tse, Mobility Increases the Capacity of Ad-hoc Wireless Networks. In *IEEE INFOCOM*, Anchorage, AL (2001).

16. P. Gupta and P. R. Kumar, The Capacity of Wireless Networks. *IEEE Transactions on Information Theory*, 46(2): 388–404 (March 2000).

17. M. Haenggi, Energy-Balancing Strategies for Wireless Sensor Networks. In *IEEE International Symposium on Circuits and Systems (ISCAS'03)*, Bangkok, Thailand (May 2003).

18. M. Haenggi, The Impact of Power Amplifier Characteristics on Routing in Random Wireless Networks. In *IEEE Global Communications Conference (GLOBECOM'03)*, San Francisco, CA (December 2003).

19. M. Haenggi, Twelve Reasons not to Route over Many Short Hops. In *IEEE Vehicular Technology Conference (VTC'04 Fall)*, Los Angeles, CA (September 2004).

20. M. Haenggi, On Distances in Uniformly Random Networks. *IEEE Transactions on Information Theory*, 51: 3584–3586 (October 2005).

21. M. Haenggi, On Routing in Random Rayleigh Fading Networks. *IEEE Transactions on Wireless Communications*, 4: 1553–1562 (July 2005).

22. M. Haenggi, Routing in Ad Hoc Networks: A Case for Long Hops. *IEEE Communications Magazine*, pages 93–101 (October 2005), Series on Ad Hoc and Sensor Networks.

23. R. Hekmat and P. V. Mieghem, Interference in Wireless Multi-hop Ad-hoc Networks. In *The First Annual Mediterranean Ad Hoc Networking Workshop (Med-hoc-Net 2002)*, Sardegna, Italy (September 2002).

24. R. Hekmat and P. V. Mieghem, Degree Distribution and Hopcount inWireless Ad-hoc Networks. In *11th IEEE International Conference on Networks (ICON 2003)*, Sydney, Australia (September 2003).

25. R. Hekmat and P. V. Mieghem, Study of Connectivity in Wireless Ad-hoc Networks with an Improved Radio Model. In *WiOpt'04*, Cambridge, UK (March 2004).

26. M. Hellebrandt and R. Mathar, Cumulated Interference Power and Bit-error-rates in Mobile Packet Radio. *Wireless Networks*, 3(3): 169–172 (1997).

27. L. Hu, Topology Control for Multihop Packet Networks. *IEEE Transactions on Communications*, 41(10): 1474–1481 (1993).

28. Y. Y. Kim and S. Li, Modeling multipath fading channel dynamics for packet data performance analysis. *Wireless Networks*, 6: 481–492 (2000).

29. B. Krishnamachari, Y. Mourtada and S. Wicker, The energy-robustness tradeoff for routing in wireless sensor networks. In *IEEE Proceedings of ICC 2003* (May 2003).

30. R. O. LaMaire, A. K. and H. Ahmadi, Analysis of a Wireless MAC Protocol with Client-Server Traffic and Capture. *IEEE Journal on Selected Areas in Communications*, 12(8): 1299–1313 (1994).

31. K. Langendoen and N. Reijers, Distributed localization in wireless sensor networks: a quantitative comparison. *Computer Networks*, 43(4): 499–518 (2003).

32. P. Larsson, Selection Diversity Forwarding in a Multihop Packet Radio Network with Fading Channel and Capture. *ACM Mobile Computing and Communications Review*, 5(4): 47–54 (2001).

33. S.-W. Lee and C.-S. Wu, A k-best paths algorithm for highly reliable communication networks. *IEICE Trans. Comm.*, E82-B: 586–590 (April 1999).

34. J. Li, C. Blake, D. S. J. De Couto, H. I. Lee and R. Morris, Capacity of Ad Hoc Wireless Networks. In *ACM International Conference on Mobile Computing and Networking (MobiCom)*, pages 61–69, Rome, Italy (July 2001).

35. L. Li and A. J. Goldsmith, Capacity and optimal resource allocation for fading broadcast channels — Part II. Outage capacity. *IEEE Transactions on Information Theory*, 47(3): 1103–1127 (March 2001).

36. X. Liu, E. K. P. Chong and N. B. Shroff, Opportunistic Transmission Scheduling with Resource-Sharing Constraints in Wireless Networks. *IEEE Journal on Selected Areas in Communications*, 19(10): 2053–2064 (October 2001).

37. X. Liu, E. K. P. Chong and N. B. Shroff, A framework for opportunistic scheduling in wireless networks. *Computer Networks*, 41(4): 451–474 (2003).

38. X. Liu and M. Haenggi, Throughput and Energy Consumption of Multihop Networks with Rayleigh Fading. In *41st Annual Allerton Conference on Communication, Control, and Computing*, Monticello, IL (October 2003).

39. X. Liu and M. Haenggi, Throughput Bounds and Energy Consumption of Mobile Multihop Networks. In *IEEE Vehicular Technology Conference (VTC'04 Fall)*, Los Angeles, CA (September 2004).

40. X. Liu and M. Haenggi, Performance Analysis of Rayleigh Fading Ad Hoc Networks with Regular Topology. In *IEEE Global Communications Conference (GLOBECOM'05)*, St. Louis, MO (November 2005).

41. X. Liu and M. Haenggi, The Impact of the Topology on the Throughput of Interference-limited Sensor Networks with Rayleigh Fading. In *Second IEEE International Conference on Sensor and Ad Hoc Communications and Networks (SECON'05)*, Santa Clara, CA (September 2005).

42. X. Liu and M. Haenggi, Throughput Analysis of Fading Sensor Networks with Regular and Random Topologies. *EURASIP Journal on Wireless Communications and Networking*, 4: 554–564 (August 2005), Special Issue on Wireless Sensor Networks.

43. X. Liu and M. Haenggi, Towards Quasi-Regular Sensor Networks: Topology Control Algorithms for Improved Energy Efficiency. *IEEE Transactions on Parallel and Distributed Systems*, 17: 975–986 (September 2006), Special Issue on Localized Communication and Topology Protocols for Ad Hoc Networks.

44. D. A. Maltz, J. Broch and D. B. Johnson, Lessons from a Full-Scale Multihop Wireless Ad Hoc Network Testbed. *IEEE Personal Communications*, 8(1): 8–15 (February 2001).

45. A. M. Mathai, *An Introduction to Geometrical Probability*. Gordon and Breach Science Publishers (1999), ISBN 90-5699-681-9.

46. R. Mathar and J. Mattfeldt, On the Distribution of Cumulated Interference Power in Rayleigh Fading Channels. *Wireless Networks 1*, (1): 31–36 (February 1995).

47. S. Megerian, F. Koushanfar, G. Qu, G. Veltri and M. Potkonjak, Exposure in Wireless Sensor Networks: Theory and Practical Solutions. *Wireless Networks*, pages 443–454 (August 2002).

48. L. E. Miller, Distribution of Link Distances in a Wireless Network. *Journal of Research of the National Institute of Standards and Technology*, 106(2): 401–412 (March/April 2001).

49. M. Neely and E. Modiano, Capacity and Delay Tradeoffs for Ad-Hoc Mobile Networks. *IEEE Transactions on Information Theory*, 51(6): 1917–1937 (June 2005).

50. R. Nelson and L. Kleinrock, The Spatial Capacity of a Slotted ALOHA Multihop Packet Radio Network with Capture. *IEEE Transactions on Communications*, COM-32(6): 684–694 (June 1984).

51. G. Németh, Z. R. Turányi and A. Valkó, Throughput of Ideally Routed Wireless Ad Hoc Networks. *ACM Mobile Computing and Communications Review*, 5(4): 40–46 (2001).

52. P. Crescenzi and V. Kann, A Compendium of NP Optimization Problems (1998), `http://www.nada.kth.se/theory/compendium/`.

53. G. J. Pottie and W. J. Kaiser, Wireless integrated network sensors. *Communications of the ACM*, 43(5): 551–558 (2000).

54. J. G. Proakis, *Digital Communications, Third Edition*. McGraw-Hill, Inc (1998), ISBN 7-5053-4885-x.

55. S. Ramanathan and E. L. Lloyd, Scheduling Algorithms for Multihop Radio Networks. *IEEE/ACM Transactions on Networking*, 1(2): 166–177 (April 1993).

56. T. S. Rappaport, *Wireless Communications – Principles and Practice*. Prentice Hall (1996), ISBN 0-13-375536-3.

57. J. A. Robert and T. J. Healy, Packet Radio Performance Over Slow Rayleigh Fading Channels. *IEEE Transactions on Communications*, COM-28(2): 279–286 (February 1980).

58. R. C. Robertson and T. T. Ha, A Model for Local/Mobile Radio Communications with Correct Packet Capture. *IEEE Transactions on Communications*, 40(4): 847–854 (April 1992).

59. V. Rodoplu and T. H. Meng, Minimum Energy Mobile Wireless Networks. *IEEE Journal on Selected Areas in Communications*, 17(8): 1333–1344 (1999).

60. E. M. Royer and C.-K. Toh, A Review of Current Routing Protocols for Ad-Hoc Mobile Wireless Networks. *IEEE Personal Communications*, 6(2): 46–55 (April 1999).

61. A. Scaglione and S. Servetto, On the Interdependence of Routing and Data Compression in Multi-hop Sensor Networks. In *Proc. ACM MobiCom*, Atlanta, GA (September 2002).

62. C. Schurgers, V. Tsiatsis, S. Ganeriwal and M. Srivastava, Optimizing Sensor Networks in the Energy-Latency-Density Design Space. *IEEE Transactions on Mobile Computing*, 1(1): 70–80 (2002).

63. S. Shakkottai, R. Srikant and N. Shroff, Unreliable Sensor Grids: Coverage, Connectivity and Diameter. In *Proceedings of IEEE INFOCOM*, San Francisco, CA (April 2003).

64. T. J. Shepard, A channel access scheme for large dense packet radio networks. In *ACM SIGCOMM*, pages 219–230 (August 1996).

65. J. A. Silvester and L. Kleinrock, On the Capacity of Multihop Slotted ALOHA Networks with Regular Structure. *IEEE Transactions on Communications*, COM-31(8): 974–982 (August 1983).

66. B. Sklar, Rayleigh Fading Channels in Mobile Digital Communication Systems Part I: Characterization. *IEEE Communications Magazine*, pages 90–100 (July 1997).

67. E. S. Sousa and J. A. Silvester, Optimum Transmission Ranges in a Direct-Sequence Spread-Spectrum Multihop Packet Radio Network. *IEEE Journal on Selected Areas in Communications*, 8(5): 762–771 (June 1990).

68. M. Stemm and R. Katz, Measuring and reducing energy consumption of network interfaces in hand-held devices. *IEICE Trans. Comm.*, E80-B(8): 1125–1131 (August 1997).

69. B. Sundararaman, U. Buy and A. D. Kshemkalyani, Clock Synchronization for Wireless Sensor Networks: A Survey. *Ad Hoc Networks*, 3(3): 281–324 (May 2005).

70. H. Takagi and L. Kleinrock, Optimal Transmission Ranges for Randomly Distributed Packet Radio Terminals. *IEEE Transactions on Communications*, 32: 246–257 (March 1984).

71. H. Takagi and L. Kleinrock, Optimal Transmission Ranges for Randomly Distributed Packet Radio Terminals. *IEEE Transactions on Communications*, COM-32(3): 246–257 (March 1984).

72. M. Tanemura, Statistical Distributions of Poisson Voronoi Cells in Two and Three Dimensions. *Forma*, 18(4): 221–247 (2003).

73. F. A. Tobagi, Analysis of a Two-hop Centralized Packet Radio Network – Part I: Slotted ALOHA. *IEEE Transactions on Communications*, COM-28(2): 196–207 (February 1980).

74. C.-K. Toh, *Ad Hoc Mobile Wireless Networks - Protocols and Systems*. Prentice-Hall (2002), ISBN 0-13-007817-4.

75. S. Toumpis and A. J. Goldsmith, Capacity Regions for Wireless Ad Hoc Networks. *IEEE Transactions Wireless Communications*, 2(4): 736–748 (July 2003).

76. A. Tsirigos and Z. Haas, Analysis of Multipath Routing—Part I: The Effect on the Packet Delivery Ratio. *IEEE Transactions on Wireless Communications*, 3(1): 138–146 (January 2004).

77. R. Wattenhofer, L. Li, P. Bahl and Y.-M. Wang, Distributed Topology Control for Power Efficient Operation in Multihop Wireless Ad Hoc Networks. In *IEEE INFOCOM*, Anchorage, AL (April 2001).

78. L. Xie and P. R. Kumar, A Network Information Theory for Wireless Communication: Scaling Laws and Optimal Operation. *IEEE Transactions on Information Theory*, 50(5): 748–767 (May 2004).

79. Y. Xu, J. Heidemann and D. Estrin, Geography-informed Energy Conservation for Ad Hoc Routing. In *In Proceedings of the ACM/IEEE International Conference on Mobile Computing and Networking*, pages 70–84, Rome, Italy (July 2001).

80. H. Y. Youn, C. Yu and B. Lee, *Routing Algorithms for Balanced Energy Consumption in Ad Hoc Networks*. CRC Press (2003), The Handbook of Ad-Hoc Wireless Networks.

81. K. Zhang and K. Pahlavan, Relation Between Transmission and Throughput of Slotted ALOHA Local Packet Radio Networks. *IEEE Transactions on Communications*, 40(3): 577–583 (March 1992).

82. M. Zorzi and S. Pupolin, Optimum Transmission Ranges in Multihop Packet Radio Networks in the Presence of Fading. *IEEE Transactions on Communications*, 43(7): 2201–2205 (July 1995).

83. M. Zorzi, R. R. Rao and L. B. Milstein, ARQ error control for fading mobile radio channels. *IEEE Transactions on Vehicular Technology*, 46(2): 445–455 (May 1997).

84. M. Zorzi, R. R. Rao and L. B. Milstein, Error Statistics in Data Transmission over Fading Channels. *IEEE Transactions on Communications*, 46(11): 1468–1477 (November 1998).